universität wien

MASTERARBEIT / MASTER'S THESIS

Titel der Masterarbeit / Title of the Master's Thesis

„A Detachment localised in the Stangalm Mesozoic (s.l.)

(Upper Austroalpine Unit, Carinthia, Austria)"

verfasst von / submitted by

Manuel Werdenich, BSc

angestrebter akademischer Grad / in partial fulfilment of the requirements for the degree of

Master of Science (MSc)

Wien, 2022 / Vienna 2022

Studienkennzahl lt. Studienblatt / degree programme code as it appears on the student record sheet:	UA 066 815
Studienrichtung lt. Studienblatt / degree programme as it appears on the student record sheet:	Masterstudium Erdwissenschaften UG2002
Betreut von / Supervisor:	Univ. Prof. Mag. Dr. Bernhard Grasemann
Mitbetreut von / Co-Supervisor:	-

Erklärung

Hiermit versichere ich, Manuel Werdenich

- dass ich die vorliegende Masterarbeit selbstständig verfasst, andere als die angegebenen Quellen und Hilfsmittel nicht benutzt und mich auch sonst keiner unerlaubter Hilfe bedient habe,
- dass ich dieses Masterarbeitsthema bisher weder im In- noch im Ausland in irgendeiner Form als Prüfungsarbeit vorgelegt habe
- und dass diese Arbeit mit der vom Begutachter beurteilten Arbeit vollständig übereinstimmt.

Wien, am 20.09.2022

I. Acknowledgements

I am in the fortunate position of having met many people with a high level of professional competence early on during my studies, who have always supported and helped me.

First and foremost, I would like to thank my supervisors Bernhard Grasemann from the University of Vienna and Christoph Iglseder from the GBA for their support and advice in the realisation of this Thesis. Christoph, thank you for the conception of this work and for sharing ideas regarding the evolution of the Alps with me. I enjoyed the fieldwork and the nice evenings in Predlitz with you, as much as I learned how to proper map a region. Also thank you for your never-ending motivation and patience in teaching me the differences between tectonic units and lithostratigraphic units and much more for pulling me out when I saw no progress.
Bernhard, thank you for your helpful input and support in microscopical and structural geological issues. Also, thanks for the given time and free space to find my way.
Special giant thanks to Marianne Sophie Hollinetz (aka. Frau Professor) thank you so much for proof reading and correcting my “farmer boy English” and for your helping hand while fieldwork and your helping brain in fruitful discussions, while I was writing this thesis. You have significantly influenced the way I think about and deal with geological issues. I learned a lot from you. You have always kept me grounded and helped me to deal with my worries.
Also big thanks to Gerd Rantitsch from the Montanuniversity of Leoben for providing the Raman Data and the instructive session in Leoben, while I was doing a few Raman measurements by my own.

I would also like to thank my mother Silvia and my sadly deceased grandmother for their financial and mental support throughout my entire time at university, without their support, none of this would have been possible. Also mentioned are my former roommates Daniela (although her role as my sister is much more important), Tobias and Anna, who have not always contributed to my productivity but have accompanied me through the difficult time of the pandemic.

I furthermore want to thank my fellow students Gerald, Moritz, Eva, Lukas, 2x Steffi, Michi, Sophia and all others for the wonderful hours after studying and working, and for the countless times when I complained about situations. Without you, the studies would never have been successful.

II. Abstract

Mechanisms of exhumation in the Upper Austroalpine Unit are rarely investigated. Based on new structural field data, microstructural observations, and Raman micro-spectroscopy on carbonaceous material a major detachment juxtaposing Drauzug-Gurktal Nappe System against the transgressive Permo-Mesozoic cover sequence of the Ötztal-Bundschuh Nappe System (Stangalm Mesozoic s. l.) with Eo-alpine top-SE kinematics has been identified in the area south of Flattnitz (Carinthia, Austria).

The hanging wall unit comprises phyllites, and graphite schists, which experienced deformation at greenschist facies conditions. Raman microspectroscopy of carbonaceous matter constrains maximum temperatures between 388°C and 409°C. Isoclinal and open folds recognized in these units are attributed to alpine deformation.

The footwall unit consists of dolomitic ultra-mylonite and impure calcitic marble ultra-mylonite corresponding to the Stangalm Mesozoic s.l. (Bundschuh Nappe). An association of meta-conglomerate and graphite schist intercalated in the Mesozoic carbonate lithologies exhibits the same structural element as the surrounding rocks. Metamorphic peak temperatures are comparable in all lithologies and range between 435°C and 519°C. Based on lithological characteristics these rocks are identified as metamorphic equivalent of the Upper Carboniferous Stangnock Formation, previously described as the Oberhof Lithodeme. The results show that this unit was incorporated during nappe stacking and was exhumed together with the Stangalm Mesozoic s.l. Therefore, it constitutes a separate nappe of the Ötztal-Bundschuh Nappe system and the term Kuster Nappe is proposed.

In all lithologies an ESE-trending stretching lineation is the pervasive structural element. C-type shear bands, flanking folds, crystal- and shape preferred orientation of mineral grains consistently indicate top-E kinematics. Any top-W deformation related to nappe stacking was entirely overprinted. From structurally lower to higher levels, a decrease of deformation temperature is identified.

Due to the observed strong coaxial deformation in quartz and carbonate rich lithologies of the footwall units ductile thinning is interpreted as main exhumation process. Trigonometrical estimation of the distance of displacement indicates approximately 60 kilometres of displacement along the shear zone. Therefore, an Eo-alpine low angle normal fault with top E kinematics is present around Flattnitz and at Mount Kuster.

III. Zusammenfassung

Die Mechanismen der Exhumation in den Oberostalpinen Einheiten sind bisher nur wenig untersucht worden. Auf Grundlage neuer strukturegeologischer Felddaten, mikrostruktureller Beobachtungen und Raman-Mikrospektroskopie Messungen an kohlenstoffhaltigem Material wurde im Gebiet südöstlich von Flattnitz (Kärnten, Österreich) eine mächtige Scherzone identifiziert, die das Drauzug-Gurktal-Deckensystem und die transgressive permo-mesozoische Bedeckung des Ötztal-Bundschuh-Deckensystems (Stangalm-Mesozoikum s. l.) mit Eo-Alpiner Top-E-Kinematik trennt.

Die hangenden Einheiten bestehen aus Phylliten und Graphitschiefern, die unter grünschieferfaziellen Bedingungen deformiert wurden. Die Raman-Mikrospektroskopie zeigt ein Temperaturmaximum der Metamorphose zwischen 388°C und 409°C. Isokline und offene Falten in diesen Einheiten werden auf Alpine Deformation zurückgeführt.

Die Liegenden Einheiten bestehen aus dolomitischem Ultramylonit und unreinem kalzitischem Marmor-Ultramylonit, welche dem Stangalm-Mesozoikum s.l. (Bundschuh-Decke) zugeordnet werden. Eine Assoziation von Metakonglomerat und Graphitschiefer, welche in den mesozoischen Lithologien eingebettet ist, weist die gleiche Strukturprägung wie die umgebenden Gesteine auf. Die Temperaturen der Metamorphose sind in allen Lithologien vergleichbar und liegen zwischen 435°C und 519°C. Aufgrund der lithologischen Merkmale werden diese Gesteine als höher metamorphes Äquivalent der karbonen Stangnock-Formation identifiziert und dem Oberhof Lithodem zugeordnet. Die Ergebnisse zeigen, dass diese Assoziation während der Deckenstapelung inkorporiert und zusammen mit dem Stangalm-Mesozoikum s.l. exhumiert wurde. Daher stellt sie eine eigenständige Decke des Ötztal-Bundschuh-Deckensystems dar und wird als Kuster-Decke bezeichnet.

In allen Lithologien ist eine ESE-streichende Lineation das vorherrschende Strukturelement. C-Typ Scherbänder, flanking structures sowie die kristall- und formpräferierte Orientierung der Mineralkörner weisen durchwegs auf eine Top-E-Kinematik hin. Jegliche Top-W-Verformung, die mit der Stapelung der Decken zusammenhängt, wurde vollständig überprägt. Von den strukturell niedrigeren zu höheren Einheiten wird eine Abnahme der Deformationstemperatur festgestellt.

Aufgrund der beobachteten starken koaxialen Deformation in den quarz- und karbonatreichen Lithologien der Liegenden Einheiten wird „ductile thinning“ als Hauptprozess der Exhumierung interpretiert. Eine trigonometrische Abschätzung der Distanz der Abschiebung deutet auf eine Versatzweiten von etwa 60 Kilometern entlang der Scherungszone hin. In der Umgebung um Flattnitz und am Berg Kuster ist eine Eo-Alpine Scherzone mit Top E Kinematik aufgeschlossen.

IV. List of abbreviations

NS	Nappe System
KWNS	Koralpe-Wölz Nappe System
ÖBNS	Ötztal-Bundschuh Nappe System
DGNS	Drauzug-Gurktal Nappe System
s.str.	sensu stricto
s.l.	sensu lato
D.	Deformation phase
SPO	Shape preferred orientation
CPO	Crystallographic preferred orientation
DPC	Dissolution precipitation creep
Qz	Quartz
Fsp	Feldspar
Wm	White mica
Wm-det	White mica detrital
Tre	Tremolite
Cal	Calcite
Py	Pyrite
Tlc	Talc
Tur	Turmaline
Fe-Ox	Iron oxide
Grt	Garnet
Chl	Chlorite
S	Schistosity planes
L	Lineation
FA	Fold axis
AP	Axial plane

Table of Content

1 Statement of aim & Introduction

Since the discovery of plate tectonics in the 1960s, the understanding of plate movement and the processes associated with mountain building has been continuously expanded. Thus, in the example of the Alps, which result from the accumulation, subsidence and exhumation of rocks and sedimentary products from different epochs of the geological era, a complex mountain range is formed. It is therefore of fundamental interest to assign the originally laterally distributed deposited (palaeographic/ lithodemic) units, which in this case form the Alps, to jointly experienced deformation mechanisms and phases (correlated to "geological events") and to classify them together in the sense of tectonic units (nappes).

For this purpose, this study investigates a major tectonic boundary located in Flattnitz (Carinthia, Austria). In this area, nappe system boundaries separating the Ötztal-Bundschuh - and the Drauzug-Gurktal Nappe System are exposed. The aim of this work is to characterize these (complex) contact/ shear zones between the nappe systems in terms of their jointly experienced deformation history, thermal evolution, and properties of the evolved nappes.

The research area is located south of the village of Flattnitz in Carinthia and extends from Mount Kuster (1669 m) to the SE flank of Mount Hirnkopf (1800 m). Based on previous mappings by Stowasser (1956) and Beck Mannagetta (1959), a revised map covering 10 km^2 is presented. From structural data from outcrop to microscope scale, the deformation history of this area is outlined. Metamorphic peak temperatures got determined by Raman microspectroscopy of carbonaceous material, that infers a temperature peak of 520°C. Using the grain size tool and the included paleo-piezometry toolbox of (Marco A. Lopez-Sanchez, 2018), the reconstruction of the paleo-differential stress regarding to deformation and subsidence of the quartz and calcite rich lithologies of both nappe systems is attempted. Based on the new data, a revised tectonic subdivision of the nappe systems in nappes and consequences for Upper Austroalpine tectonics is presented.

2 State of the Art

2.1 Geology of the Eastern Alps

The Eastern Alps were formed as the result of the continuous collision of the European plate and the Adriatic plate. Accumulation of microcontinents, slope sediments and oceanic deposits resulted in a mountain range with a complex structure. The division of major tectonic units in the Eastern Alps is based on their paleogeographic origin from the European Continent, Penninic Oceans, Neo-Tethys Ocean, and Adriatic Continent (Froitzheim et al., 2008; Schmid et al., 2004). In the latter named units an intracontinental subduction event (Janak et al., 2004; Stüwe & Schuster, 2010) took place during the Cretaceous. The associated high-pressure metamorphism and deformation is referred as the Eo-Alpine event (Thöni & Jagoutz, 1993), which lead to the formation of the Upper Austroalpine nappe stack. This nappe stack is subdivided into several nappes belonging to several nappe systems with different metamorphic and structural characteristics. The units are built of partly polymetamorphic crystalline basement, Paleozoic and Permo-Mesozoic (meta-)sediments (Schuster, 2015; Schuster et al., 2010). The Austroalpine Unit was earlier subdivided in a Lower, an Upper and a Middle Austroalpine Unit after the nomenclature of Tollmann (1977). Insights of Schmid et al. (2004) suggested that the Middle and the Upper Austroalpine Unit are summarized in the Upper Austroalpine Unit, just the latter one is of relevance in this study. The Upper Austroalpine Unit consists of upper crustal nappe systems that experienced ductile (Veitsch-Silbersberg NS; Tirolic-Noric NS) and brittle deformation (Bajuvaric and Juvavic NS) as well as poly-metamorphic basement nappe systems. These are, from structurally highest to lowest level, the Drauzug-Gurktal Nappe System (DGNS), the Ötztal-Bundschuh Nappe System (ÖBNS), the Koralpe-Wölz Nappe System (KWNS). Cretaceous eclogites only occur in the KWNS which comprises the deepest subducted part. During extrusion of these HP units the metamorphic gradient in the hanging wall records normal and in foot wall inverted metamorphic gradients. The structurally lowest unit is the Silvretta-Seckau Nappe System (SSNS).

This study focuses on the transition between the (paleographic) Ötztal-Bundschuh Nappe System and Drauzug-Gurktal Nappe System and their interaction during Cretaceous nappe stacking followed by Upper Cretaceous normal faulting.

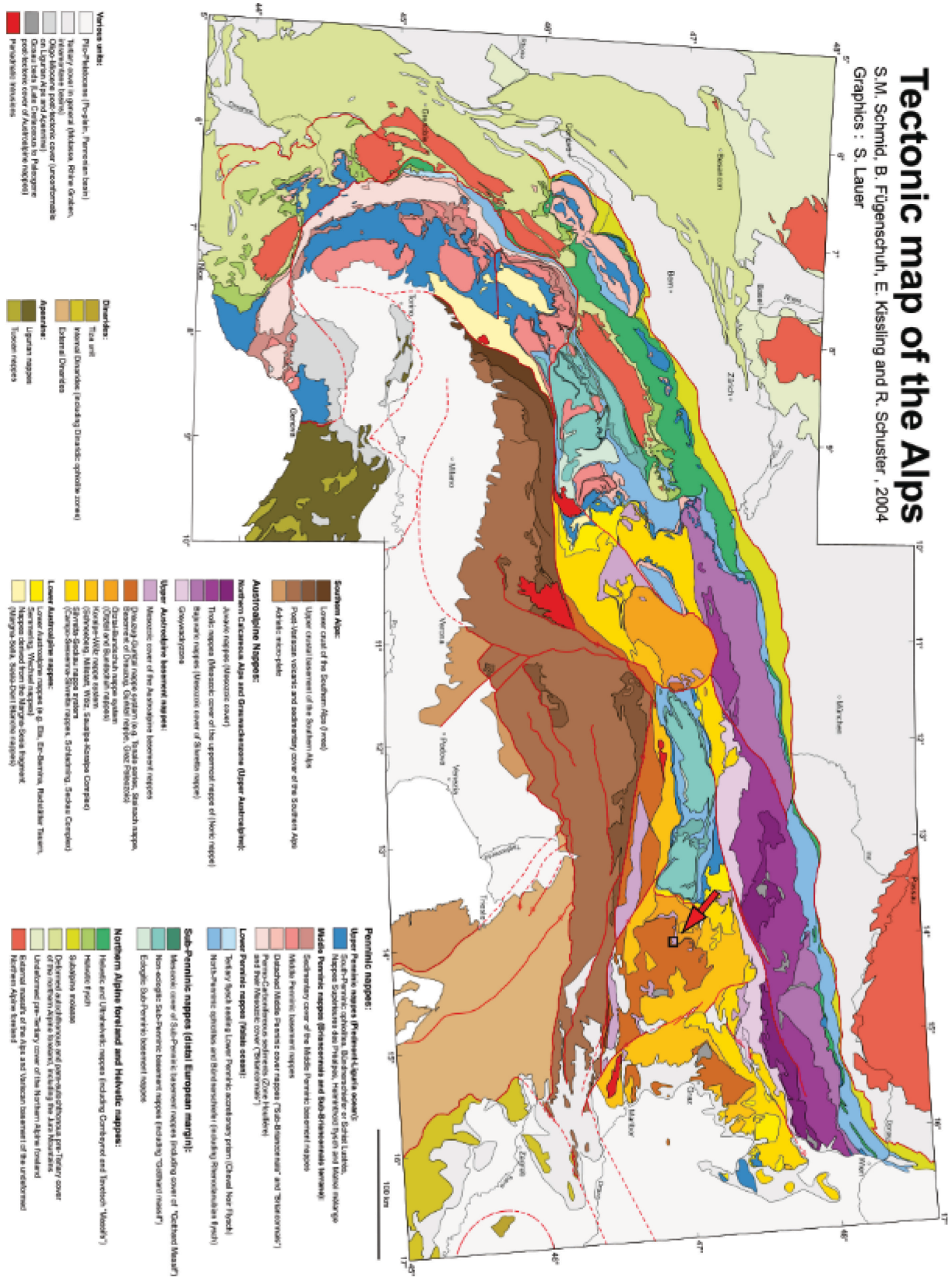

Figure 1: Tectonic map of the alps by Schmid et al.; the black box and the red arrow mark the research area. Coordinates of Mount Kuster N46.931197, E14.039298 (Carinthia, Austria).

2.2 Gurktal Alps

The Gurktal Alps are built from nappes of the Koralpe-Wölz NS, the Ötztal-Bundschuh NS and the eponymous Drauzug-Gurktal NS. Lithologically, these units consist of (1) a crystalline basement, (2) pre-Variscan metasediments, (3) a post-Variscan (Pennsylvanian-Cisuralian) cover, (4) a Permo-Mesozoic cover and (5) a Cretaceous-Paleogene cover, although these constituents comprise different proportions of the tectonic units.

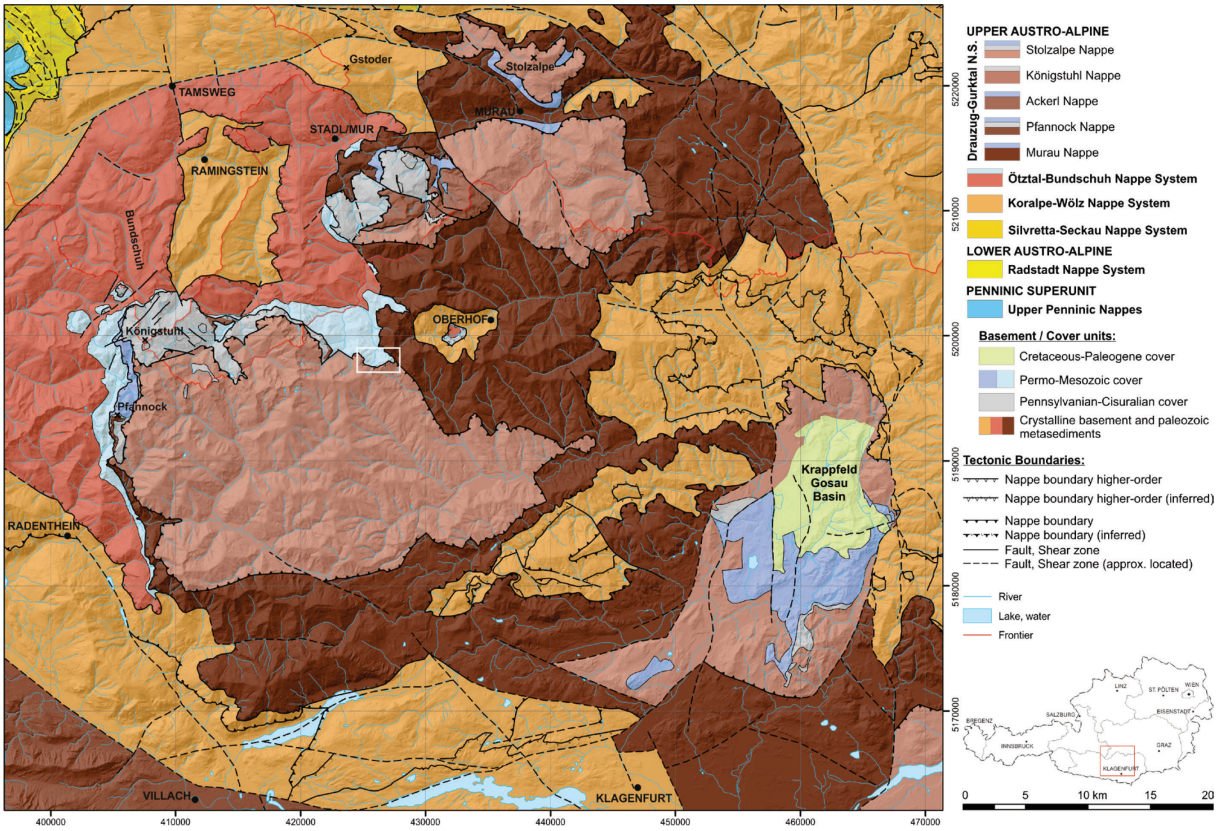

Figure 2: Tectonic map of the Gurktal Alps; the white square indicates the position of Figure 4; from and modified after Rantitsch et al., 2020.

The structurally lowest units can be assigned to the uppermost part of the Koralpe-Wölz NS (Gstoder Nappe and undefined mica schist nappes). The main lithostratigraphic unit in the Gstoder Nappe is the Radenthein Complex, which shows a heterogeneous assemblage of metapelites with amphibolite and hornblende bearing mica schists, marble, and graphite schist (crystalline basement type 2 according to Schuster, 2015). This nappe experienced a tectono-metamorphic overprint during the Eo-Alpine event at metamorphic peak conditions of c. 550-600°C and 9-11 kbar (Koroknai et al., 1999; Kaindl & Abart, 2002; Hoinkes et al., 2010; Krenn et al., 2011; Hollinetz et al., 2018; Iglseder et al., 2018). Raman micro

spectroscopy temperatures yielded temperatures of around 540-580° C in the Ramingstein window (Iglseder et al., 2018; Rantitsch et al., 2020) and 520-550°C in the Oberhof window (Hollinetz, 2018). The metamorphic peak is constrained by ^{144} Sm/^{143} Nd garnet dating and occurred at 84-100 Ma (Schuster & Frank, 1999). ^{40}Ar/^{39}Ar muscovite ages and Rb/Sr biotite ages document subsequent exhumation at 83-86 Ma and further cooling below 300°C between 72-77 Ma (Schuster & Frank, 1999; Hollinetz et al., 2018; Iglseder, 2019).

The overlying Bundschuh Nappe of the Ötztal-Bundschuh NS is lithostratigraphically subdivided in a basement of the Bundschuh-Priedröf Complex that consists of garnet-bearing mica schist, paragneiss, and Ordovician intrusions of the Bundschuh-Orthogneis Lithodeme (crystalline basement type 1 according to Schuster, 2015), as well as a Permo-Mesozoic cover (Stangalm Mesozoic s.str. after Stowasser, 1956; respectively s.l. after Iglseder, 2019; Iglseder et al., 2019).
Two-phased garnets in the crystalline basement document a polyphase metamorphic overprint with peak conditions at 600-650 °C and 10-11 kbar (Koroknai et al., 1999; Schuster & Frank, 1999). Eo-Alpine peak conditions are constrained by petrological investigations and Raman microspectroscopy measurements at 520-560 °C and 10 kbar in the Eastern parts of the Bundschuh Nappe (Hollinetz, 2018; Hollinetz et al., 2019). Raman data from structural lower levels yields temperatures of 510-590 °C in the Basement and in covering parts 450-530 °C, which indicates a normal metamorphic gradient (Iglseder et al., 2018; Rantitsch et al., 2020). The age of the Eo-Alpine overprint is determined form U-Th-Pb monazite dating and ^{40}Ar/^{39}Ar muscovite ages that range between 99 and 82 Ma (Neubauer et al., 1998; Schuster & Frank, 1999; Iglseder et al., 2018; Hollinetz et al., 2019). Cooling below 300 °C documented by Rb/Sr biotite ages occurred between 81 and 87 Ma (Schuster & Frank, 1999; Iglseder et al., 2018).

Five previously identified nappes corresponding to the Drauzug-Gurktal NS and comprise the uppermost part of the nappe stack in the Gurktal Alps (Huet, 2015; Iglseder et al., 2016). The structurally lowest unit is the Murau Nappe, which consists of pre-Variscan siliciclastic metasediments in the basal part (“Murau Group”), and carbonate dominated lithologies (“Murau Limestone”) in the structurally upper proportions. In the Northern parts, a Permo-Mesozoic cover is also present (Neubauer et al., 2019). The Murau Nappe is overlain by the Ackerl (Ackerl crystalline Complex) and Pfannock Nappes (Pfannock orthogneiss). Both nappes contain metasediments that transgressed on the crystalline basement and range from the Carboniferous (Stangnock Formation) to the Triassic (e.g., Lantschfeldquarzite, “Pfannock Trias”) (Iglseder & Huet, 2019 and references therein). The overlying Königstuhl Nappe contains a pre-Variscan low-grade metamorphic basement made of pyroclastic

metavolcanic and (siliciclastic) metasedimentary rocks as well as dolomite marbles (Kaser Complex, Iglseder et al., 2019). Large proportions of the nappe consist of Upper Carboniferous continental metasediments of the Stangnock Formation (Schönlaub, 2014a). This formation is built of coarse to fine-grained molasse-type sediments of a braided river network composed of quartz-rich polymictic conglomerates at the base, sandstones and arenaceous shales with a sub-greenschist facies overprint in the region around Turrach (Iglseder et al., 2019). Relative dating of plant fossils suggests an age of 310 – 305 Ma of the Upper Carboniferous (Fritz et al., 1990; Fritz & Krainer, 2007; Kabon & Iglseder, 2019 and references therein). These are overlain by the Lower Permian (Cisuralian) Werchzirm Formation (Iglseder, 2019).

The tectonically uppermost unit is the Stolzalpe Nappe, which consists of pre-Variscan siliciclastic metasediments (Spielriegel Complex) and Upper Ordovician metavolcanics (Kaser Complex, Iglseder et al., 2018, Iglseder, 2019). In structurally higher levels of this nappe, post-Variscan metasediments of Upper Permian to Cisuralian age of the Stangnock Formation and Werchzirm Formation occur, as well as a Permo-Mesozoic and Cretaceous-Paleogene cover in the South-Eastern areas of this unit. Which experienced a low-grade metamorphic overprint due to the Eo-Alpidic event.

The peak of metamorphism in these five nappes range from upper greenschist facies at basal proportions (Frimmel, 1987; Koroknai et al., 1999; Neubauer, 1987) to sub-greenschist and very-low-grade facies in structural higher levels (Rantitsch et al., 2020; Huet, 2015; Iglseder et al., 2016; Von Gosen et al., 1985). Garnet growth at the base of the Murau Nappe indicates Variscan amphibolite facies conditions during the metamorphic overprint. The Eo-Alpine peak and overprint occurred at 460-500°C (Koroknai et al., 1999). Raman microspectroscopy show for the structurally uppermost nappes (Stolzalpe and Königstuhl Nappe) a Variscan peak of metamorphism of 350°C and an Eo-Alpine overprint of average 250°C (Iglseder et al., 2016).

2.3 Geology of the research area

Introductory structural and lithologic features are described in lithostratigraphic and lithodemic units belonging to nappes in higher ranked nappe systems. Based on their definition (Schmid et al., 2004; Froitzheim et al., 2008; Schuster, 2015 and references therein) nappe systems correspond to rock units and their paleogeographic position at +/- Jurassic times before involved in Alpine orogenesis. Nevertheless, most nappe definitions correspond to Alpine tectonics and superposition. In the following, I tried to use the description of features in a lithostratigraphic/ lithodemic unit. Sometimes, for better understanding I use the Stratigraphic + Tectonic combination.

The research area is located south of the village of Flattnitz in Carinthia and extends from Mount Kuster (1669 m) to the SE flank of Mount Hirnkopf (1800 m). The exposed rocks correspond to nappes of the ÖBNS and the overlying DGNS. In the following, the lithostratigraphic units that build up these nappes are described in more detail:

In a large part of the study area, rocks of the Permo-Mesozoic cover of the Bundschuh nappe are found; in contrast, no evidence of a crystalline basement is described in the area of mount Kuster (Stowasser, 1956). The occurrence of a crystalline basement is described in northern parts of the research area (Weissenbacher, 2015). The Permo-Mesozoic Cover consists predominantly of carbonate lithologies with siliciclastic intercalations. Formerly known as the “Flattnitz Trias” (Von Gosen et al., 1985), it corresponds to the Stangalm Mesozoic s.l. (Iglseder, 2019 and references therein; Iglseder et al., 2019). The protolith age of the metasediments ranges from the uppermost Permian to the Jurassic and is based on correlation with undeformed, non-metamorphic equivalents that occur in the Northern Calcareous Alps. Pistotnik (1976) interpreted a transgressive contact to the basement of the Bundschuh nappe and proposed a stratigraphic classification where the cover lithologies are subdivided in several formations. However, in the Flattnitz area the stratification sequence as described cannot be found due to a pronounced tectonometamorphic overprint that occurred during the Eo-Alpine tectonics. Thus, a subdivision in lithodemic units seems more appropriate, as recent research by Iglseder et al., (2019) suggests. Their classification of the Stangalm-Mesozoic s.l is used in this work and briefly summarized in the following:

The Weißwände Lithodeme (formerly “Unterer Dolomit” after Stowasser, 1956; “Wettersteindolomit” after Tollmann, 1958; Pistotnik 1973, 1974) consists of bright, fine-grained banded dolomites and is interpreted as metamorphic equivalent of the Wetterstein dolomite (Iglseder et al., 2019). Phyllites

and mica schists of the Bockbühel Lithodeme (formerly “Bockbühel Schiefer”, Stowasser, 1956) comprise a metamorphic equivalent of the Partnach Formation (Weissenbacher, 2015; Iglseder et al., 2019) and occur intercalated in the Weißwände Lithodeme. The Karnerboden Lithodeme (formerly “Oberer Dolomit”, “Trümmerdolomit”, Stowasser, 1956) consists of dark greyish medium-grained dolomites and is interpreted as metamorphic equivalent of the Hauptdolomit (Iglseder et al., 2019). The uppermost Leckenschober Lithodeme (formerly „Kalkschiefer, Mergelschiefer, Kieselkalkschiefer“, Stowasser, 1956; “Aptychen-Kalkschiefer“, Tollmann, 1977) is comprised by platy limestones with intercalated phyllitc layers, and interpreted as metamorphic equivalent of the Allgäu- and Ammergau Formation (Iglseder et al., 2019 and references therein).

A special unit (of importance for the investigated area) was documented by Beck-Mannagetta (1959) incorporated into the Stangalm-Mesozoic. He described the occurrence of a well delimited lithological association consisting of strongly foliated quartz conglomerates, mica-rich meta-sandstone, and partly graphitic mica schist in the area between Johanniswand and Mount Kuster. He saw the lithologic affiliation of these lithologies as part of the Upper Carboniferous Stangnock Formation. Similarities to the Oberhof Lithodem (Hollinetz, 2018; Hollinetz et al., 2019) are suggested and are a main part of this study, defining a new tectonic unit, named the Kuster Nappe (see chapter 5.4).

The structurally higher parts belong to units of the DGNS. The Murau Group within the Murau Nappe is the structurally lowest lithostratigraphic unit in the research area and comprise pre-Variscan metasediments as garnet bearing, graphitic phyllites respectively mica schists. This is overlain by lithologies of the Stolzalpe Nappe namely the Spielriegel Complex. It comprises meta-sandstones in exchangeable layering with meta-siltstone and quartz-phyllite as well as rarely occurring layers of graphite-schist, chlorite-phyllite, chlorite-schist, greenish-slate, meta-tuff, meta-tuffite and quartzite. Subordinated dolomite marble ("iron dolomite") and calcite-marble exist. Towards upper structural levels, the occurrence of chlorite schist, chlorite, and quartz-phyllite is increasing (Iglseder, 2019).

2.4 Deformation phases (in the Gurktal Alps)

Rocks exposed in the study area were subjected to polyphase deformation. In the following, the main pre- and alpidic deformation phases are presented. Based on earlier studies (Frimmel, 1987; Schuster, 1994; Huet, 2015; Hintersberger et.al., 2017; Iglseder & Huet, 2019), the main deformation phases of the research area are explained. Pre-Variscan structures belong to deformation phase D_0 only obvious in the Spielriegel Complex. Deformation phases D_1–D_2 related to the Variscan event (after Hintersberger et al.; 2017) are obvious in the metasediments of the Spielriegel Complex. The D_3-D_4 deformation phases are related to the Eo-Alpine event (after Hintersberger et al.; 2017), followed by the D_5 deformation phase corresponding to the Neo-Alpine event (after Hintersberger et al.; 2017). These are most prominently expressed in the Permo-Mesozoic Stangalm-Mesozoic s.l. and Oberhof Lithodeme, partly in metasediments of lowermost parts of the Spielriegel Complex.

The oldest structural features (D_0) are observed in lithologic units of the Stolzalpe-Nappe and are classified as sedimentary and volcano-clastic sedimentary layering. These features comprise convolute bedding, cross bedding, and ripples are only preserved in regions that experiences less deformation during the following Variscan event. In most areas, these structures are largely overprinted by a penetrative axial plane schistosity. The sedimentary layering shows kilometre ranged domains of coherent layering dipping shallowly towards SE (Huet, 2015). Furthermore, the formation of the earliest phase is described as symmetric isoclinal parallel-folds (D_1). This phase is shown in lithologic units of the Stolzalpe-Nappe (Spielriegel Complex and Kaser Complex) in shallow NW–SE dipping fold axis. Locally these folds show S-, Z-, and M-geometries. In the Murau Group this phase is indicated by folded quartz veins which pervasively overprint the sedimentary layering (Frimmel, 1987). The D_2 phase is represented by ENE verging, asymmetric kink folds with cm to km extent. The overprint of D_1 folds by D_2 folds results in an interference pattern. Structural elements related to D_2 are a crenulation lineation parallel to the fold axis and a stretching lineation perpendicular to the fold axis. The Murau Group shows in this phase isoclinal folds parallel to the schistosity planes (s2) (Frimmel, 1987). However, due to the stronger overprint of later deformation phases, the D_1 and D_2 elements may be ambiguous in the Murau Group.

Structures interpreted as Eo-Alpine (Cretaceous) structures can be subdivided into two major phases: (A) (D_{3a}) related previous WNW-verging close folds and brittle-ductile shear structures with WNW-directed kinematics are assigned to nappe stacking and thrusting. These structures got subsequently overprinted.

(B) (D_{3b}) top-to ESE directed structures related to WNW-ESE-directed extension due to exhumation and normal-faulting (Iglseder & Huet, 2019). These phases are expressed to a different degree in different units depending on the prevailing metamorphic grade during deformation and the magnitude of later overprint. This can be observed in the Radenthein Complex, Bundschuh-Priedröf Complex, Stangalm Mesozoic s.l., Murau Group, and in the Spielriegel Complex. Therefore, the structural features in the Spielriegel Complex corresponding to the (D_{3a}) phase shown by WNW-verging, closed folds. Also, brittle-ductile transition shear structures with top-to WNW-directed kinematics are included. C'-type-shear bands with slickensides have a shallow dip towards SW to NW. Less common are conjugated shear planes. Phase D_{3b} in the Spielriegel Complex described by Huet (*2015*) is shown by normal faults dipping to ESE or WNW. These structures cut all pre-existing features. It could be shown that the maximum compressive principal stress axis (σ1) is oriented vertically, and the minimum compressive principal stress axis (σ3) is horizontally (N 280) oriented. The (D_{3b}) structures especially are localised at nappe boundaries to and of the Königstuhl- & Bundschuh-Nappe (Iglseder & Huet, 2019, ATA, 2019 and references therein).

The structural overprint of the Murau Group can also be assigned to the Eo-Alpine event. (D_{3a}) structures are ENE-WSW dipping fold axes as well as stretching lineation and partly top to the W thrusting (Neubauer, 1987). (D_{3b}) structures are correlated with WNW-ESE extension and top to the E shearing which leads to the formation of C'-type shear bands (Hollinetz et al., 2018; Iglseder et al., 2018).

The units of the Stangalm Mesozoic s.l. show asymmetric isoclinal N-verging folds with E-W orientated fold axes originated from WNW thrusting while nappe stacking (D_{3a}). There are geometric similarities of the (D_{3b}) related isoclinal folds and therefore the formation of schistosity planes and ESE-WNW-directed mineral lineation parallel to the sedimentary layering (Frimmel 1987). Frimmel reported evidence for the formation of isoclinal folds and corresponding axial plane schistosity during this phase. They mostly occur in conjunction with C'-type shear bands with a detaching top to the ESE kinematic (Iglseder & Huet, 2019; Iglseder et al., 2019).

The D_4 phase is referred to the Neo-Alpine (Late Cretaceous-Neogene) event and therefore expressed as open obtuse to acute-angle folds in cm to dm scale. A diffuse crenulation lineation indicates a NNW-SSE shortening. Due to cross cutting relationships this event overprints further deformation phases and can be interpreted as tectonic structure (Huet, 2015). In the Stangalm Mesozoic s.l. this phase/ structure is presented in open asymmetric folds, which refold the older Eo-Alpine ones. Fold axes are orientated from E-W to ESE-WNW with slightly steeper orientated axial planes as in the D_{3b} event.

D_5 is expressed as a brittle deformation feature by steep joint sets.

2.5 Geomorphology

Geomorphological observations were included into mapping of the area around Flattnitz, which experienced in the Würm massive overprint by glacial erosion of the Mur Glacier and northern parts of the Drau Glacier (Van Husen, 2019). This glacial activity originated from the eastern end of the Hohe Tauern. The ice was flowing in eastern direction via the Lungau into the Murtal. More southern proportions flowed in south-eastern direction via the Lieser- and Maltatal to the northern boundary of the Drau Glacier. In this ice accumulation area, a closed ice flow network was active. Due to the thick ice layer, the flow of ice from the accumulation area and the resulting accompanying pressure, a flow off in northern direction was not possible. Therefore, in the region of Turrach and Flattnitz the ice of the Mur Glacier drifted further to the south and formed SE of Turrach a transfluence with the Drau Glacier and in Flattnitz an overflow of Mount Kuster and an ice fall. Van Husen (2019) shows that the ice flow in the region of Turracher Höhe had a width of 1500 meters and thickness of 300 meters. At Flattnitz he showed a filling of the valley of 3500 meters width and a thickness of the ice layer of 400-500 meters, documented by glacial erratic blocks. This leads to massive glacial erosion as deepening of the valley bottoms and steepening of mountain flanks, what enables mass movements as the ice retreated. In the Würm LGM the ice cover reaches its maximum.

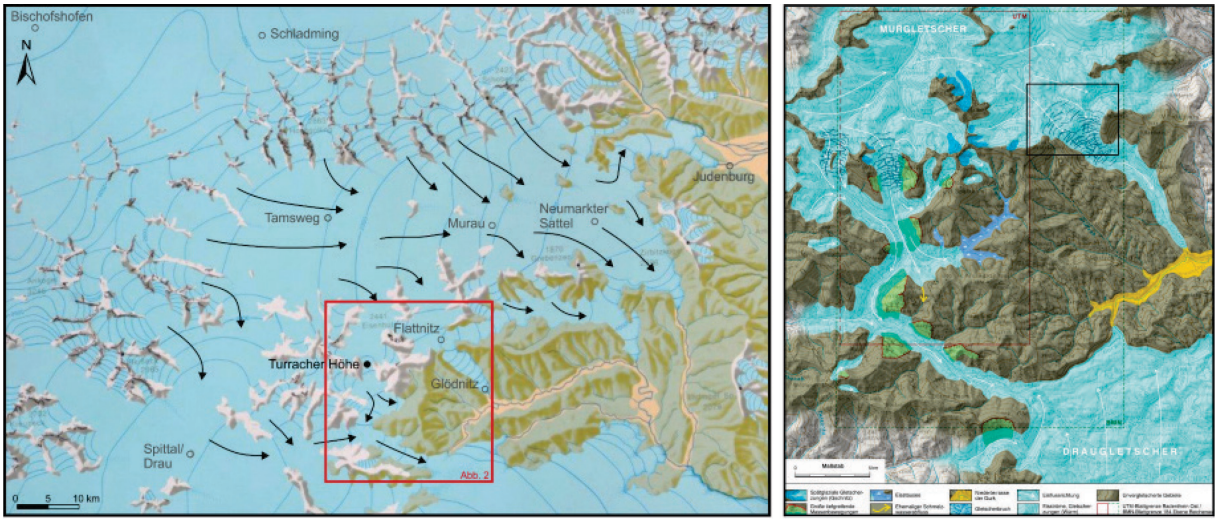

Figure 3 left: Reconstruction and iceflow from glacier system of the Mur glacier during the last ice age (Würm); Right: Reconstruction of glaciation in the region of Turrach & Flattnitz; Figures from Van Husen, 2019.

3 Methods

The aspiration of this work is the presentation of a revised map, structural interpretation, and deformation history with correlation of the maximum thermal evolution of the area around Mount Kuster S of Flattnitz.

3.1 Mapping, Field work & Sampling

Geological mapping focused on the lithological units, structural geological and tectonic aspects, metamorphic overprint, and the quaternary development. The tectonic and stratigraphic position of the lithodemic units as well as their geological affiliation were identified by detailed mapping of a 10 km² extended area around Flattnitz in Carinthia, including Mount Kuster.

Samples of all units were taken and prepared for microscopical and structural investigations. The thin sections were compounded in the thin section laboratory of the Department of Geology and Department of Lithospheric Research at the University of Vienna.

3.2 Raman micro-spectroscopy

Carbonaceous material especially graphite schist and graphite-bearing metasediments were systematically mapped and sampled. The sample set comprises 17 samples which were taken during the mapping for this thesis and from preceded mappings by C. Iglseder from the Geological Survey of Austria, partly published in Rantitsch et al., 2020. Carbonaceous matter for the Raman measurements was isolated from the rock matrix using hydrochloric and hydrofluoric acid treatment described by Rantitsch et al., (2004). Raman spectra were acquired by using a Dilor confocal Raman spectrometer equipped with a frequency-doubled Nd-YAG laser (100 mW, 532 nm), a diffraction gratings of 1800 grooves/mm and a Peltier-cooled, slow-scan, CCD matrix-detector. Laser focusing and sample viewing were performed through an Olympus BX 40 microscope fitted with a 10 × long working distance objective lens. To obtain a better signal to noise ratio five scans with an acquisition time of 30 s in the 700–2000 cm−1 region was averaged. Minimum 20 spectra for each sample were recorded. The results were provided by Professor Dr. Gerd Rantitsch from the University of Leoben.

3.3 Microstructural analysis & Imaging

Microstructural and thin section analysis has been done with the optical microscope Nikon Optiphot2-Pol. Images from thin sections were taken with the optical camera microscope Leica DM 4500 P.

3.4 Quantification

3.4.1 Refold structures

Measurements of axial planes and fold axis of different deformation phases were taken to classify the type of refold structure after the nomenclature of Grasemann et al., (2004). These measurements are used to present a ternary diagram (vector-triangle plot), which allows a simple representation of a complex three-dimensional structure.

3.4.2 Paleo-piezometry

The size of dynamical recrystallised grains in highly deformed monomineralic rocks is a function of differential stress. This method to measure the magnitude of paleo differential stress is called paleopiezometer (Twiss, 1977). Consequently, for a particular differential stress during deformation, different minerals have each particular grainsize depending on the deformation mechanism, water content of grains and deformation temperature (Passchier, 2005).

Generally, the four main deformation mechanisms are (1) cataclasis, which means deformation and displacement by cracks and microcracks of rigid particles. (2) Diffusive mass transfer by solution (DMT) or dissolution and precipitation, this is understood as deformation by the movement of lattice defects, ions, atoms, and molecules driven by chemical potential gradients. Natural examples are cleavage domains, SC, and SCC' fabrics. (3) Intracrystalline plasticity is shown in permanent misorientation of the crystal lattice. This deformation is driven by the movement of extra half planes, seen in grain boundary sliding and twinning. (4) Solid-state diffusive mass transfer is expressed as phase transformation commonly seen in mineral reactions and chemical zonation (Blenkinsop, 2000).

The estimation of the differential stress is carried out using the toolbox coded in Phyton by Marco Lopez Sanchez (2018). Therefore, the grains of nearly monomineralic samples were considered and mapped. The area of each grain was calculated using the software ImageJ. Further on the circular diameter of each measured grain area must be calculated by the formular: $d = 2 * \sqrt[2]{(\frac{Area}{\pi})}$. Depending on the piezometer used, the distribution of the grain sizes must be given in the form of the arithmetic mean or in the form of the rooted mean squared. The script provides different piezometers which were calibrated using different sets of natural samples and experiments, therefore different piezometers provide slightly different values for the differential stress.

4 Results

4.1 Mapping

The areal mapping of the research area leads to the following map (Fig. 4). In this thesis, all coordinates are given in the WGS 1984 UTM Zone 33N coordinate system. Lithological, structural geological and geomorphological issues were considered during mapping. Mount Kuster and Mount Hirnkopf SW of Flattnitz (Carinthia), which are mostly built of lithologies of the Mesozoic cover unit of the Bundschuh Nappe the so called Stangalm Mesozoic s.l. overlain and juxtaposed by units of the Drauzug-Gurktal Nappe System. The resulting map and the corresponding legend are presented below. For better readability, fold axes of the different deformation events are shown in chapter 4.3 (Fig. 19 A & B). An interpreted lithological and tectonic profile from field observations and measurements is provided (Fig. 5 & 6)

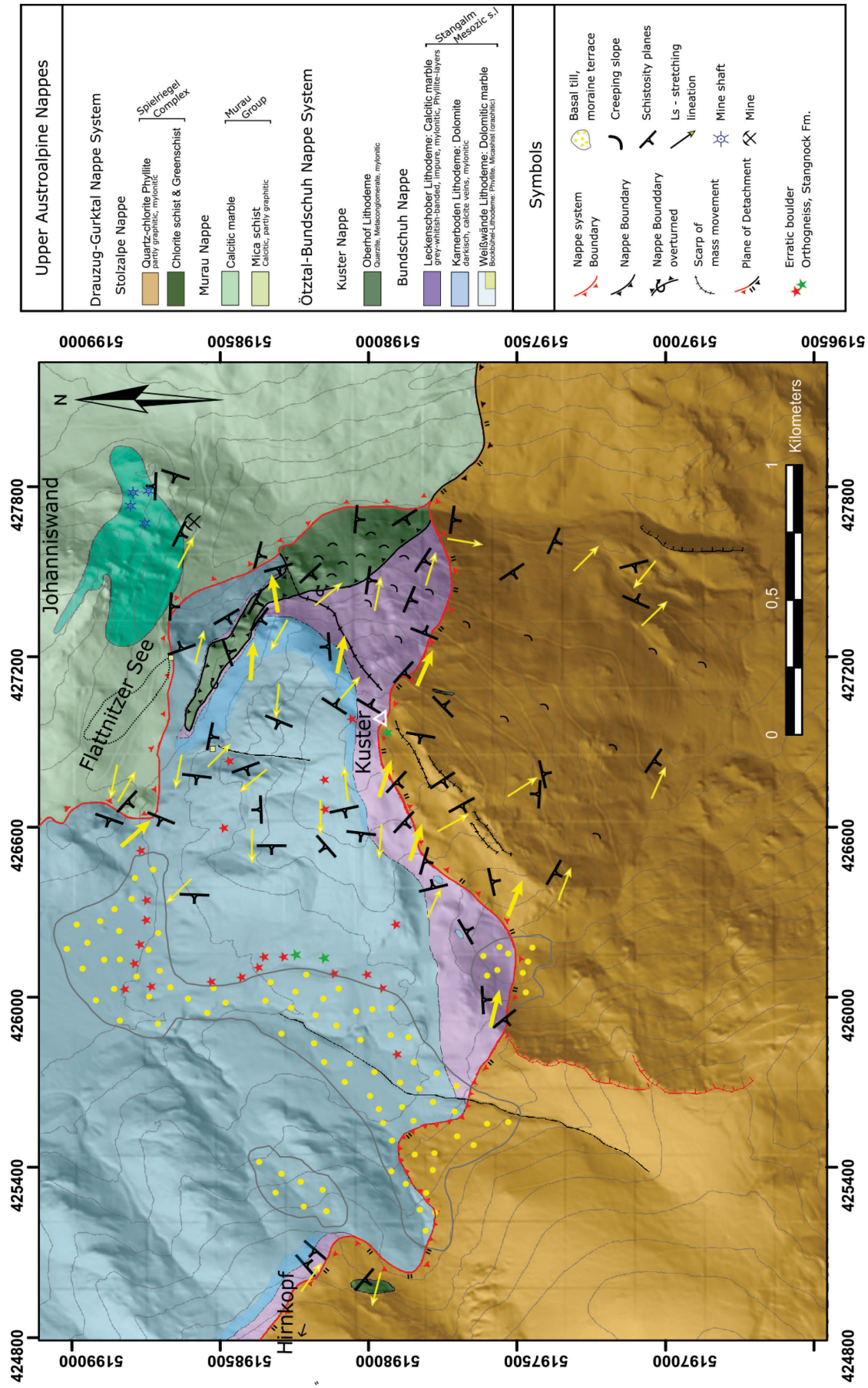

Figure 4: Geological map of the research area, drawn in ArcGis v.10.7.

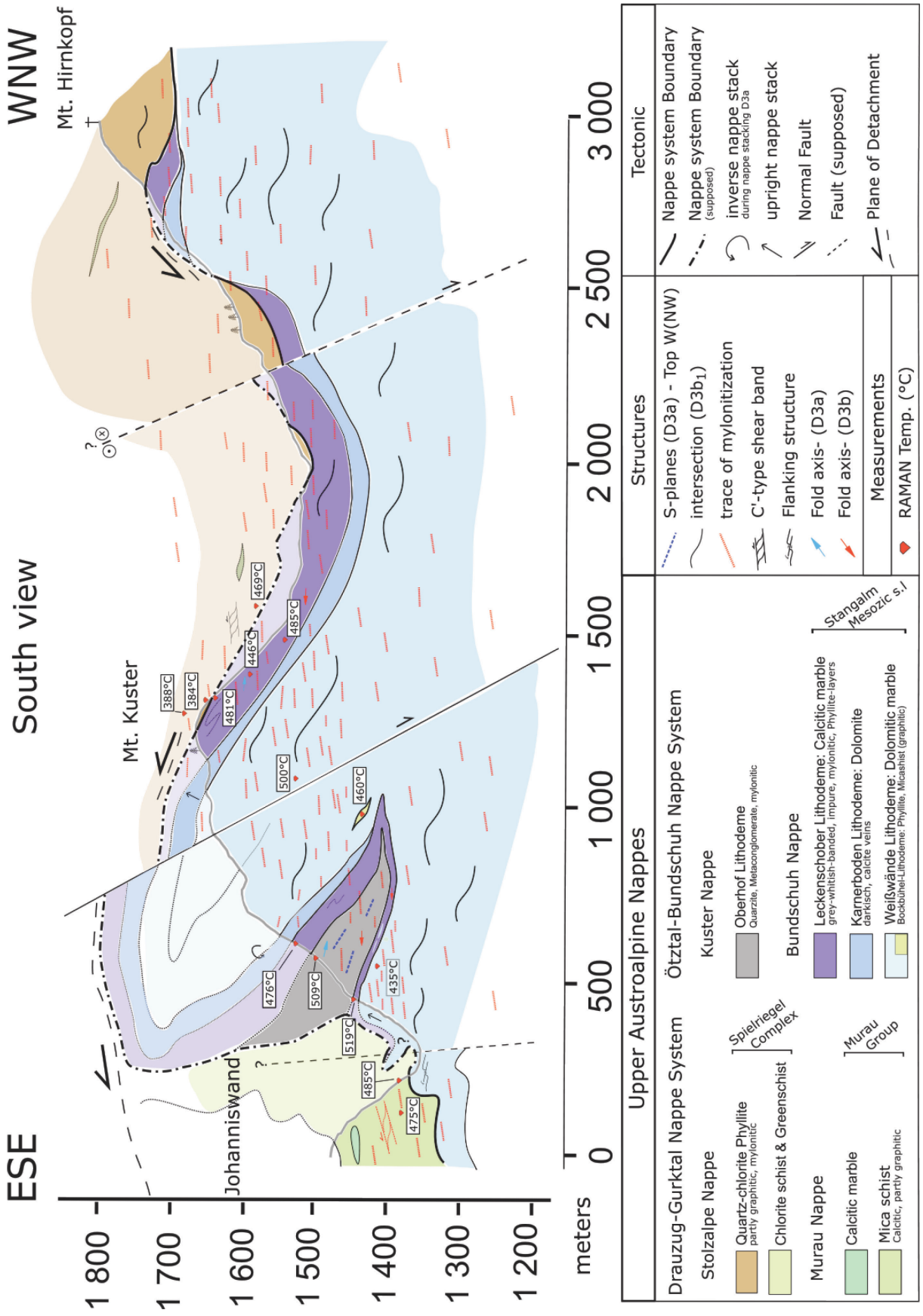

Figure 5: Interpreted profile of Eo-Alpine nappe stacking structure with incorporated Oberhof Lithodeme, overprinted by the D3b phase.

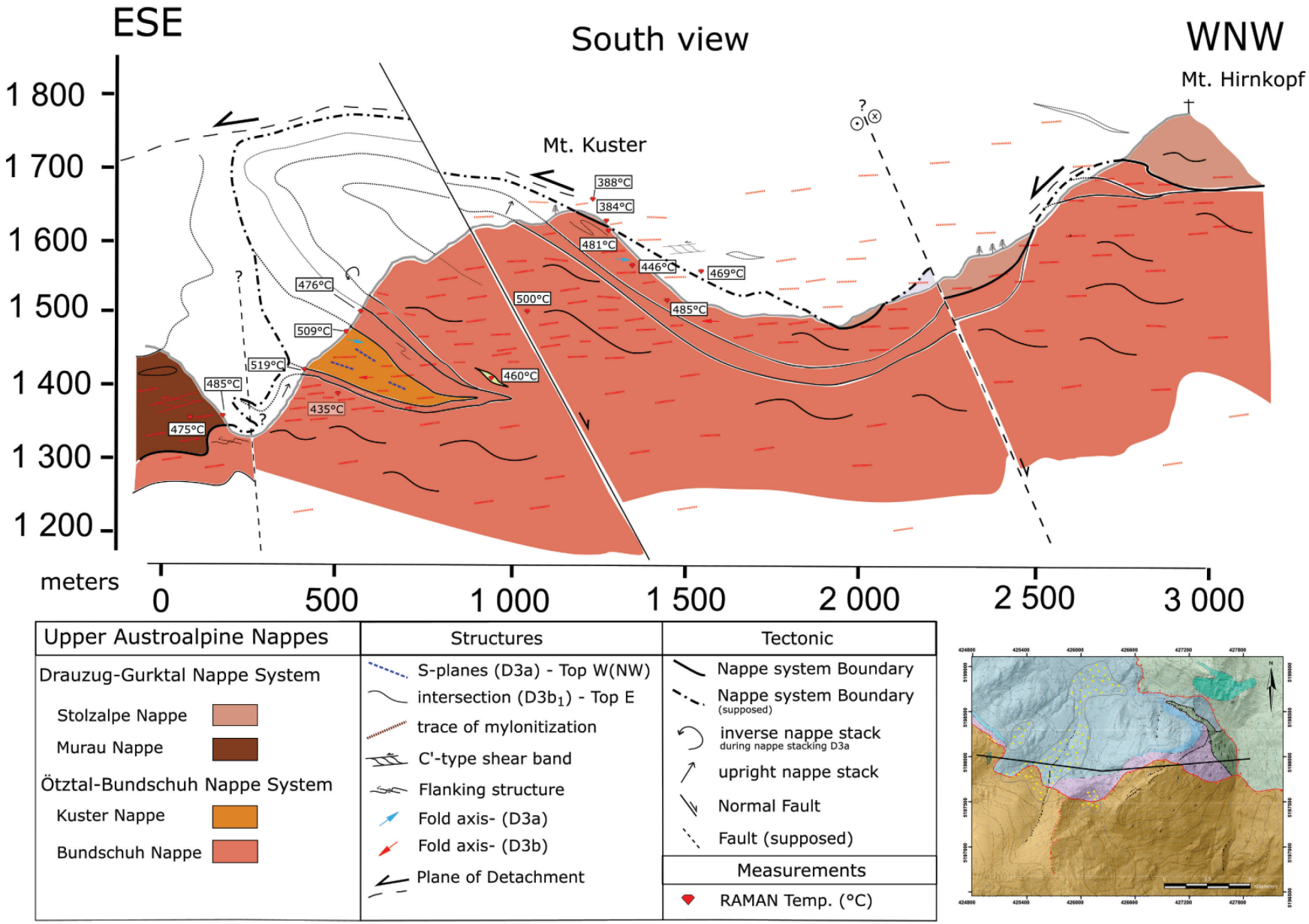

Figure 6: Interpreted tectonic profile, Ötztal-Bundschuh Nappe System in footwall position (Kuster Nappe & Bundschuh Nappe), Drauzug-Gurktal Nappe System in hanging wall position.

4.2 Description of Lithologies of the lithostratigraphic units / Lithodemes

In this part, a description of the lithodemic units and their corresponding lithologies using the nomenclature of Iglseder et al., (2019) and Iglseder (2019) (Fig. 7) based on macroscopically observations in the field as well as microscopic investigations of the samples is provided. The description follows from structurally lower to structurally higher units.

4.2.1 Stangalm Mesozoic s.l.

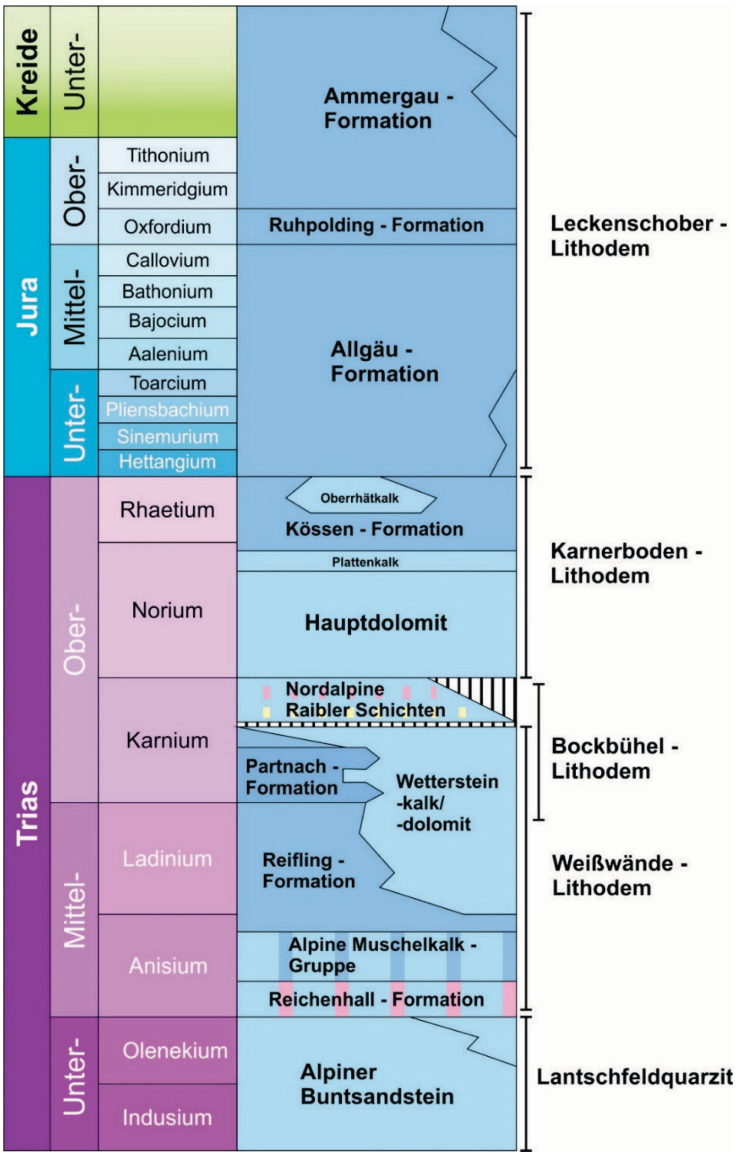

Figure 7: Ideal profile of the Stangalm Mesozoic s.l. & comparison with units of the Northern Calcareous Alps from Iglseder et al., (2019).

4.2.1.1 Weißwände Lithodeme

The Weißwände Lithodeme comprises the lowermost structural and lithological unit in the study area and covers around 4km² S and W of the village Flattnitz. It is exposed at the waterfall 300 meters E from Lake Flattnitz and in the orographic western side of the corresponding valley as well as on the northern flank of Mount Kuster. It shows in the investigated area a thickness of approximately 800 meters increasing towards NW.

The Weißwände Lithodeme is characterised by a whitish and greyish banded ultra-fine-grained dolomite marble (Fig. 8 A & B). In the field, these dolomite marbles have a massive and dense/consolidated appearance. The outcrops are mostly strong fractured by mainly two joint sets (Fig. 8 D), whereby the fracture density is increasing towards hanging wall direction. The surface of these rocks is mostly covered with whitish weathering products.

Macroscopic observations show a very fine-grained fabric. Tests with hydrochloric acid (3%) indicates that these rocks are mainly build up from dolomite grains. Furthermore, newly formed white mica in submillimetre scale on the schistosity planes can be observed. In ruptures perpendicular to the schistosity planes whitish and greyish layers at millimetre scale can be seen. In hanging wall direction, the fine-grained occurrence of these rocks is decreasing. This means a change in colour towards a darker greyish appearance, which is cut by a branched network of calcite veins. In some fractures whitish radially grown amphibole identified as tremolite (Fig. 8 C) can be detected as well as yellowish to brownish iron precipitations.

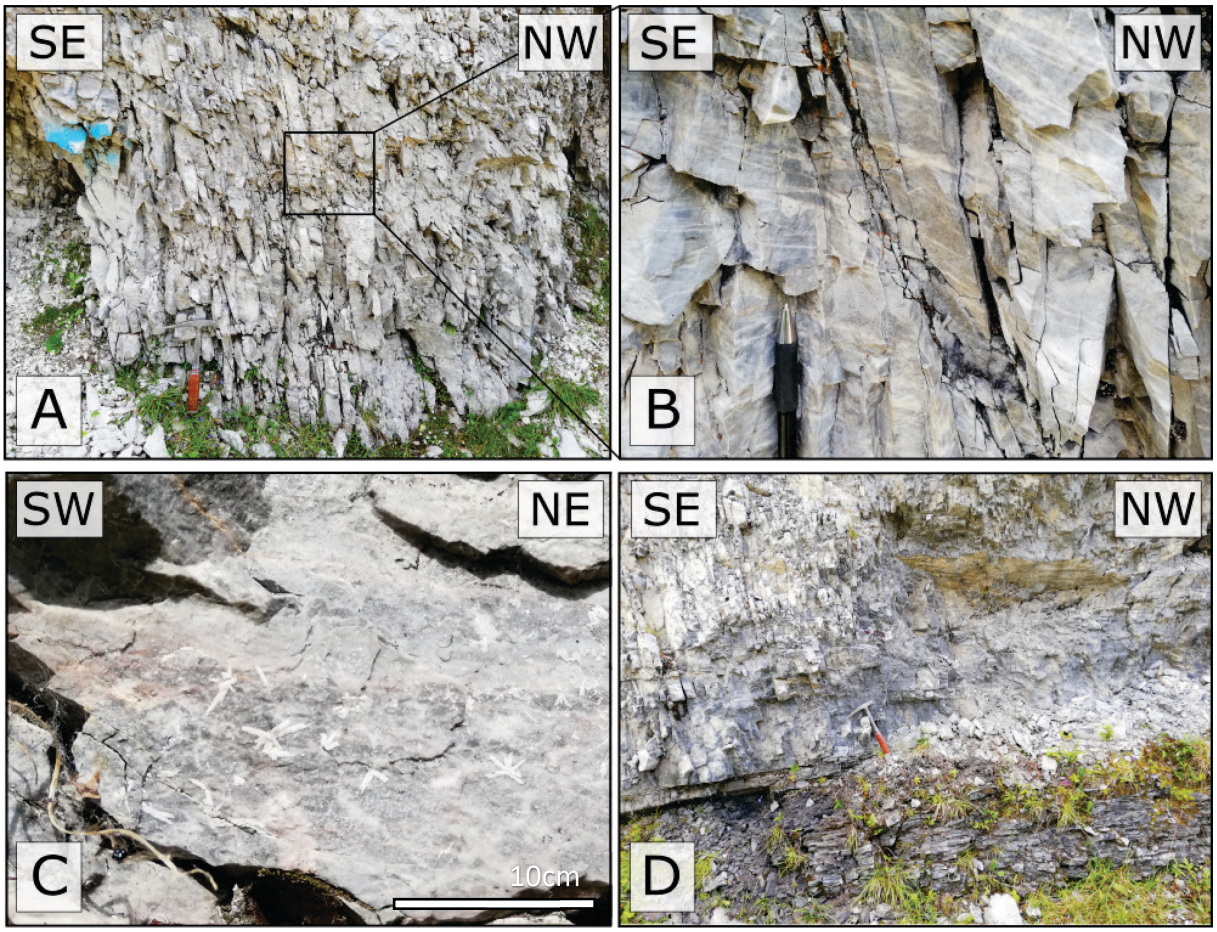

Figure 8: Outcrop of fractured dolomite mylonite; B: Detail photo of calcitic veins in dolomite marble (A & B UTM 33N: 0426970/5198332 – sample MW 1906); C: Joint in dolomite with Tremolite (UTM 33N: 0426991/5198299); D: Contact of dolomite of the Weißwände Lithodeme and the Karnerboden Lithodeme (UTM 33N: 0426893/5198525).

4.2.1.2 Bockbühel Lithodeme

Graphite and mica schist corresponding to the Bockbühel Lithodeme occur in only two small outcrops in the research area (indicated as greenish squares in Fig. 4). One spot is at the SE end of lake Flattnitz. The other location is approximately 100 m in the S of the lake. These rocks have a macroscopically different appearance compared to mica schist in other lithodemic units. On the side at the end of the lake a graphite schist is cropping out, it has a pronounced layering and lacks detrital white mica. On the elevated side the outcrop has a dimension of one cubic meter; the rocks are distinguished as mica schist corresponding to the mica schist type (intermediate type) as Weissenbacher (2015) described in his thesis. These rocks made of quartz, feldspar, and millimetre sized white mica. A detailed description of the Bockbühel-Lithodeme is given by Weissenbacher (2015) and Iglseder (2019).

4.2.1.3 Karnerboden Lithodeme

The dolomite of the Karnerboden Lithodeme can be found at the summit and on the northern flank of mount Kuster as well as at the NE flank of mount Hirnkopf. This unit reaches a maximum thickness of 50 metres at mount Kuster and approximately 100 metres at mount Hirnkopf.

Macroscopically, this lithology is characterised by a dark-greyish medium to fine grained, partly mylonitic, massive dolomite-marble. Often these rocks are permeated by a branched network of calcite (Fig. 9 A) and subordinate quartz veins (Fig. 9 B) that are deformed. Close to the contact zones to the Leckenschober Lithodeme these dolomites are cataclastically overprinted. Mylonitisation of this unit can be observed in a few outcrops in the northern part of the summit of mount Kuster. In contrast to the Weißwände Lithodeme, the grain size is generally larger. Stowasser (1956) reported the occurrence of fossil, however no evidence for such fossils was found during fieldwork.

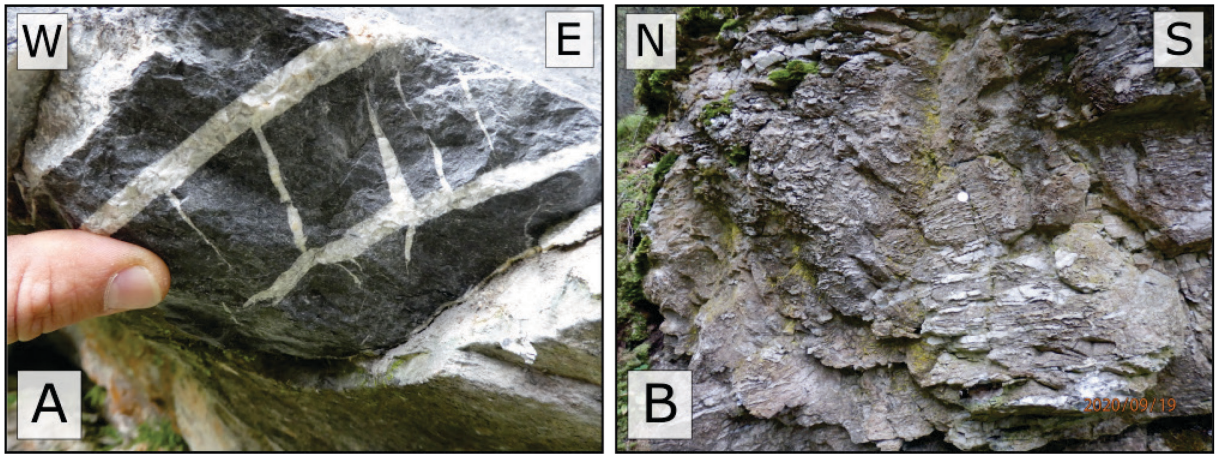

Figure 9 A: En-echelon veins with an orientation of 45 degree to the extension in the Karnerboden Lithodeme, view to N (UTM 33N: 0426229/5197682); B: Dolomite with isoclinal and open folded quartz mobilisates, view to E (UTM 33N: 0426413/5197747).

4.2.1.4 Leckenschober Lithodeme

The Leckenschober Lithodeme is the uppermost unit of the Stangalm Mesozoic s. l. In the research area, it mainly consists of fine to medium-grained dark greyish impure calcite-marble, which show brownish crusts on the weathered surface (Fig. 10 A). Greyish-whitish-blueish banded calcite-marble-mylonite with S-parallel phyllitic intercalations is typical for this lithodemic unit as well (Fig. 10 B). Strongly sheared graphite-, chlorite- and clay-schists occur rarely with a maximum thickness of 0.5 meters (Fig. 10 B). Sometimes meter scaled boudins of dolomite are observed (Fig. 10 C).

Macroscopically, this lithology shows strongly elongated phyllite lenses and a well pronounced lineation on the schistosity planes. Throughout the entire Leckenschober Lithodeme isoclinal folds are prominent. Cubic mostly strongly weathered pyrite are regularly distributed in the coarse-grained layers of this unit (Fig. 10 D).

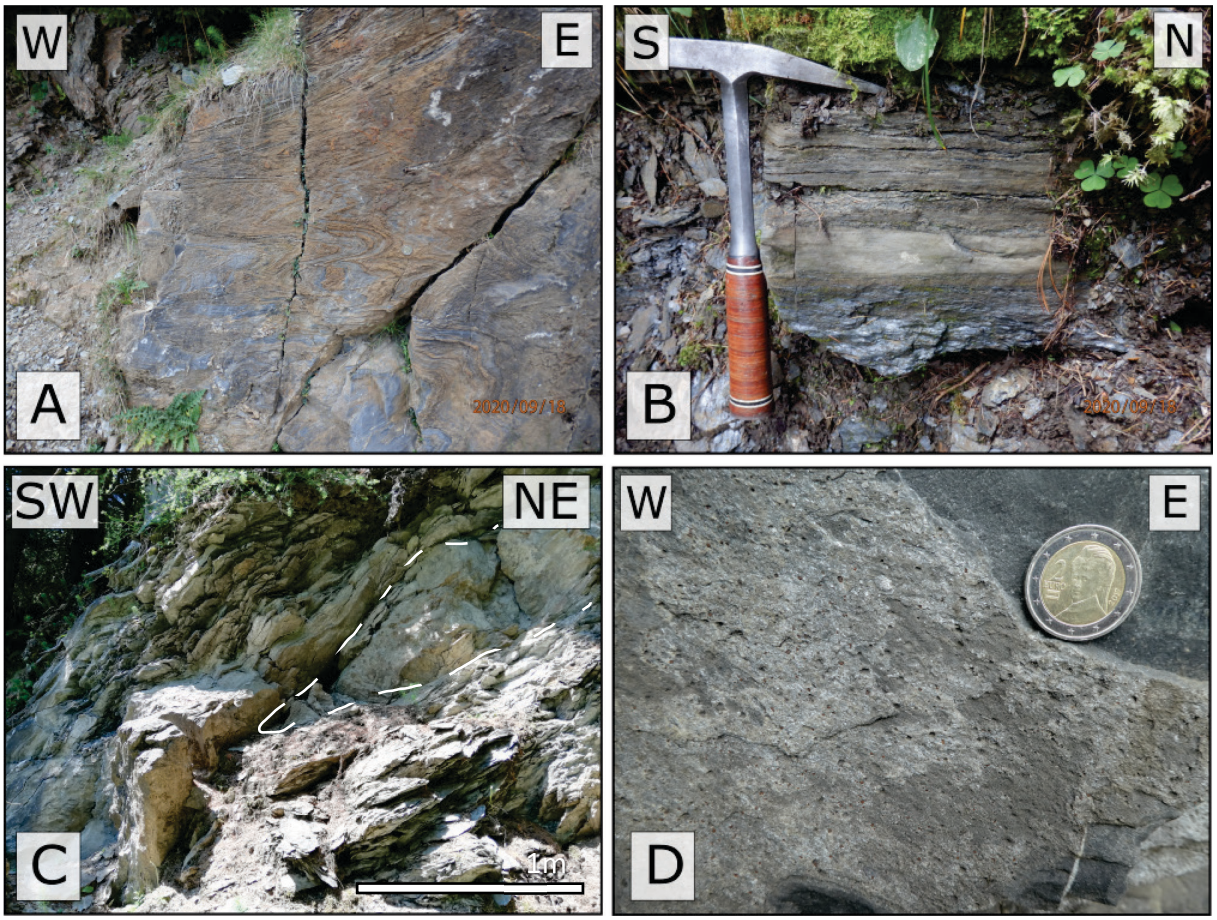

Figure 10 A: Isoclinal folded calcite-marble with brownish weathering layers (UTM 33N: 0427115/5197866); B: Banded calcite-marble; C: Calcite-marble with graphite schist layer & dolomite boudin in Leckenschober Lithodeme (UTM 33N: 0427531/5197799); D: Pyrite inclusion in impure calcite-marble (UTM 33N: 0426021/5197596).

4.2.2 Oberhof Lithodeme

A heterogeneous association of meta-conglomerate and graphitic mica schist forms an elongate, NW to SE striking body on the NE flank of Mount Kuster. Its extent corresponds to the description of Beck-Mannagetta (1959). Following Hollinetz (2018), these lithologies are assigned to the Oberhof Lithodeme. South of lake Flattnitz, this unit shows an apparent thickness of approximately 50 m, increasing towards SE. Boulders of several cubic meters of carbonaceous schists with a large amount of irregular white mica grains reaching up to one millimetre in size are observed. Further to the SE, the lithology gradually changes to massive and dense meta-conglomerate and quartzite with increasing thickness. This lithology dominates in this occurrence of the Oberhof Lithodeme and shows characteristic quartz components (Fig. 11 A; B; C). The deformed pebbles have a size of several centimetres to decimetres and are embedded in a dark greyish quartz rich and white mica poor matrix. The long axis of the elongated clasts is E-W oriented, and they occasionally show isoclinal and open folding (Fig 11 A). Further towards the SW a strongly foliated mica schist is cropping out. In the contact zone to the Leckenschober Lithodem in upper structural levels, strongly foliated very fine-grained mylonitic quartzite boulders occure.

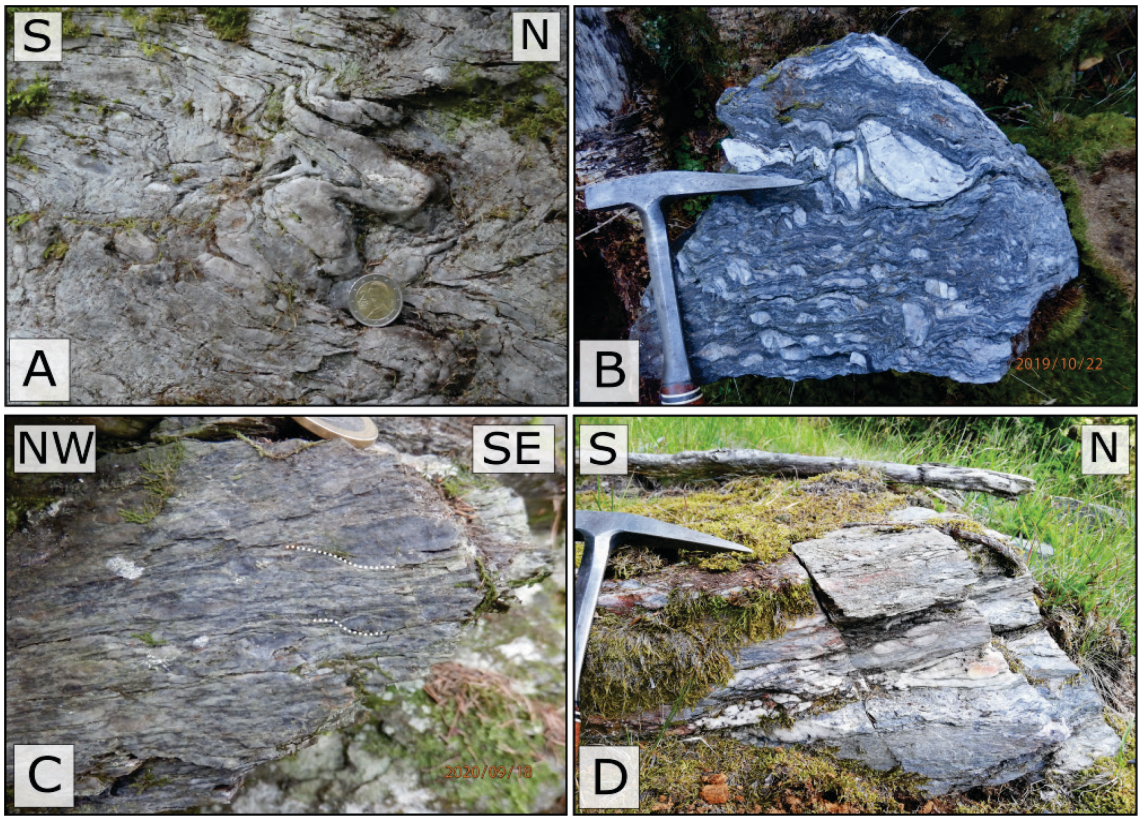

Figure 11 A: Folded quartz clast of meta-conglomerate in outcrop, view parallel to fold axis (UTM 33N: 0427008/5198587); B: Boulder of meta-conglomerate (UTM 33N:0427453/5198180); C: Quartzite with shear band geometries (UTM 33N: 0427267/5198410); D: Outcrop of meta-conglomerate & sample location MW 1918 (UTM 33N: 0427453/5198194).

4.2.3 Murau Group

Lithologies corresponding to the Murau Group are present in the NE of the mapping area and mainly build up parts of the Johanniswand. Outcrops can be found along the Flattnitztal Landstrasse (L63), as well as in the N and W region of lake Flattnitz.

Typical lithologies are quartzite, quartz-phyllite (Fig. 12 B & C), mica schist with coarse grained white mica and subordinate graphite schist (Fig. 12 B) and calcite-mica schist (Fig. 12 D).

Macroscopically and structurally these lithologies are very similar to lithologies of the Spielriegel Complex. The main difference is the lower chlorite content in the Murau Group which, results in a brighter appearance of the rocks. Moreover, a higher white mica content consisting of larger grains can be observed.

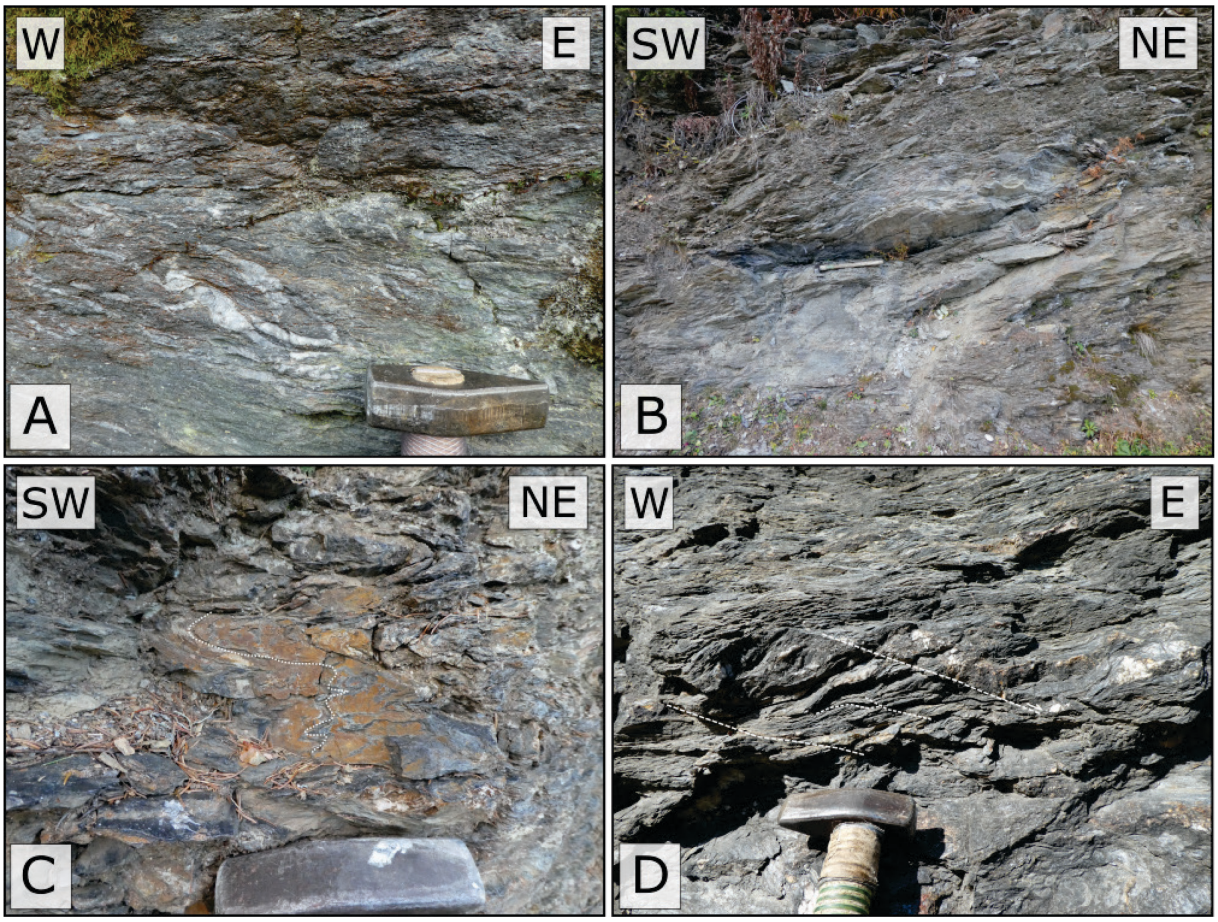

Figure 12 A: Quartz rich lithology with deformed quartz veins of the Murau Group (UTM 33N: 0427774/5198134); B: Graphite schist layer; C: isoclinal folds B & C (UTM 33N: 0426711/5198738); D: Calcitic mica shist with C'type shear bands record top E shear sense (UTM33N: 0427589/5198622).

4.2.4 Spielriegel Complex

In the study area, the Stolzalpe Nappe represents the uppermost tectonic unit. The occurring lithologies are assigned to the Spielriegel Complex. These lithologies crop out on the southern shares of the summit, the southern flank of Mount Kuster and in the southwestern area of Mount Hirnkopf.

In the Spielriegel Complex quartzite, chlorite- & quartz-rich phyllites with changing amounts of fine-grained white mica and chlorite is distinguished as the main lithologies. A continuous transition between chlorite-rich packages and quartz-rich bodies is observed (Fig. 13 B). The rocks are completely dissected by quartz mobilisates up to centimetres thick in the form of isoclinal and openly folded veins (Fig. 13 C), which occur parallel to the foliation. Mostly brownish and reddish iron oxides are found in these veins (Fig. 13 C). Macroscopically the phyllites show well pronounced schistosity planes with a lepidoblastic fabric and crenulation lineation, therefore a platy appearance with dark greenish to blackish surfaces, depending on the amount of chlorite in the samples (Fig. 13 A). The quartz-rich lithologies, on the other hand, have silvery shiny surfaces with a much lower chlorite content.

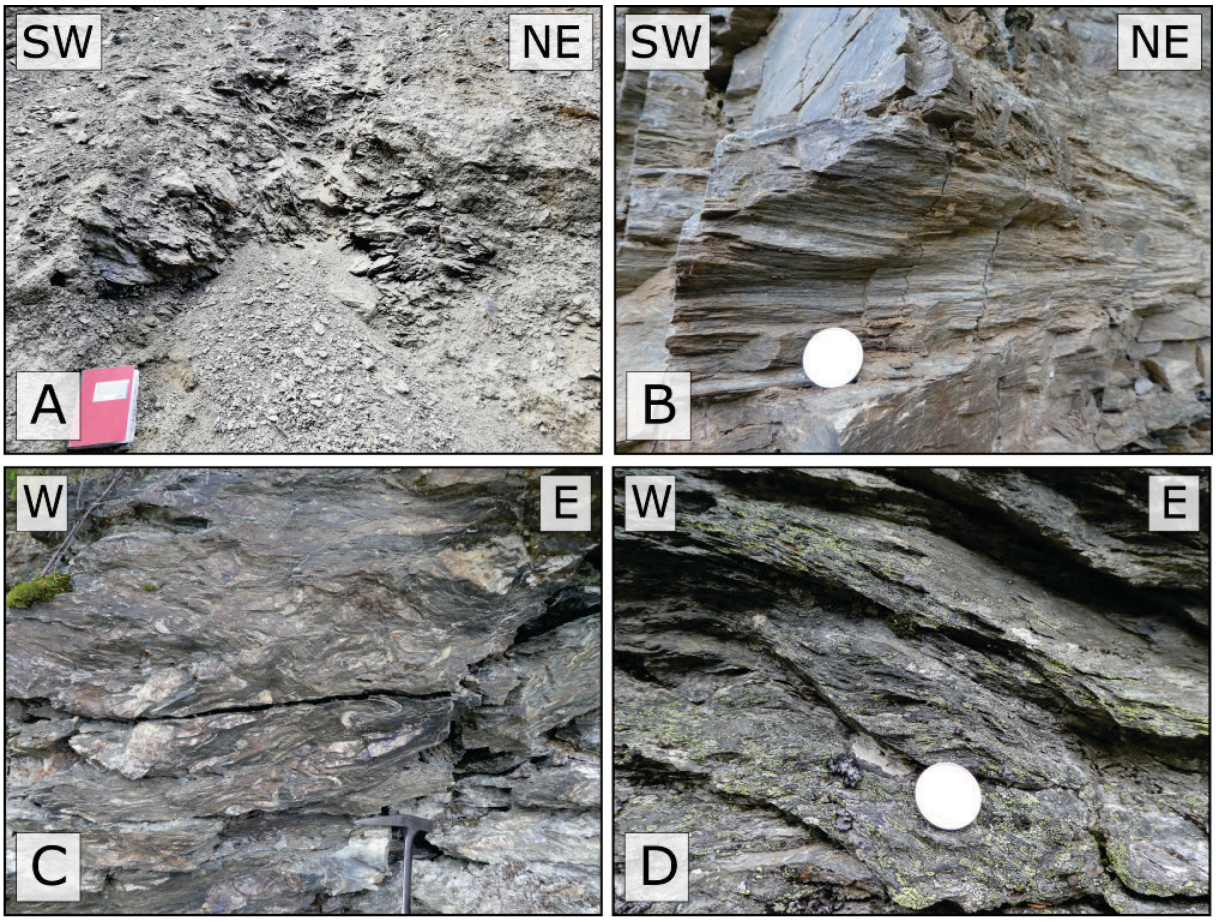

Figure 13 A: Excavation of Quartz-chlorite-Phyllite (UTM 33N: 0427580/5197373); B: Deformed quartzite next to nappe boundary & sample location MW 1910 (UTM 33N: 0427115/5197866); C: Quartzite with deformed quartz veins (UTM 33N: 0426609/5197420); D: C'-Type shear bands give top-to-the E shear sense (UTM 33N: 0426410/5197375).

4.3 Structural observations & measurements

Based on field observations and measurements of planar and linear features, different deformation phases can be distinguished in the area around mount Kuster. These phases are named according to their temporal occurrence, starting with the oldest-"event" D_0 to the youngest structural overprint D_4. Essentially, pre-Alpidic and alpidic phases can be distinguished by superposition of the different fold structures, the different orientation of the axial plane surfaces of the folds and crosscutting relationships of the structures. In the following plots the coloured great cycle shows the best fit great cycle of the fold axial plane poles to plot a π-diagram. The different deformation phases have been outlined before in chapter 2.4.

In the research area, no evidence for structures related to the sedimentary and volcano-sedimentary deposition of lithologies in the Murau and Stolzalpe nappes (D_0, Iglseder, 2019; Huet, 2015) is observed.

D_1 corresponds to the first observable folding event. Pre-existing centimetre thick quartz mobilisate layers are observed which show relicts of isoclinal folds with shallow dipping fold axis towards W-NW (Fig. 14 D1-isoclinal folds & Fig. 19 A). Theses folds commonly are refolded by a later event. The D_1 event is only present in the lithologies of the Spielriegel Complex (i.e., Stolzalpe Nappe).

D_2 is mostly recognised in the Spielriegel Complex. This event is shown in open, asymmetric folds with slightly steeper fold axis as in the D_1 event recorded (Fig. 14 D2-open asymmetric folds & Fig. 19 A). The orientation of these fold axes varies from NW to SW. D_1 and D_2 structures are related to the Variscan event (*Huet, 2015*).

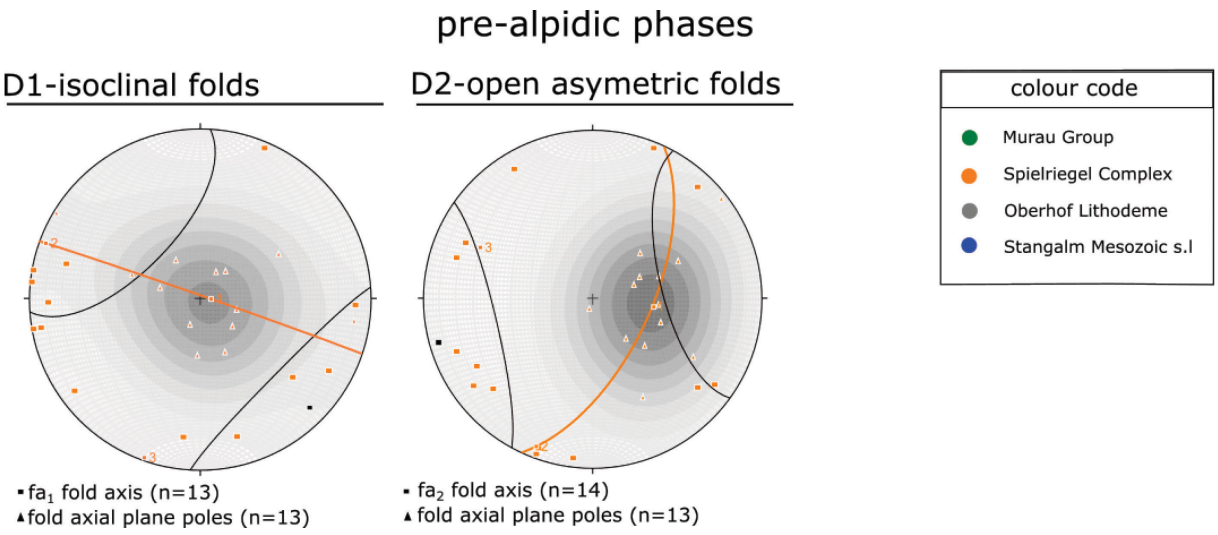

Figure 14: lower hemisphere stereoplots of pre-Alpidic deformation phases D1 & D2. Plotted with Stereonet v.11.

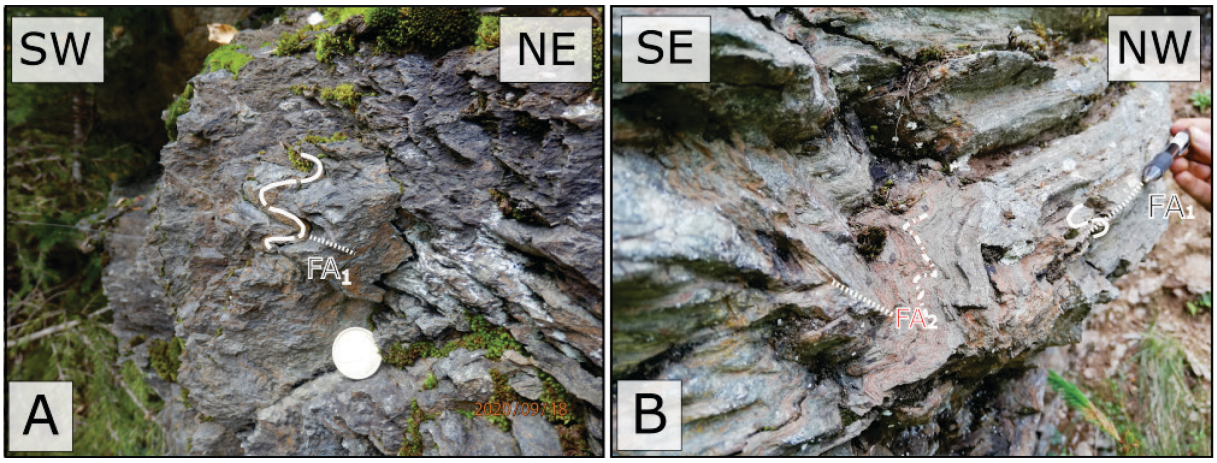

Figure 15: Lithologies of the Spielriegel Complex A: Quartz-chlorite phyllite with isoclinal folded quartz vein FA1 dipping shallowly towards W (UTM 33N: 0426930/5197444); B: Chlorite-schist/greenschist isoclinal fold FA1 dipping towards W, open asymmetric folds with FA2 dipping WSW (UTM 33N: 0427008/5197884).

D_3 represents structures related to the Eo-Alpidic event, which can be observed in the research area. Since the D_{3b} phase shows the most dominant structural imprint of the research area, no evidence for D_{3a} structures was found. Structural elements related to the D_{3b} phase are observed in all units. This deformation pattern can be subdivided into three major phases, which can further get subdivided into high temperature structures and low temperature structures, discussed in chapter 5.2.1

1) Formation of isoclinal folds: These folds can be distinguished from meter to centimetre scale. Mostly the folds show shallow dipping E-W oriented fold axis and sub-horizontally orientated axial planes to the main schistosity (Fig. 17 D_{3b}-isoclinal folds & Fig. 19 B). The measured schistosity planes follow the same systematic as the axial planes and are commonly sub-horizontally orientated and dipping in nearly all directions with an angle of approximately 10-20 degrees. These folds are best seen in the lithologies and quartz clasts of the Oberhof Lithodeme (Fig 11 A), units of the Spielriegel Complex near the nappe system boundary (Fig. 18 C), and in the calcite-marble of the Leckenschober Lithodeme (Fig. 18 A).

   Further structures correlated with this phase (ductile top to the E shearing) are expressed by the mylonitisation of the previously mentioned units and the formation of a pervasive stretching lineation and mineral lineation with an ESE-WNW directed alignment and shallow dipping orientation towards SE and NW which is best seen in the carbonatic and dolomitic marbles of the Stangalm Mesozoic s.l. (Bundschuh Nappe) and units of the Stolzalpe Nappe next to the nappe boundary. The dolomitic marble rarely shows flanking structures with a top to the E kinematic (Fig. 18 B). Boudins of dolomitic rocks can be spotted in the calcite-marble of the Leckenschober Lithodem (Fig 10 C).

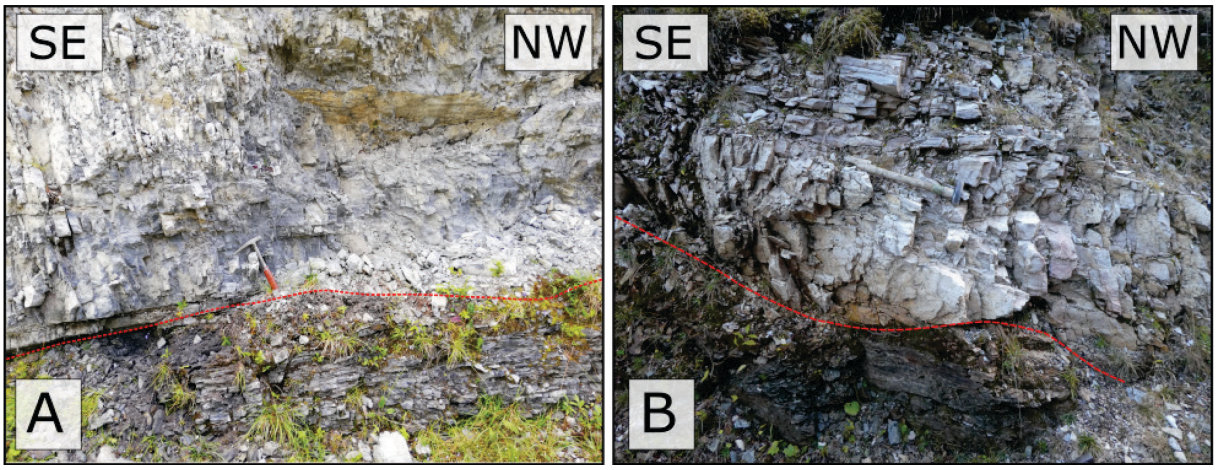

Figure 16 inverse nappe stack evidence for km scaled isoclinal folds A: Weißwände Lithodeme in hanging wall position of Karnerboden Lithodeme (UTM 33N: 0426893/5198525); B: Weißwände Lithodeme on top of the Murau Group (UTM 33N: 0426656/5198730).

2) D_{3b} related ductile to brittle-ductile transition is recorded in C'-type shear bands. These are a very common feature in the area. They are overprinting the whole fabric of schistosity planes, folds, and axial planes of the older fabric. These have a normal fault character dipping towards E. The fault planes show quartz fibres and striations with a top to the (E)SE kinematic (Fig 17 D_{3b}-shearbands & Fig. 18 E). Commonly seen in lithologies of the Murau and Stolzalpe Nappe, less common in the calcite-marble of the Leckenschober Lithodeme and not present in the dolomite marble of the Weißwände Lithodeme and the Karnerboden Lithodeme.
3) The last phase of folding in this area can be distinguished by the superposition of isoclinal folds of the D_{3b} event in outcrop and thin section scale. These folds have steep to moderate steep axial planes and shallow dipping EW oriented fold axis (*Decker, 1998*). The crenulation lineation follows the same trend as the fold axes of open folding (Fig. 17 D_{3b}-open folds, Fig. 18 D & Fig. 19 B).

D_4 brittle deformation is recorded in steep mostly conjugated and sometimes orthogonal joints occurring in mainly two sets (Fig. 17 D4, Fig. 8 A & Fig. 18 F). The first joint set is orientated NE-SW with steeply dipping fault planes towards SE. The second one is oriented NE-SW with steeply dipping fault planes towards NW. The sets show an angle between of approximately 10-20 degrees. The joints cut all pre-existing structures and are observed predominantly in the dolomite marble of the Weißwände Lithodeme.

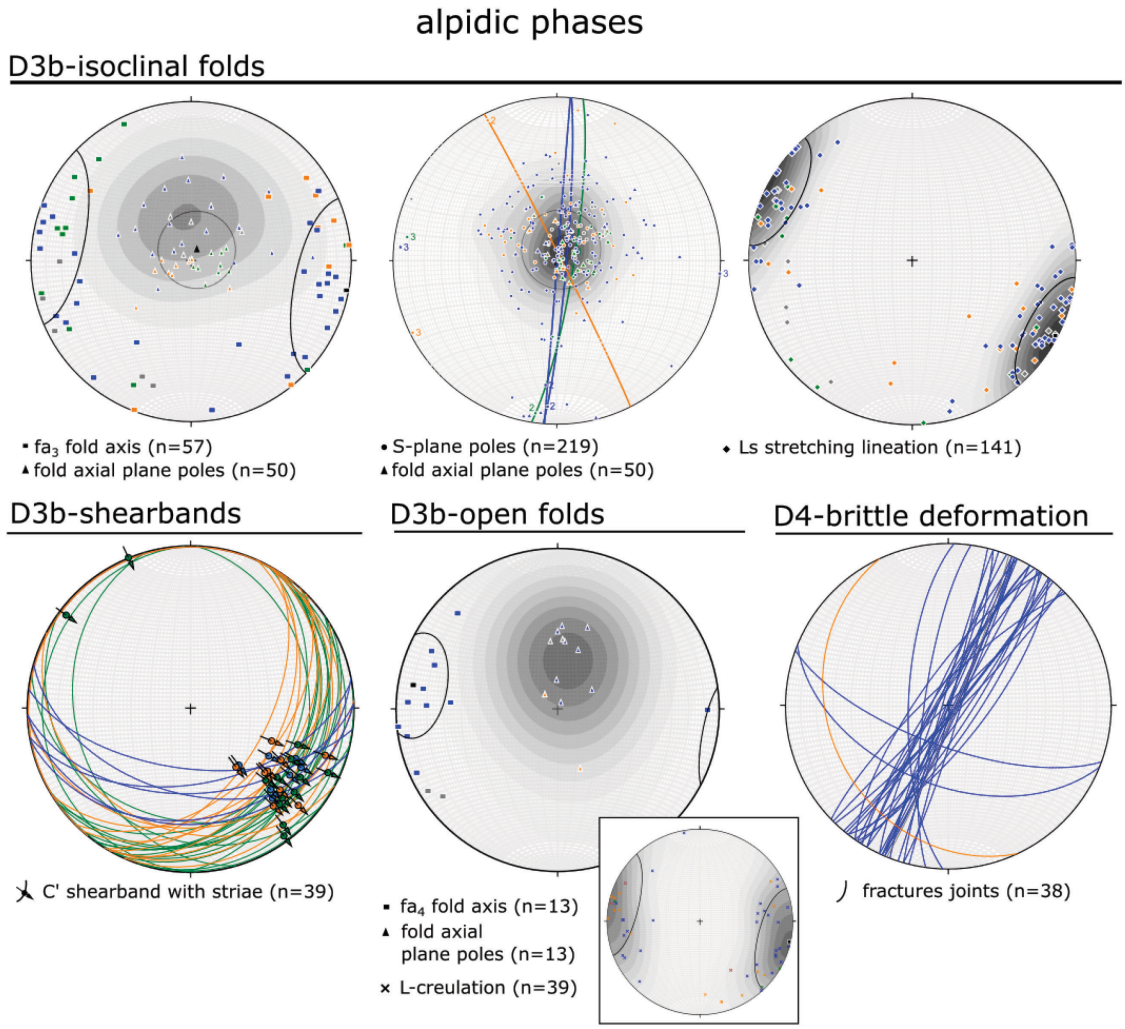

Figure 17: Lower hemisphere stereoplots of alpidic phases of deformation D3b & D4. The same colour code as in figure 14 is used.

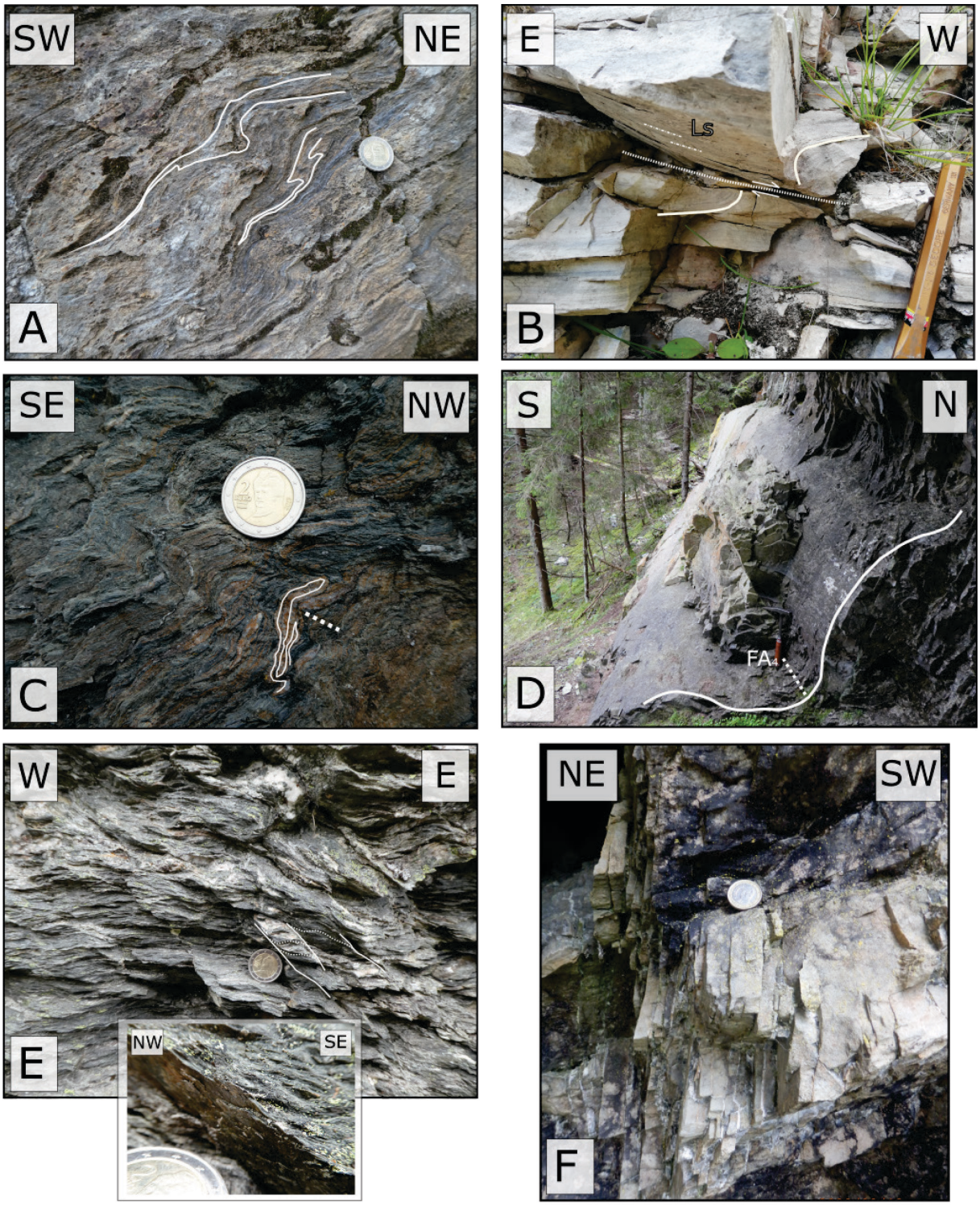

Figure 18 A: Isoclinal folds in calcitic-marble (Leckenschober Lithodeme) refold structure type 3, refolded by later open folding event (FIP - D_{3b}) (UTM 33N: 0427115/5197866); B: Top to the E flanking structure, stretching lineation (Ls) in dolomite marble ultra-mylonite & sample location MW 1911 (Weißwände Lithodeme) (UTM 33N: 0426656/5198730); C: Refolded isoclinal folds of quartz veins D^{3b} related (Spielriegel Complex) with FIP (UTM 33N: 0425887/5197547); D: Open folds of the Weißwände Lithodeme bounden to D_{3b} (UTM 33N: 0427303/5198372); E: C'-type shear bands with quartz fibres with top to the SE shear sense (Spielriegel Complex) (UTM 33N: 0426741/5197439); F: Steep NW-oriented fractures in Dolomitic marble (Weißwände Lithodeme) (UTM 33N: 0427292/5198387).

In the following maps the structures related to the different deformation events are plotted.

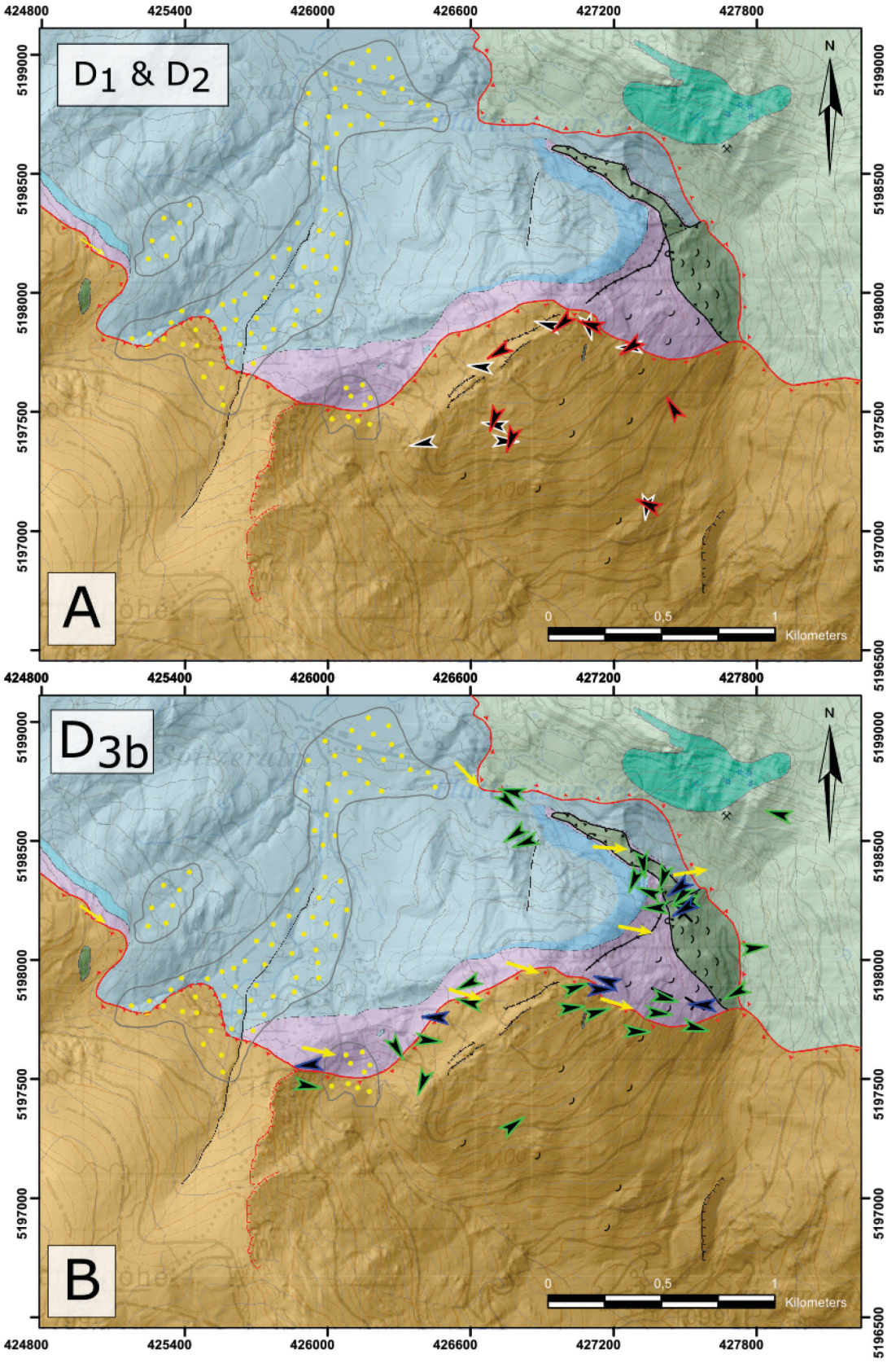

Figure 19 A: Isoclinal folds of D1 (white arrows) & open asymmetric folds of D2 (red arrows); B: Isoclinal folds (green arrows) & open folds of D3b phase (blue arrows). Legend as in Figure 4.

4.4 Microstructural observations

4.4.1 Weißwände Lithodeme & Karnerboden Lithodeme

In the microscope the footwall shares of the dolomites of the Weißwände Lithodeme consists mainly of ultra-fine-grained dolomite. These grains reach a minimum size from 12.5 µm to maximum 25 microns (Fig. 20 A). Along cracks bigger aggregates of dolomite, rarely feldspar, subordinate quartz, and calcite grains can be detected. The calcite grains often show twinning lamella. The silicate minerals feldspar and quartz furthermore occur in the dolomitic matrix. Quartz and feldspar have a larger grain size than dolomite and often show a xenomorphic, elongated shape. Along the long axis the grains have a size from 125 µm up to 750 µm in cracks. White mica occurs frequently in the thin sections especially on the schistosity planes (Fig. 20 A). They show a well pronounced E-W regulation and sizes up to 100 µm, with crossed nicols they show undulose extinction. Minor amounts of a cubic opaque phase can be seen, which is arranged in S-parallel planes with sizes up to 125 µm.

Towards the hanging wall, the appearing dolomite of the Weißwände Lithodeme show microscopically similar properties. Differences are shown in grainsize and their distribution. Therefore, in comparison, a bimodal grain size distribution can be recognised in these samples. The bigger grain fraction reach dimensions of 500 µm the smaller grain size fraction have an extent up to 20 µm. The grains show hypidiomorphic grain shapes. Subordinate they show twinning lamellae. The grains arranged in an E-W regulation. The coarse-grained layers often display boudins between the fine-grained layers (Fig. 20 D). White mica occurs in minor amounts in the hanging wall shares than in footwall proportions. In the uppermost parts of the hanging wall the absence of these can be shown. Minor amounts of hypidiomorphic feldspar and quartz with a length of up to 200 µm can be distinguished. A reddish to nearly opaque iron phase is identified as siderite or ankerite. Along from cracks tremolite is observed which reach a size up to 200 µm (Fig. 20 B).

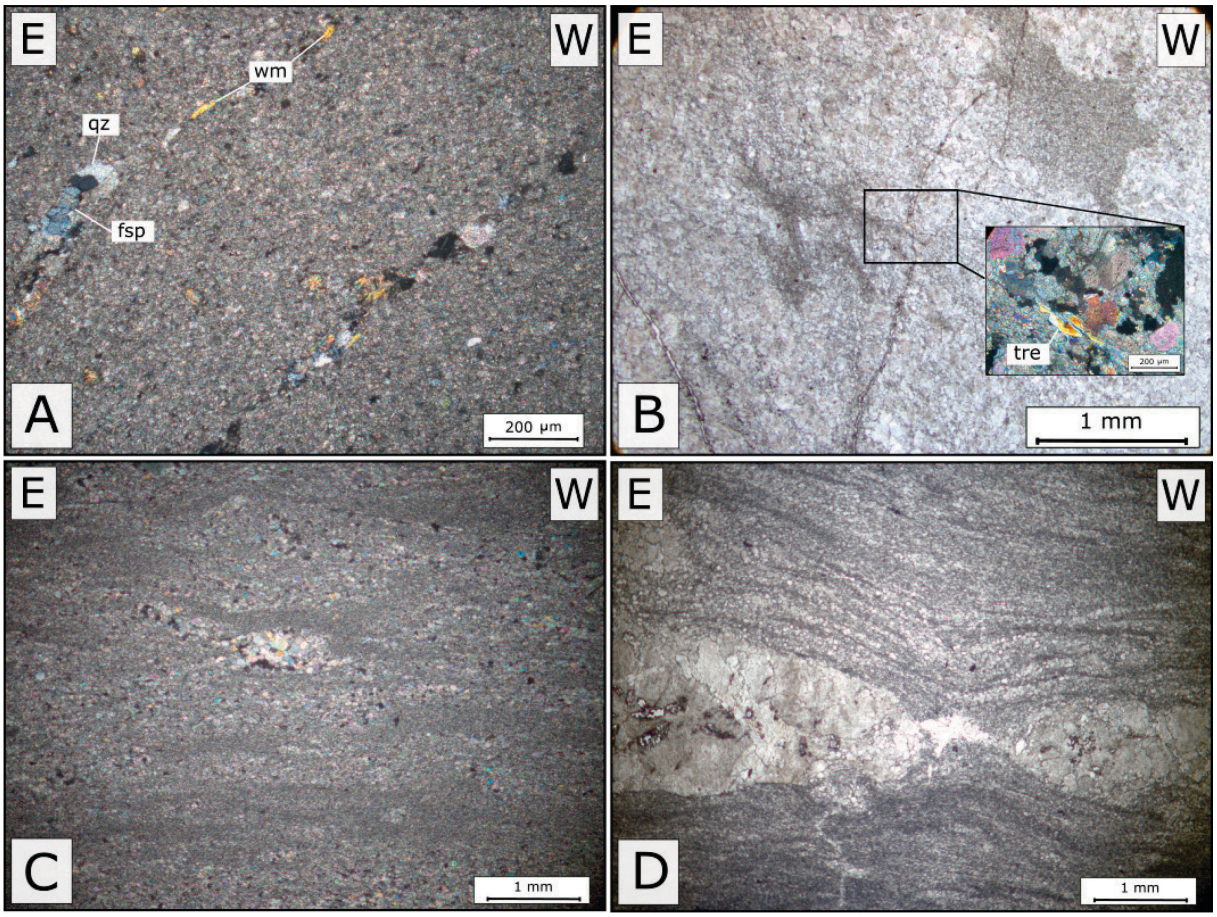

Figure 20 (Weißwände Lithodeme) A: Dolomite ultra-mylonite, white mica, quartz, and feldspar occur parallel to the S-planes Sample MW1911B (UTM33N: 0426656/ 5198730); B: fractured dolomite with tremolite in cracks sample MW1906 (UTM33N: 0426991/ 5198299) ; C: aggregate of bigger dolomite grains in fine grained matrix sample MW1904; D: Boudin in dolomite mylonite sample MW1904 (UTM33N: 0426787/ 5198431).

In contrast to the dolomite of the Weißwände Lithodeme the dolomite of the Karnerboden Lithodeme show much bigger grainsize and no banded appearance. This lithology also consists mainly of dolomite grains, which are bigger developed and show a maximum size of 150 µm. In the footwall shares and intercalated in the Leckenschober Lithodeme, this dolomite shows mylonitisation, but to a much lesser extent than in the Weißwände Lithodeme. A difference is seen in the occurrence of quartz in the samples, which are more likely and bigger in size in the Karnerboden than in the Weißwände Lithodeme (Fig. 21 C). Pyrite is also found in the samples (Fig. 21 D). Structurally the dolomite of the Karnerboden Lithodeme shows lesser ductile deformation, therefore the formation of stylolites which truncate the fabric (Fig. 21 B) and in the contact zone to the Leckenschober Lithodeme a cataclastic overprint is seen.

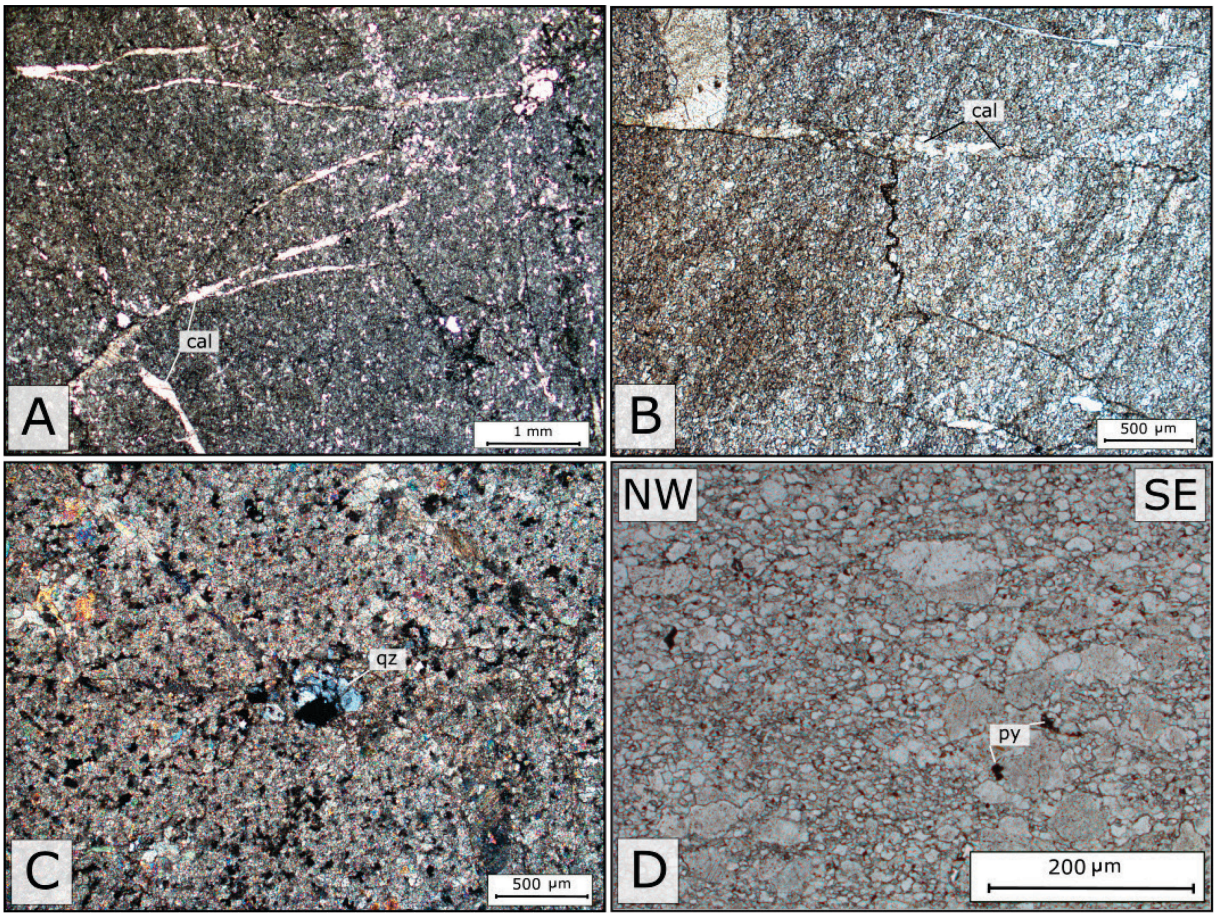

Figure 21:(Karnerboden Lithodeme) A: calcite veins in dolomite, Sample Foss1A (no orientation); B: Stylolite in Sample Foss1B; C: Intersection of quartz vein in Foss1A (UTM33N: 0426356 /5197828); D: Dolomite grains in Sample MW1905.

4.4.2 Leckenschober Lithodeme

In the microscope this calcite-marble shows a variety of minerals, listed below according to their frequency. The most frequent mineral in this lithology is calcite, it builds up 80 percent of the analysed samples. The grains show sizes from 50 µm to 750 µm with mostly slightly irregular grain boundaries and E-W regulated grains (SPO) (Fig. 22 A). The large grains show twin lamella of type 2 and type3 according to Passchier (2005) (Fig. 22 C). White mica appears abundantly, the mineral is spread homogeneously across the thin sections. It reaches sizes from 100 µm to 1 cm. The small white mica grains are associated with the smaller calcite grains. The grains bigger than 500 µm show a well pronounced E-W directed regulation and subordinated a mica fish with a top to the E sense of shear (Fig. 20 D). Subordinated kinked white mica grains occur which show undulatory extinction. The grains show sizes from maximum 500 µm to 125 µm. In the sample MW1920 white mica occur in isoclinal

folded “pellets” (Fig. 22 D). Feldspar is not abundant and mostly of irregular rounded shape, but these grains can be found in the whole section. They have a dimension of 100 µm to 500 µm and occasionally show growth twins. Quartz occurs mostly as rhombic porphyroclasts due to the rhombic habit no consistent sense of shear can be derived from these clasts. On the one side the grains have a length up to 2.5 mm and show undulose extinction, on the other side these grains look strongly elongated and have small, delimited grains with sizes to maximum 25 µm and no noticeable undulose extinction (Fig. 20 C bulging). The opaque phase is dispersed in all thin sections. Idiomorphic grains showing a cubic habit were identified as pyrite. Furthermore, in the thin sections the mineral dolomite which shows less twinning and bigger grain sizes than calcite can be seen. The dolomite grains preferably appear in layers. At the boundaries of calcite grains, feldspar and quartz grains talc occurs (Fig. 22 C).

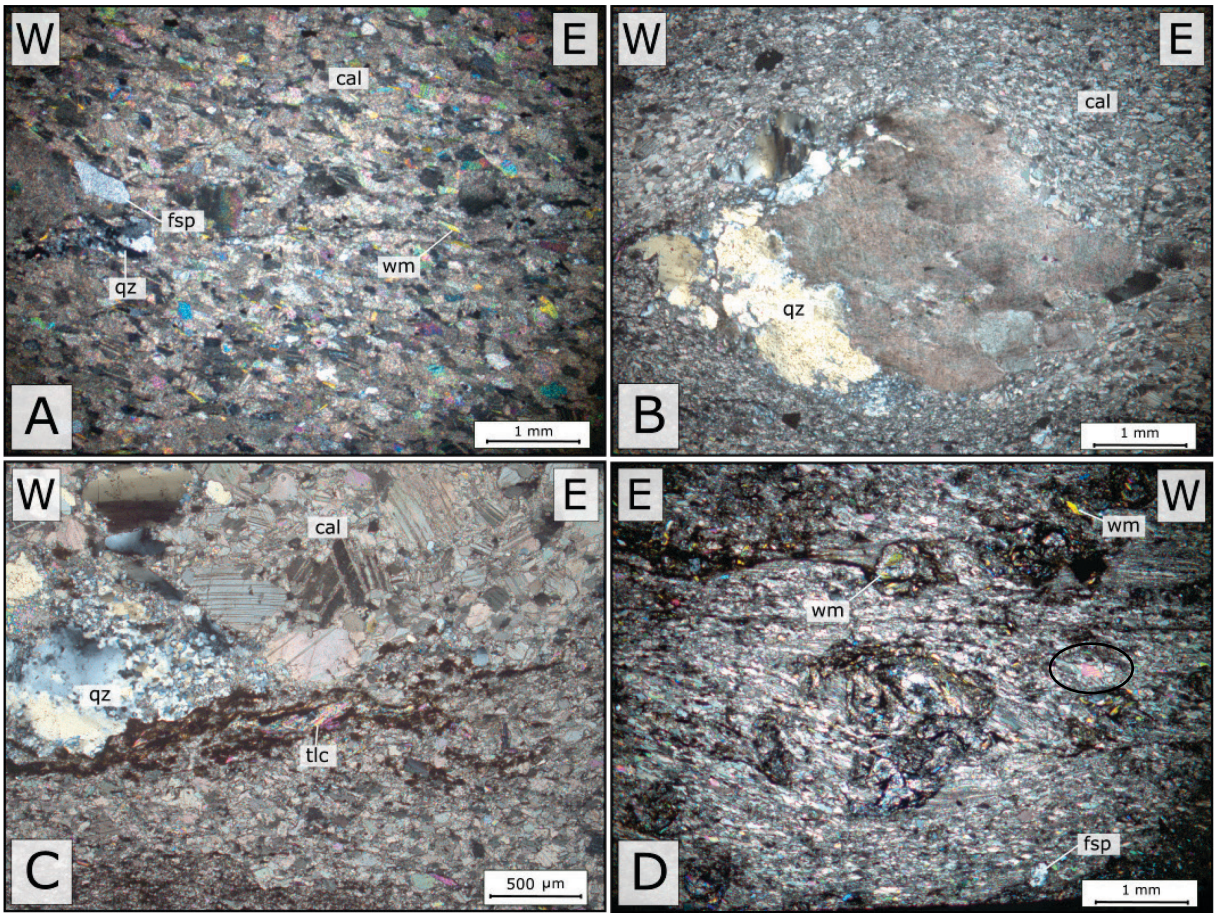

Figure 22 (Leckenschober Lithodeme) A: Impure calcite-marble Sample MW1902 (UTM33N: 0427256/ 5198578); B: Quartz porphyroclast in fine grained calcite matrix; C: Stylolite in impure calcite marble, quartz grains show bulging, calcite grains twinning of type 2 & 3, B & C sample MW1909A (UTM 33N: 0427115/5197866); D: Isoclinal folded white mica layer & mica fish texture top to the E kinematics (black circle) in calcite-marble sample MW1920 (UTM33N: 0427342/5198370).

4.4.3 Oberhof Lithodeme

Microscopic observations of the samples exhibit that the main minerals which build up the Oberhof Lithodem at Mount Kuster are quartz, white mica, chlorite, feldspar and rarely tourmaline. Accessory minerals are zircon and apatite. Opaque phases are pyrite and iron oxides which mostly occur along cracks. Quartz is the most abundant mineral and occurs with a frequency of 90 percent in the samples. The quartz grains show a bimodal grain size distribution with hypidiomorphic to xenomorphic grain shapes. The bigger quartz grains are settled in the deformed quartz clasts. These grains can reach up to one centimetre in length and show a strong E-W elongation and oscillatory extinction with crossed nicols (Fig. 23 A). In the rim area of the quartz clasts the formation of smaller grains is observed. Therefore, they reach a maximum size of approximately 200 µm, while the quartz grains, which build up the matrix have a size of 50 µm. The smaller grains are found in all layers around the clasts, they show hypidiomorphic grain shape and an E-W elongated shape partly deformed by shearbands. The appearance of the quartz grains as well as the chlorite content changes with respect to the sample position. Towards higher structural levels, the formation of subgrains is increasing and there is no evidence for sutured grain boundaries. Moreover, the overall grain size is decreasing towards the nappe boundary in hanging wall direction. Additionally, the quartz pebbles are stretched and observed shear band boudinages indicates a top to the E shear sense (Fig. 23 D). White mica occurs in the thin sections mostly in S parallel planes, in corresponding folds and arranged in shear bands (Fig. 23 C & D). Frequently single white mica grains are observed in the matrix determined as detrital white mica. These grains reach sizes up to 250 µm (Fig. 23 E). Both types show a well pronounced E-W regulation. The grains have dimensions up to 200 microns. A few grains in the matrix with a mica fish texture are observed which indicates a top to the E shearing. Chlorite is less abundant than white mica but behaves in a similar way as the arranged ones. Close to the nappe boundary, the chlorite content is increasing as the white mica content is decreasing. A few grains of feldspar can be spotted in the sections. Most of them show irregular grain boundaries and polysynthetic twinning. Greenish pleochroitic tourmaline is observed (Fig. 23 B) in the quartz rich layers with a maximum size up to 150 µm.

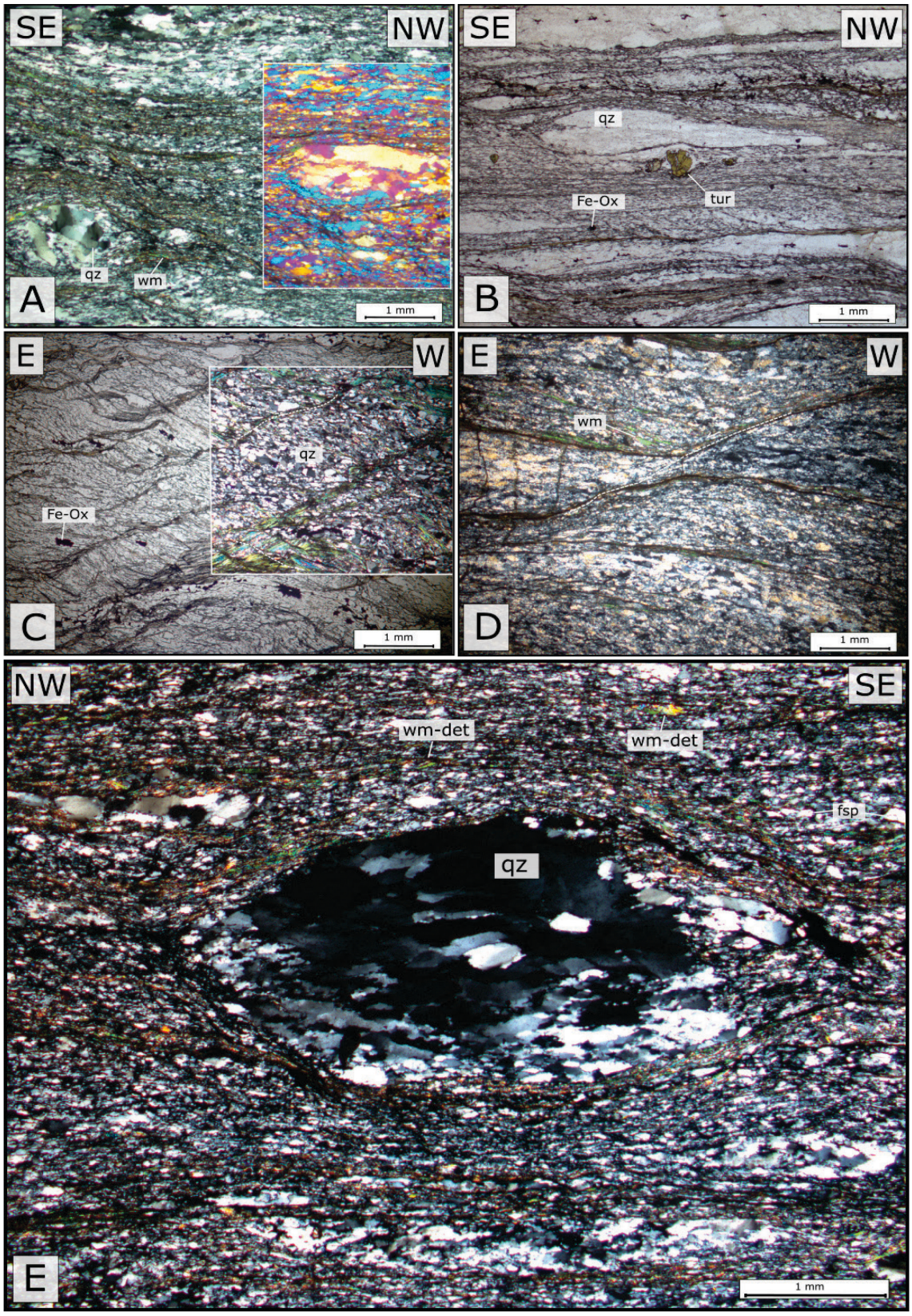

Figure 23 (Oberhof Lithodeme) A: Meta-conglomerate clast geometries; B: Meta-conglomerate with accessory tourmaline A & B sample IGL 20/52 I; C: Crenulation in mica rich layers (sample MW1918, UTM33N: 0427453/5198194); D: Shearband Boudinage (Top to E) Sample (MW1919B, UTM33N: 0427303/5198370); E: Quartz clast with rhombic geometry & detrital white mica in matrix (mica fish texture top to E) Sample IGL 20/52 II.

4.4.4 Murau Group

Microscopically the lithologies of the Murau Group mainly made of quartz (approximately 80% in modal composition). Most grains have a size of around 200 µm and are well E-W elongated. With crossed nicols less grains show undulose extinction. Another microstructural type of quartz is found in S-parallel layer distinguished as deformed veins, which have a maximum length of 750 µm. With crossed nicols the grains have a strong oscillatory extinction with an angle of 20 degrees to the main schistosity. In the rim area of those grains, the formation of the first grain type is observed. White mica occurs as aggregates in layers, as well as isolated grains between the layers and rarely between quartz grains. The single mica grains have a length of 100 µm to maximum 750 µm; most of these grains are arranged parallel to the S-planes, the bigger ones grow oblique to the S-planes. The mica layers follow the S-planes with smaller sizes and show oscillatory extinction. The white mica grains, which are oblique to the S-planes are often kinked or cracked. Chlorite grains have the same systematic as white mica grains but show smaller grain sizes and they occur more frequently in quartz rich layers. Feldspar can be found in the whole thin section with sizes up to 100 µm and hypidiomorphic grain shapes. With crossed nicols a few grains show twinning. Rare, hypidiomorphic garnet is found in mica rich layers reaching sizes of up to 100 µm (Fig. 24 A & B). No biotite was found in the samples of the Murau Group. Accessory minerals are identified as zircon, tourmaline, iron oxides occur along cracks.

Structurally the schistosity planes with big white mica grains, bigger quartz grains, and C'-type shear bands (Fig. 24 C) are the most obvious features in the lithologies of the Murau Group.

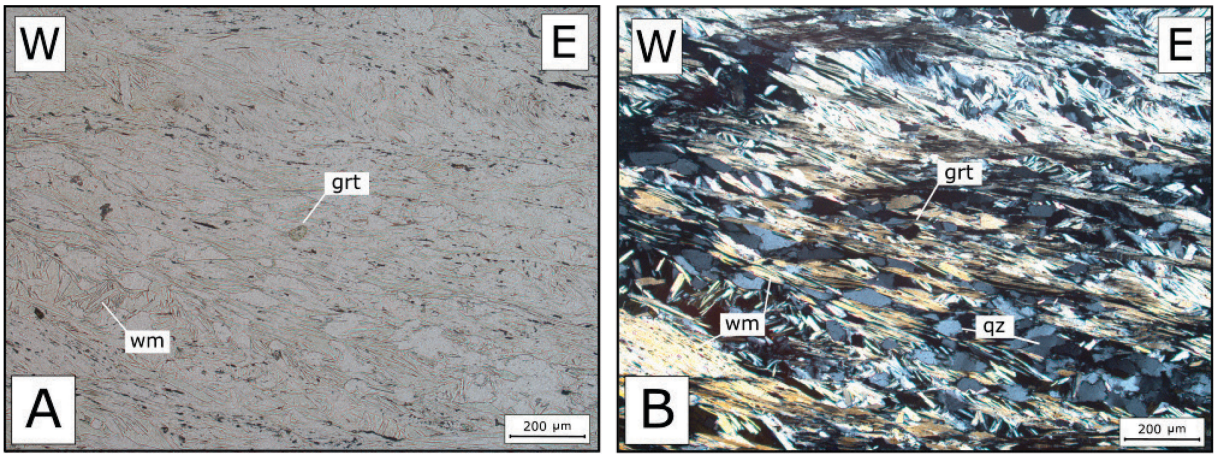

Figure 24 (Murau Group) Sample: MW1903 (UTM 33N: 0427115/5197866). A: Mica shist with small garnet grain & SPO of white mica, B: with crossed nicols.

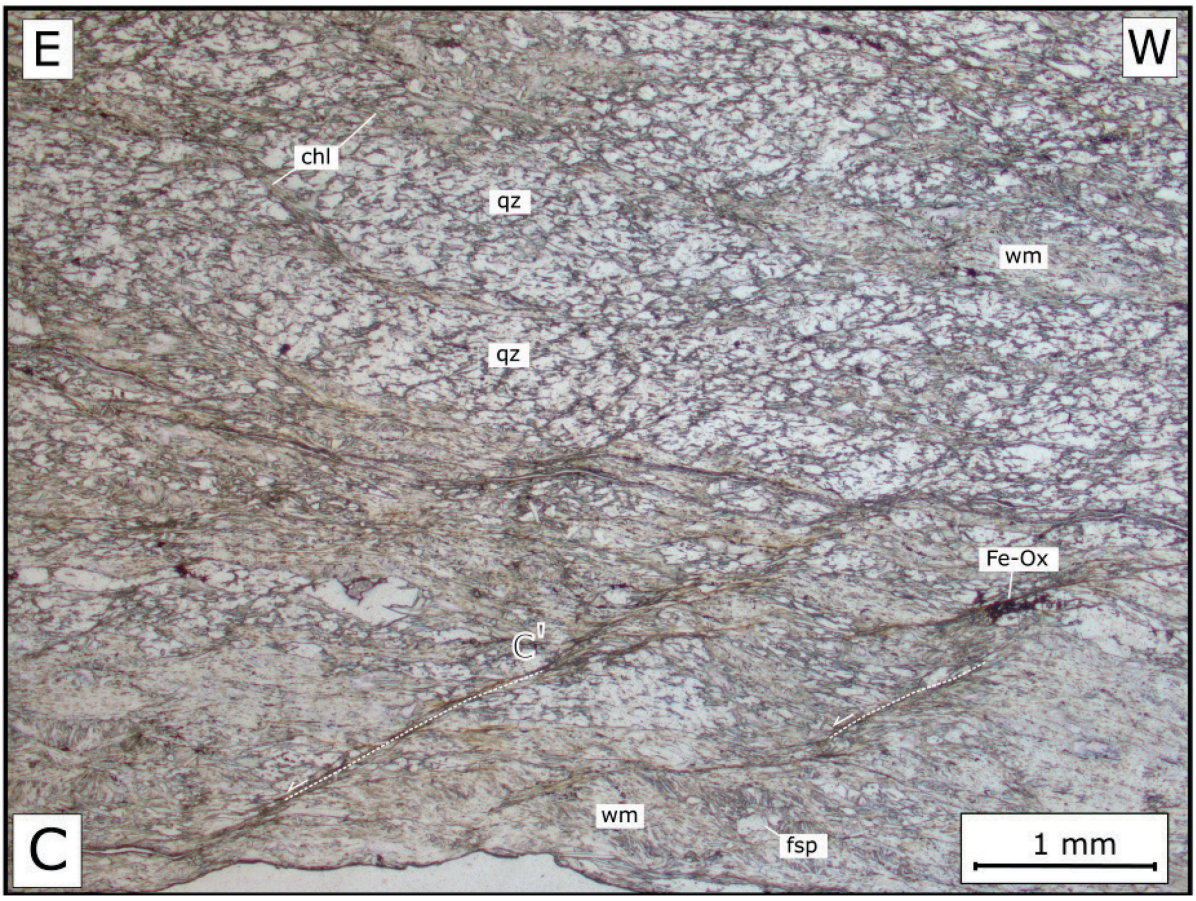

Figure 24 (Murau Group) C: C'-Type shear bands (top to the E sense of shear).

4.4.5 Spielriegel Complex

Microscopic observations show that the lithologies of the Spielriegel Complex consist mainly of quartz, white mica, chlorite, and subordinate chloritized biotite. A few grains of tourmaline can be seen (Fig. 25 A & C). The rocks exhibit a well pronounced lepidoblastic fabric. Quartz occurs in different grainsizes. The biggest grains occur in quartz veins with undulating grain boundaries. They are well aligned to the schistosity and have an extent up to 500 µm and show strong oscillatory extinction. Smaller grains build up most of the quartz in the samples and their grainsize differs from 10 µm to 50 µm. All of them show nearly straight grain boundaries and hardly any undulose extinction. White mica, biotite and chlorite only can be observed in S-parallel layers with a bimodal grain size distribution.

Small grains occur in the same areas as the small quartz grains and have similar sizes. Big grains have an extent of 400 µm and occasionally a mica fish texture.

Feldspar can be observed in all thin sections and occurs as rounded, partly rotated grains spread over the thin sections. They have an extent of 200 µm with a rhombic geometry. In the strain shadows small quartz grains are observed.

They show the same systematics as the quartz grains, which build up the matrix (Fig. 25 B). Due to the symmetric distribution of strain shadows, these clasts are not suitable as shear sense indicators. Rarely occurring quartz clasts with stair stepping and rotated minerals indicate a top to the E shearing (Fig. 25 A). Most obvious are C'-type shear bands with a top to the E sense of shear (Fig. 25 C & D). Structurally, however, they show the same characteristics than the quarzitic mica shist of the Murau Group. Major differences are seen in the occurring minerals as garnet in the Murau Group, the grainsize of white mica and quartz grains.

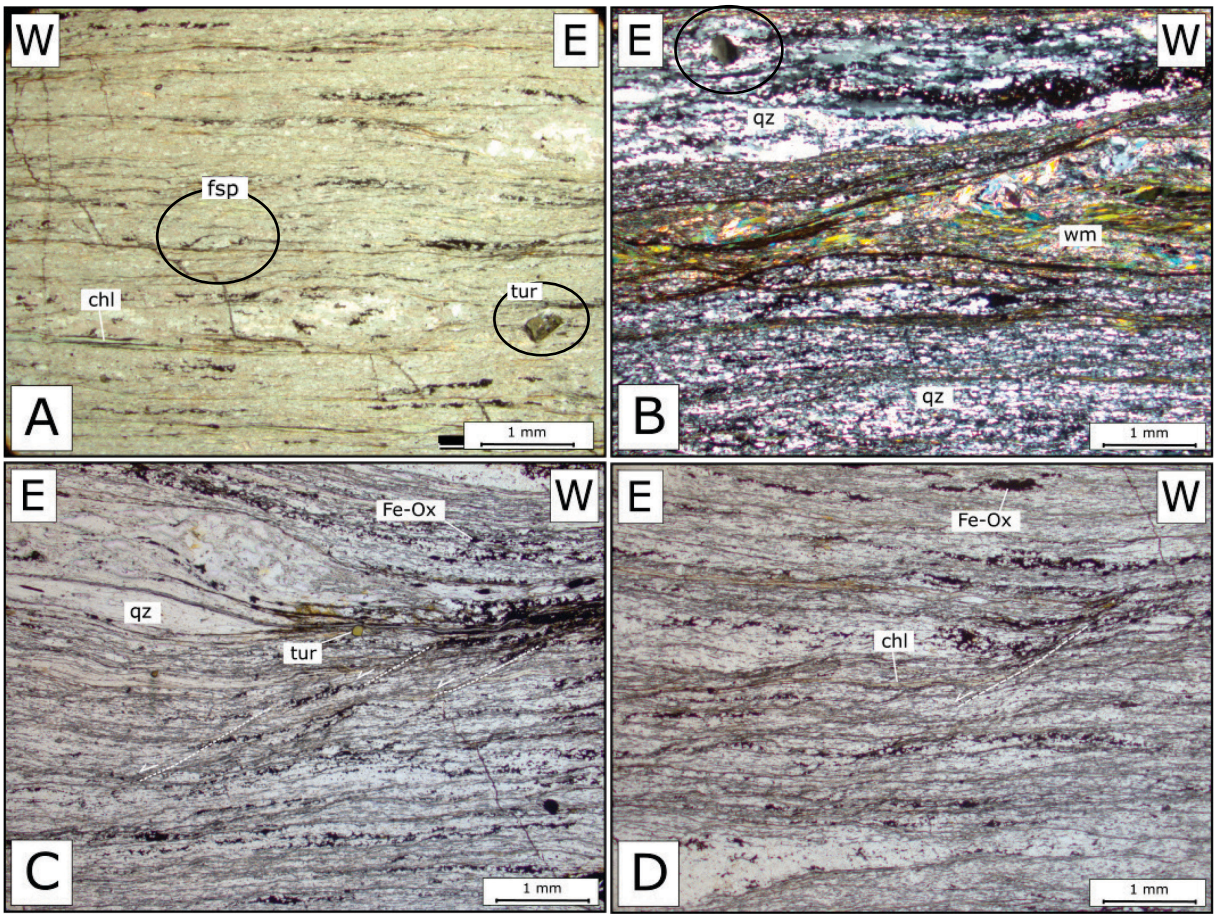

Figure 25 (Spielriegel Complex) Sample MW1910 (UTM 33N: 0427115/5197866) A: Quartz rich mylonite with rotated mineral (Top to the E sense of shear), B Mica rich layer and rounded clast with rhombic geometry, C & D: C'-Type shear bands (top to the E sense of shear).

4.5 Refold structures

Due to the occurrence of different folds with associated fold axes and axial planes resulting from older and younger deformation phases (folding events) it is possible to quantify them in the form of a vector triangle plot according to Grasemann et al., (2004). In this study, the 6 endmembers of possible refold structure types get discussed and a possibility to represent these endmembers by a direction-cosine matrix is explained. This matrix can be used to classify the angle between overlapping folds and display them in a triangular diagram.

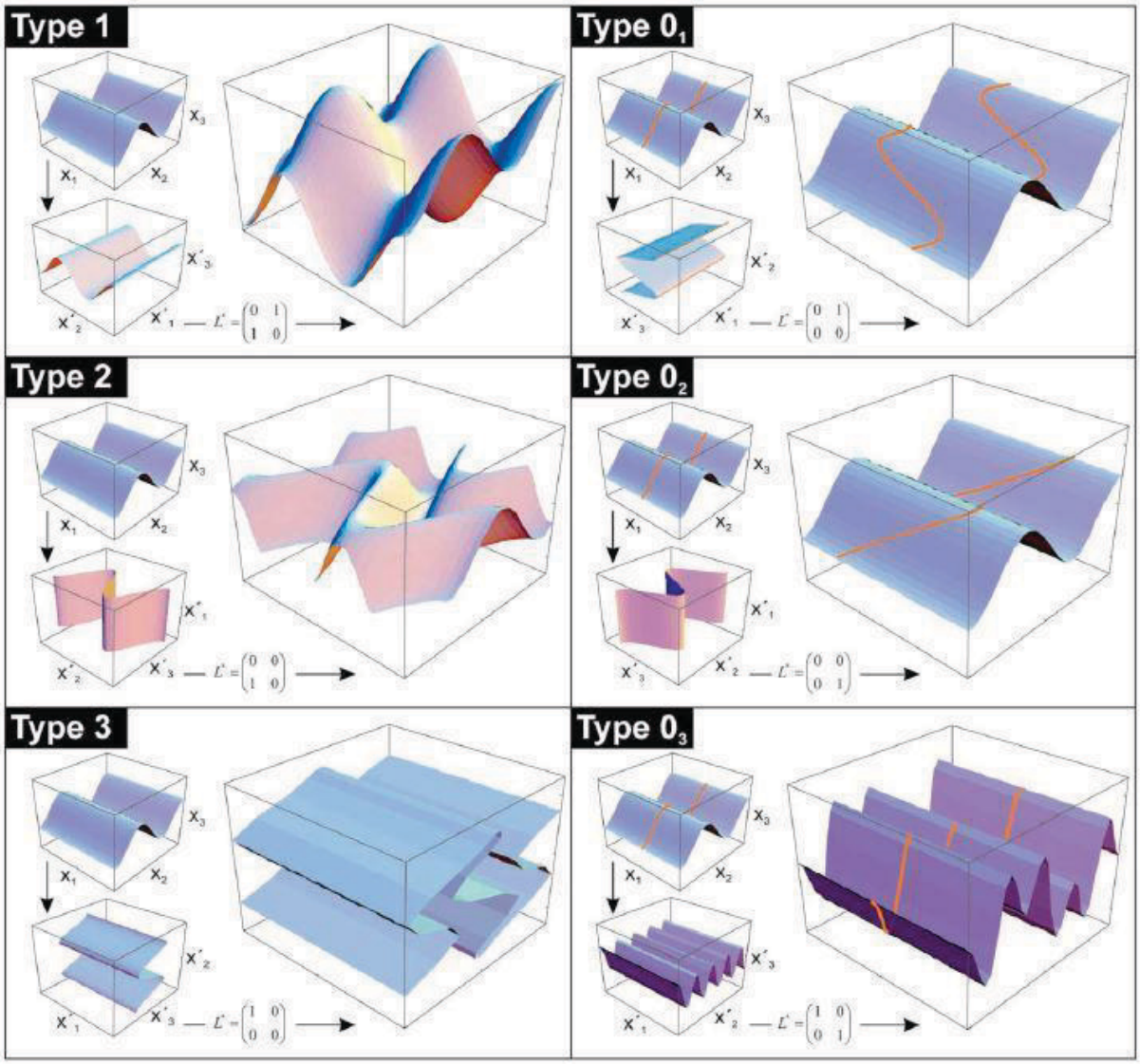

Figure 26: Representation of the 6 endmember types of superposition of folds. (Figure from Grasemann et al., 2004).

From measurements and observations of superposition of folds in the field, the matrix L* can be calculated. The calculation requires the fold axis of the older fold (FAo - x_1) and the pole of the corresponding older axial plane (APo - x_2), as well as the fold axis (FAy - x'_1) and the pole of the axial plane (APo - x'_2) of the younger superposing fold (Tab. 1). The conversion of the respective l_{ij} -value is done by calculating the angle between the linear features, shown in Fig. 27 C, according to Grasemann et al., (2004).

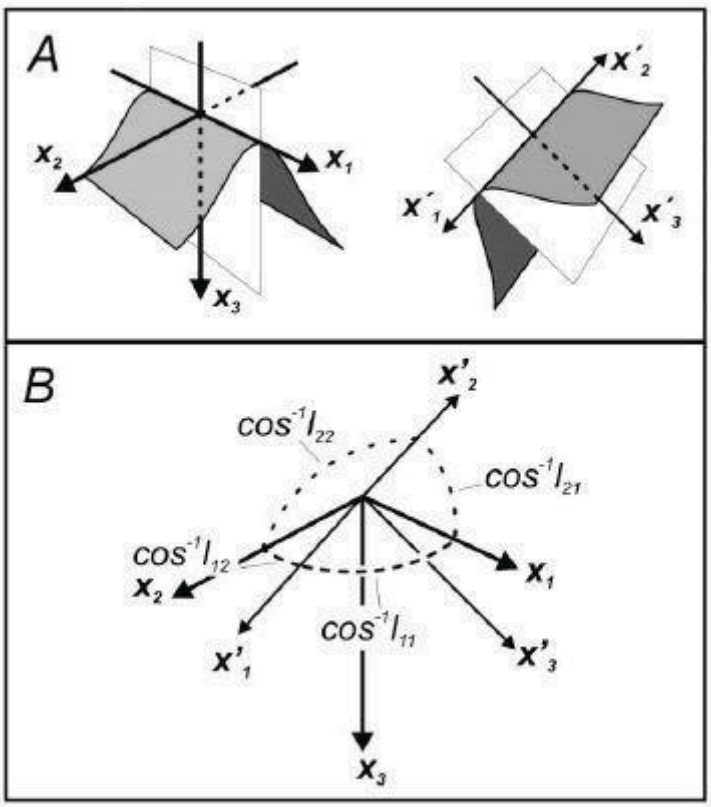

C

$$L^* = \begin{pmatrix} l_{11} & l_{12} \\ l_{21} & l_{22} \end{pmatrix}$$

$$\begin{pmatrix} \cos^{-1} l_{11} = < x_1' x_1 ; \cos^{-1} l_{12} = < x_1' x_2 \\ \cos^{-1} l_{21} = < x_2' x_1 ; \cos^{-1} l_{22} = < x_2' x_2 \end{pmatrix}$$

Figure 27 A: shows the geometric relation of the fold events, fold axis (x1 & x'1) and the poles of the axial planes (x2 & x'2).

B: shows the components lij which are required for the construction of the triangular plot

*C: shows the calculation of the angles between the linear features and the position in the matrix L**

Figure from Grasemann et al., (2004).

Field measurements Data table:

point	unit	generation	FAo(x1)		Apo		APo(pole)(x2)		FAy(x'1)		Apy		Apy(pole)(x'2)	
			dip dir.	dip	dip dir.	dip	dip dir.	dip	dip dir.	dip	dip dir.	dip	dip dir.	dip
001	Murau	F2-F3	241	14	329	04	149	86	084	03	337	09	157	81
008	Murau	F2-F3	255	10	268	09	088	81	244	16	325	06	145	84
														90
018	St.M	F3-F4	130	08	200	30	020	60	290	20	240	20	060	70
073	St.M	F3-F4	115	08	220	42	040	48	277	16	189	30	009	60
110	St.M	F3-F4	096	10	050	22	230	68	273	08	199	32	019	58
113	St.M	F3-F4	100	20	160	40	340	50	264	01	339	32	159	58
027	Oberhof	F3-F4	237	10	228	19	048	71	236	09	179	36	359	54
017	Stolzalpe	F1-F2	194	16	207	25	027	65	216	13	233	28	053	62
017	Stolzalpe	F2-F3	216	13	233	28	053	62	084	01	309	21	129	69
018	Stolzalpe	F1-F2	165	18	240	44	060	46	287	17	251	21	071	69
018	Stolzalpe	F2-F3	287	17	251	21	071	69	075	10	271	20	091	70
046	Stolzalpe	F1-F2	276	01	003	27	183	63	249	15	245	25	065	65
056	Stolzalpe	F1-F2	285	20	286	18	106	72	240	22	275	32	095	58
056	Stolzalpe	F2-F3	240	22	275	32	095	58	141	01	180	20	000	70
069	Stolzalpe	F1-F2	187	20	278	80	098	10	294	19	019	05	199	85
081	Stolzalpe	F1-F2?	130	30	110	35	290	55	050	37	054	52	234	38
081	Stolzalpe	F1-F2	269	12	106	20	286	70	125	13	246	46	066	44
081	Stolzalpe	F2-F3	246	21	270	31	090	59	092	15	352	05	172	85
081	Stolzalpe	F1-F2	260	01	310	20	130	70	234	14	312	34	132	56
081	Stolzalpe	F2-F3	234	14	312	34	132	56	075	19	140	20	320	70
101	Stolzalpe	F1-F2	092	10	335	28	155	62	200	03	333	55	153	35
101	Stolzalpe	F2-F3	200	03	333	55	153	35	054	12	126	50	306	40
106	Stolzalpe	F1-F2	280	01	022	13	202	77	200	07	289	35	109	55

Table 1: Table of field measurements of superposing folds. Fold axis singed by FA, axial planes by Ap and corresponding poles.

		I_{11} FAo(x1)-FAy(x'1)	I_{12} FAy(x'1)-APo(pole)(x2)	I_{21} Apy(pole)(x'2)-FAo(x1)	I_{22} Apy(pole)(x'2)-APo(pole)(x2)	fold axis
Murau group	001	28	85	75	5	F2-F3
	008	12	82	82	8	F2-F3
Stangalm Mesozic s.l	018	34	73	76	19	F3-F4
	073	30	82	89	22	F3-F4
	110	18	66	75	52	F3-F4
	113	26	80	57	72	F3-F4
Oberhof Lithodeme	027	1	80	80	27	F3-F4
Spielriegel Complex	017	22	78	84	12	F1-F2
	017	50	65	77	30	F2-F3
	018	67	76	75	24	F1-F2
	018	42	59	88	7	F2-F3
	046	30	66	70	44	F1-F2
	056	42	81	78	15	F1-F2
	056	82	67	79	39	F2-F3
	069	81	33	65	81	F1-F2
	081	65	75	82	41	F1-F2?
	081	44	84	60	62	F1-F2
	081	44	44	68	31	F2-F3
	081	29	82	71	14	F1-F2
	081	39	56	82	54	F2-F3
	101	73	68	61	27	F1-F2
	101	37	90	80	79	F2-F3
	106	80	70	56	38	F1-F2

Table 2: Calculation table for fold interference pattern, each value calculated in the way described in figure 27 C shows the angle between mentioned linear features.

4.5.1 Vector Triangle plots:

The following diagrams show the intersections of the folds that appear in the research area. These are plotted by the values l_{11} & l_{12} which define the origin of the vector, and by the values l_{21} & l_{22} which define the direction and the end point.

This method applied to all interfering folds encountered in the lithologies gives an overview of the interference structures that can be found in the study area. The arrows shown in Fig. 28 A & B get compared with the arrows on the outside of the triangle plot. If the direction of the arrows resembles that of the outer ones, the respective fold interference type is present.

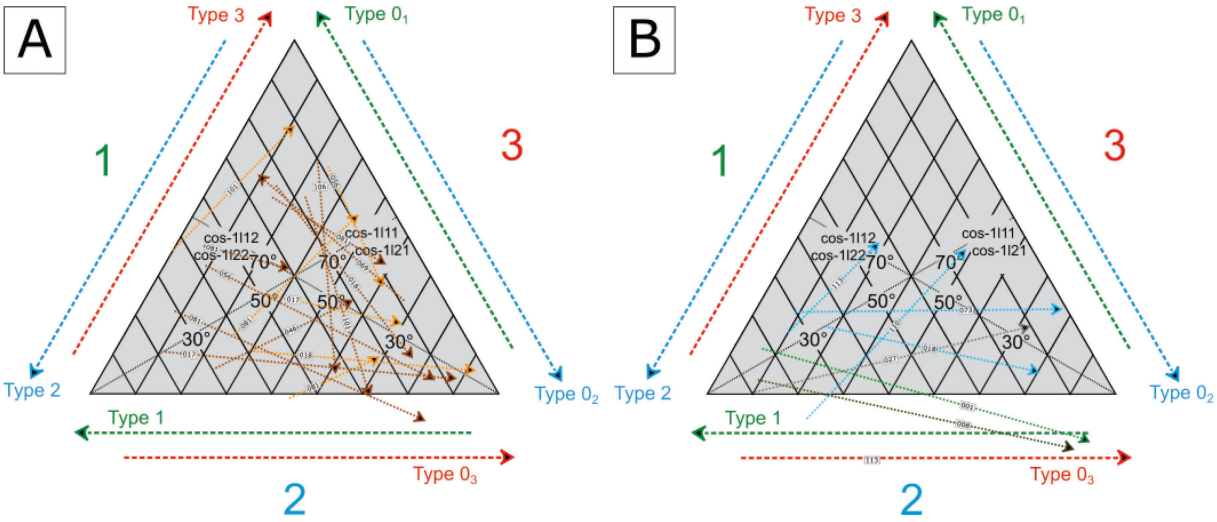

Figure 28: Vector triangle plots A: Fold interference pattern of lithologies of the Spielriegel Complex. B: Superposing folds of lithologies of the Stangalm Mesozoic s.l. (blueish), Oberhof Lithodem (greyish) and the Murau Group (greenish). The number on the arrows indicates the number of the outcrop point.

The triangular plots illustrate the present fold interference structures as shown in Fig. 26. The lithologies of the Spielriegel Complex (Fig. 28 A) show mainly refold structures of type 0_3 & 0_2. In a few outcrops a type 3 refold structure can be detected. A similar picture presents itself for the lithologies of the Stangalm Mesozoic s.l. (Fig. 28 B). This shows interferences of type 0_3 and type 3. The lithologies of the Oberhof Lithodeme and the Murau Group present exclusively refold structures of type 0_3.

4.6 Results from Raman micro-spectroscopy

In this part the results of the applied RAMAN microspectroscopy of the graphite bearing units of the research area are presented and shown in the map.

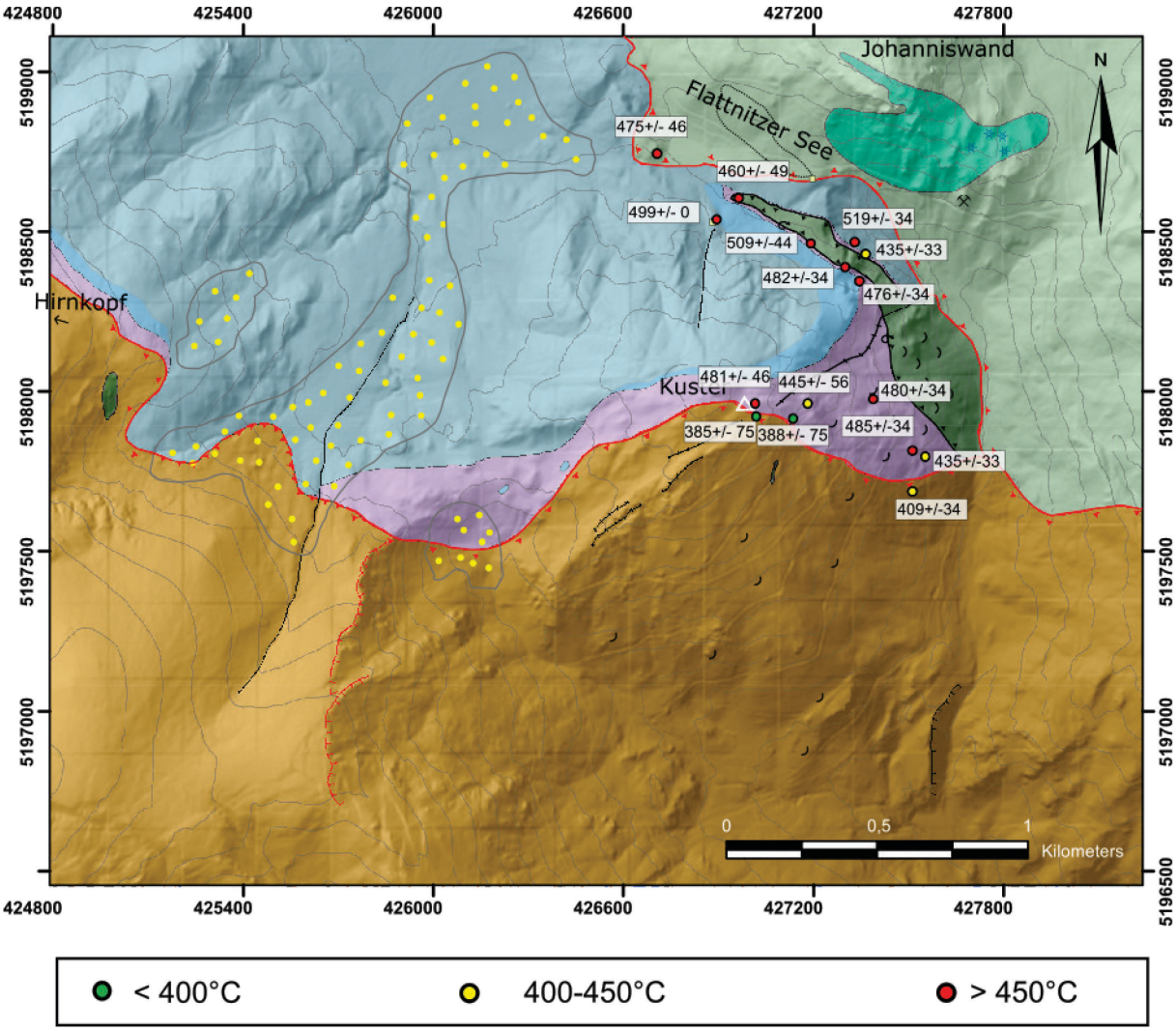

Figure 29: RAMAN micro-spectroscopy data plotted on the map in the boxes are the values of T-max in °C +- Error; the measurements are colour coded temperatures < 450°C in red, 400-450°C in yellow, < 400°C in green. Legend as in Figure 4.

All graphite-bearing units were sampled and analysed using RAMAN microspectroscopy carried out by Dr. Gerd Rantitsch from the University of Leoben [8 samples, highlighted in green in Table 3 are New Data, the other samples highlighted in yellow are already published in Rantitsch et al., 2020]. These temperatures show the maximum temperature during metamorphism (Lünsdorf et al., 2017). The maximum temperatures are plotted on the map above and colour coded. The structurally lower

lithologies of the Stangalm Mesozoic s.l. as well as the Oberhof Lithodem experienced the highest temperatures, while structurally higher units as the Murau Group and the Spielriegel Complex show lower peak temperatures. Graphite was found in the dolomite-marble of the Karnerboden Lithodeme in the contact zone to the Weißwände Lithodeme. The maximum thermal overprint shows a temperature of 499°C. In the Leckenschober Lithodeme graphitic schist layers with a maximum thickness of 0.5 m alternating with impure calcite-marble layers occur. The measurements show temperatures from 480°C to 435°C. The graphite bearing lithologies of the Oberhof Lithodeme are distinguished as carbonaceous schists with a big amount of detrital mica grains. The samples show a peak of temperature at 519°C. Graphite can also be found in quarzitic mica schists of the Murau Group. this usually can be found in thin layers with a thickness of a few centimetres distributed along the schistosity planes. These show a temperature of 475°C. A decrease in temperature is observed in structurally higher lithologies of the Spielriegel Complex. Here, the analyses show temperatures of 388°C - 409°C.

Probe_NR	UTM33_N	UTM33_E	Lithology	Lithodemic unit	Temp [°C]	+/-
IGL19/14	5198421	427367	Dol-Mbl-myl, graphitic	Weißwände	435	33
IGL17/22	5198596	426968	Meta-marl, graphitic	Bockbühel	460	26
IGL18/03	5198530	426899	Graphite schist	Bockbühel	500	29
IGL18/15	5197952	427020	Phyllite, graphitic	Leckenschober	482	34
IGL18/18	5197951	427185	Phyllite, graphitic	Leckenschober	446	47
IGL19/06	5197785	427556	Graphite schist in Cal-Mbl-myl	Leckenschober	435	33
RAMAN 1	5197803	427515	Graphite layer in Cal-Mbl-myl	Leckenschober	485	34
RAMAN 2	5197964	427392	Graphite layer in Cal-Mbl-myl	Leckenschober	480	34
RAMAN 3	5198336	427348	Graphite layer in Cal-Mbl-myl	Leckenschober	476	34
IGL19/13	5198459	427333	Graphite schist	Oberhof	519	34
RAMAN 4	5198454	427196	Graphite schist	Oberhof	509	44
RAMAN 5	5198381	427303	Graphite schist with detr. wm	Oberhof	482	34
IGL17/26	5198738	426711	Graphite Schist	Murau Group	475	26
RAMAN 6	5197675	427515	Graphitic Qz-phyllite	Spielriegel	409	34
RAMAN 7	5197911	427023	Graphite Schist	Spielriegel	385	75
RAMAN 8	5197904	427139	Graphite Schist	Spielriegel	388	75
IGL18/14	5197941	426829	Graphite Schist - Erratic block	Stangnock	349	32

Table 3: Result table from Raman micro spectroscopy, the data highlighted in green are new data, the yellowish are already published in Rantitsch et al., (2020).

4.7 Results from Paleopiezometry

The estimation of the differential stress is carried out using the toolbox coded in Phyton by Marco Lopez Sanchez (2018). The recrystallized grains of nearly monomineralic samples of the Leckenschober Lithodeme, the Oberhof Lithodeme, and from the Spielriegel Complex were investigated.

The different values in the calculation table are given in [MPa] and show the differential stress for each published piezometer. These values give the differential stress in the lithospheric crust while dynamic recrystallisation and the distribution plots indicate the apparent grain size of the corresponding lithologies and shows the different mean values, as the arithmetic mean, the geometric mean, and the median. Therefore, the Leckenschober Lithodeme and the Spielriegel Complex show differential stresses of approximately 60 MPa and a mean of grain sizes of 16.91 µm and 20.47 µm. The Oberhof Lithodeme shows lower differential stress of 20-50 MPa. The mean diameter of the grains is varying from 28.32 – 32.60 µm.

				piezometer Quartz (SGR) in [Mpa]					piezometer calcite in [Mpa]		
sample	lithology	Lithodemic unit	def mech	Twiss	Holyoke	Stipp_Tulis	Cross	Cross_hr	Barnhorn	Rutter corr	Rutter
1909A	Calcite	Leckenschober	SGR						61,02	77,95	67,51
1910	Quartz	Spielriegel	SGR	326,73	73,73	100,61	109,62	102,46			
1910_1				67,18	41,10	56,08	64,84	64,30			
1910_2				65,03	42,74	58,32	67,15	66,33			
1918_8	Quartz	Oberhof	SGR	48,95	25	34,12	41,48	43.25			
1919B_7				26,98	15,13	20,64	26,41	28,98			
1923_3				53,87	34,29	46,79	55,1	55,65			

A

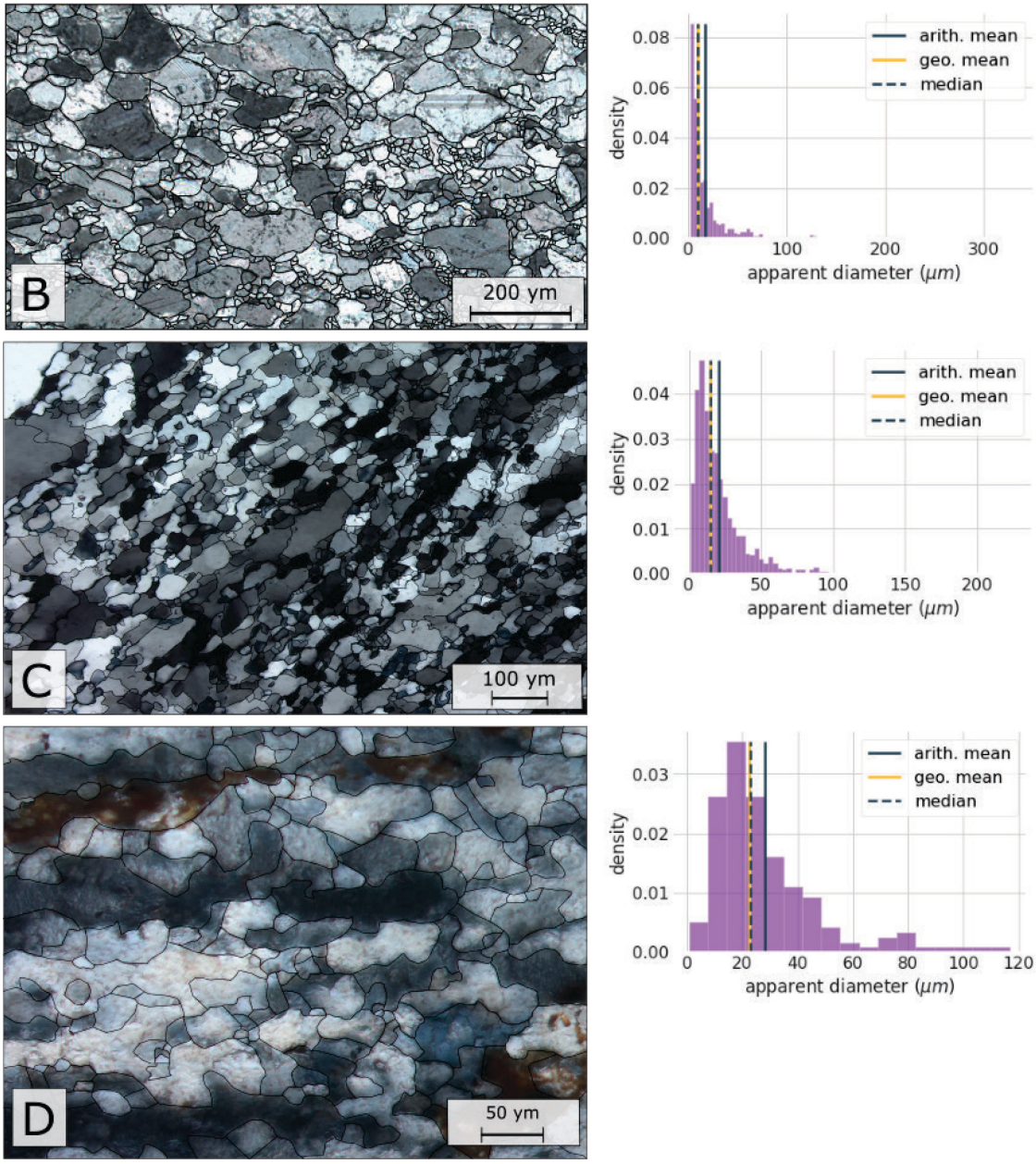

Table 4 A: Calculation table for paleopiezometry; Figure 30 B: Sample 1909A calcite-marble of the Leckenschober Lithodeme with drawn outlines of subgrains; C: Sample 1910 Quartzite from Spielriegel Complex (B & C UTM 33N: 0427115/5197866); D: Sample 1923 Quartzite from Oberhof Lithodeme (UTM 33N: 0427338/5198343).

5 Discussion & Interpretation

5.1 Structural evolution & metamorphism (during D_{3a}):

The investigated lithologies contain few minerals that allow accurate estimates about the P-T conditions during metamorphism using geothermobarometry. However, microstructures of quartz and calcite (e.g., different grain sizes, different twinning in calcite) allow estimates of the temperature during deformation. Combined with the Raman microspectroscopy data, metamorphic conditions during the structural evolution can be interpreted.

Sedimentary structures are not found in the investigated area. Compositional layering observed in many lithologies may be inherited from the protolith, but this feature is completely recrystallized and overprinted by younger deformation phases.

Structures originated and related to the oldest observable deformation phase are interpreted as Pre-Alpine. The D_1 & D_2 related structures only can be observed in structurally higher levels of the Spielriegel Complex, where the Eo-Alpine overprint was less pronounced. In this sense the isoclinal folds of D_1 and the asymmetric open folds of the D_2 phase cannot be used for deriving kinematics of these “old” deformation phases. But the same top-to the W-NW kinematics are assumed as in earlier studies discussed (Neubauer, 1987; Ratschbacher et al., 1989; Schuster, 1994).

The Eo-Alpine event is the dominant feature in the research area and therefore subdivided into different phases as described in chapter (2.4). From cross-cutting relationships of different structural elements, and microstructures that are indicative for a particular deformation phase, a relative chronology is established.

In lithologies of the Stangalm Mesozoic s.l., the chronology starts with the transgressive deposition of the Weißwände Lithodeme and the Bockbühel Lithodeme onto the Bundschuh Priedröf Complex which was followed by the Karnerboden Lithodeme and the Leckenschober Lithodeme. This package was overthrusted by older lithologies of the Spielriegel Complex, the Murau Group, and the former Stangnock Formation (nowadays Oberhof Lithodeme). This phase is described as D_{3a} phase of the Eo-Alpine event (Iglseder & Huet, 2019). In this phase the peak of metamorphism occurred, due to the deepest subduction of all units. The Raman microscopy data suggest a thermal peak of the structurally lowest units (Stangalm Mesozoic s.l. and Oberhof Lithodeme) of 435°C-519°C. This temperature is consistent with the observed microstructure of the ultra-mylonite of the Weißwände Lithodeme, which is interpreted as ductile recrystallization at peak temperatures. This leads to the interpretation that both units jointly experience this peak, which is discussed in more detail in chapter (5.4). The

measured maximum temperature is decreasing in structural higher levels. Peak temperatures of the Murau Group show 475°C, therefore the growth of garnet is possible (Hollinetz et al., 2019). Koroknai et.al., (1999) interpreted occurring garnets at the base of the Murau Nappe as Variscan but recent investigations from Hollinetz et al. (2019) shows evidence for single-phased garnet growth during the Eo-Alpine event of this Nappe. The rarely occurring garnet in the sample from Mount Kuster are very small in size and can be interpreted as inherited as well as newly formed. However, the overlaying Spielriegel Complex show a significant drop in temperature and a peak at 388°C which is the highest measured temperature of units of the Stolzalpen Nappe but indicates an upright Eo-Alpine metamorphic gradient in this unit.

The comparison of grainsize and habit of quartz and white mica of similar lithologies of the Murau Group and the Spielriegel Complex also gives a hint on deformation temperature and deformation mechanism discussed in more detail in chapter 5.2.2. Further on the exhumation related deformation of D_{3b} phase of this nappe stack, the retrograde metamorphism, and cooling of the system took place. Due to the low diversity in the mineralogical composition this phase is mostly recognised in deformation structures.

In the regime of brittle deformation, the presence of a fluid phase is shown by the occurrence of tremolite in the different steep joint sets of the Weißwände Lithodeme. Therefore, a mixed fluid reaction can be used for this hydration-decarbonation reaction, which is strongly dependent on the availability of CO_2.

$$5Dol + 8\,Qtz + H_2O = Tr + 3Cal + 7CO_2$$

5.2 The Detachment

5.2.1 Structures of the shear zone

Structures related to phase D_{3b} result in the main structural overprint of all units, whereby all traces of earlier D_s and D_{3a} phase got lost, except in the Stolzalpe Nappe. However, the preserved structural overprint is bounden to the D_{3b} phase. All observed structures in the research area which are used to reconstruct a sense of shear consistently indicate a Top to the E sense of shear. This is indicated by flanking structures in the dolomite ultra-mylonite (Fig. 18 B), mica fish textures, and clast geometries in other lithodemic units. Furthermore, structures are identified which indicate a strong coaxial deformation bounden to D_{3b}. The formation of a pervasive stretching lineation dipping mainly towards SE, as well as isoclinal folds with E-W oriented fold axis in nearly all lithodemic units and the formation of corresponding axial plane schistosity is observed. Further on the formation of meter to centimetre scaled boudins of dolomite, as well as the consistent E-W oriented shape preferred orientation (SPO) of mineral grains indicate strong coaxial deformation.

Further cooling is reflected by the formation of brittle-ductile transition structures in the quartz rich lithologies and rarely in the calcite-marble occur in form of C'-type shear bands, that overprint the whole fabric and accumulate minor amounts of displacement. No shearbands were observed in the dolomite-marble of the Weißwände and the Karnerboden Lithodeme. Since dolomite marble is monomineralic and fairly massive, no glide horizons to form shearbands exist. Instead, the formation of stylolites is observed (Fig. 21 B, 22 C). The last recognisable step is recorded in centimetre to kilometre open folds which overprint the whole nappe stack and result in refold structures. This phase can be interpreted as independent phase of NNW-SSW shortening as Huet (2015) described, or as last syngenetic exhumation phase of D_{3b}.

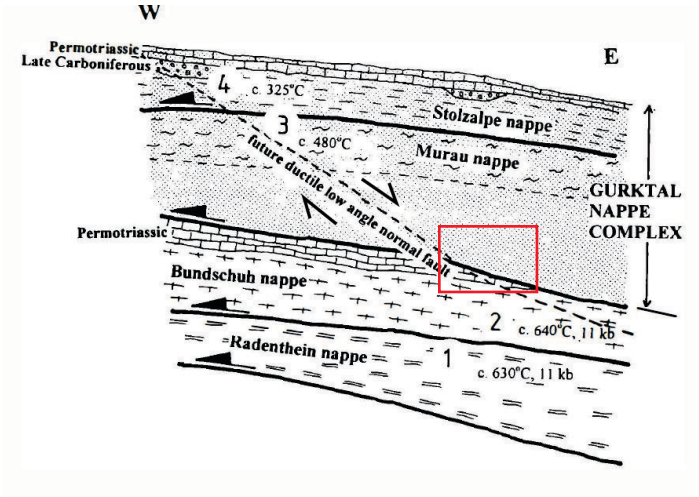

Figure 31: Schematic sketch of the low angle normal fault in the upper Austroalpine unit, from and modified after Neubauer et al., 1998, The red square indicates the position of the research area in the nappe stack.

5.2.2 Shear zone evolution

In active ductile shear zones, the higher the strain-rate at low temperatures the smaller is the stable recrystallized grainsize (Passchier, 2005). Mylonites also may undergo grain growth during dynamic recrystallisation in a shear zone to reach the stable grain size (Masuda and Fujimura, 1981). Dynamic recrystallisation leads to a balance between grain size reduction and growth processes. (De Bresser et al. 2001). The grainsize distribution plots shown in chapter 4.6 indicates a grain size reduction in hanging wall direction This can be interpreted as lower deformation temperatures in structural higher levels. Microstructural evidence of the preserved structures that were briefly described above indicates different deformation mechanisms were active and are subdivided into high temperature structures and low temperature structures mentioned in chapter 4.3.

The main active deformation mechanisms are diffusive mass transfer as dissolution & precipitation creep (DPC) and intracrystalline plasticity seen in twinning, recovery of grains as bulging (BLG) and subgrain rotation (SGR). Along phase boundaries in mica rich lithologies and in the dolomite ultra-mylonite grain boundary sliding was active.
In this sense, the different lithologies and syngenetic phases of exhumation are subjected to different deformation mechanisms. In the very fine-grained dolomite ultra-mylonite grain size sensitive flow was active (Herwegh et.al. 2001), which commonly occurs at high temperatures (Passchier, 2005). The deformation temperature is decreasing in structural higher levels, seen in the change of deformation mechanism. Lithologies in upper levels, therefore, show dominantly microstructures indicative of DPC such as a spaced foliation, cleavage and less common microlithon domains. DPC microstructures are best seen in the calcite-marble of the Leckenschober Lithodeme, where soluble material is dissolved, and insoluble material as white mica and phyllitic/graphitic material remains with an E-W orientated shape preferred orientation (SPO). Calcite is recrystallising and shows the same SPO. DPC is also evident from the formation of strain caps and strain shadows around porphyroclasts where newly formed small grains are observed in the quartz rich lithologies. Hereby the isoclinal folds and the penetrative axial plane schistosity were formed seen in isoclinal folded pyllitic inclusions of the Leckenschober Lithodeme (Fig. 20 D).

Ongoing deformation during exhumation also caused intracrystalline deformation in quartz grains and quartz porphyroclasts. Where at the expense of the rim area of big clasts and preexiting veins, which show a highly undulose extinction, newly formed subgrains are observed. The deformation mechanism is interpreted as SGR. This deformation concerns all quartz rich lithologies and indicates a deformation temperature of minimum 400°C according to Passchier (2005).

At decreasing temperature, the impure calcite-marble on the one hand commonly show twinning of type 2 and 3 of large, recrystallised grains which indicates temperatures of deformation of ~200°C. On the other hand, quartz in these samples often show bulging which is in good correlation of the deformation temperature suggested by the twinning (Fig. 22 C). In later phases of exhumation also the DPC occurred like formation of stylolites in the dolomitic and calcitic-marble, whereas in quartz- and mica-rich lithologies the formation of C and C'-type shearbands is most prominent. This formation is related to high finite strain accommodated by grain boundary sliding which leads to a grain size reduction (Ree, 1994; Schmid et al., 1987; Walker et al., 1990).

Since the deformation mechanism in the nearly monomineralic systems is consistently identified as SGR, which is best seen in large, deformed grains which subsequently replaced by small unstrained grains, the confining pressure of lithologies was calculated with piezometry. It is shown that both units The Leckenschober Lithodeme and the Spielriegel Complex which defining the nappe system boundary experienced the same pressure. This is an indication that both nappes were exhumed together and formed an several 100 m thick Top ESE shear zone which is most localised at the nappe system boundary between the Drauzug-Gurktal Nappe System and the Ötztal-Bundschuh Nappe System mostly in the Stangalm Mesozoic s.l. These observations are in good correlation with research from Hollinetz (2018) who investigated detaching structures on top of the Gstoder Nappe and saw evidence for a detachment in structural higher levels. Weissenbacher (2015) also found evidence for Top E orientated detaching structures in the Bundschuh Priedröf Complex but did not assign them to a major detachment localised in the Stangalm Mesozoic.

Results of paleopiezometry must be interpreted with caution due to the following reasons: (1) the investigated samples are not perfectly monomineralic. (2) some degree of error may arise from errors in grain mapping; (3) deformation mechanisms other that SGR may have been active. For more precise results of paleopiezometry, it is highly recommended to use EBSD maps. EBSD measurements allows the calculation of the flow law and an accurate description of the deformation mechanism and the grain boundaries. Which further leads to more precise values of the confining pressure.

5.2.3 Geochronological Data

For a better understanding of the temporary relationships and the cooling history, the following section will explain the available geochronological data related to the shear zone in the study area. The geochronological interpretation is based on published data from Iglseder & Huet (2019) respectively Iglseder et al. (2019) & references therein.

The cooling history of the Bundschuh nappe shows a cooling below 300°C between 81-87 Ma based on Rb/Sr data of biotite. A further cooling below 150 °C based on U-Th-He measurements on zircons of between 45-50 Ma. For the structurally higher Murau nappe there is an $^{40}Ar/^{39}Ar$ plateau age measured on muscovite, which shows cooling at 86 Ma. A U-Th-He age on zircon in the Stolzalpe nappe indicates cooling below 150° C by about 76 Ma.

These cooling ages show in connection with the detachment the exhumation of the units of the nappe stack, whereby the structurally deeper units start to exhume first and this movement is progressing continuously to higher crustal levels. Therefore, it can be shown that the shear zone at mount Kuster is a cretaceous ductile shear zone which exhumed units from the Ötztal Bundschuh Nappe System together with units from the Drauzug Gurktal Nappe System from 87 – 76 Ma.

5.2.4 Low angle Detachment vs. ductile thinning

Deformation in the Earth's crust occur in localised fault planes. Depending on temperature and strain rate, both brittle or ductile processes can occur. Crustal detachments play an important role in the exhumation of deeply subducted units. Generally, these detachments are defined by an increase of mylonitic deformation in the footwall. The detachment plane is defined by a zone of cataclasis which get formed as a result of exhumation. (Daniel et al., 1996; Gautier et al., 1993; Grasemann et al., 2012; Haertel and Herwegh, 2014; Jolivet et al., 1994). These criteria are used to discuss the existence of a large-scale detachment at Mount Kuster, where structural lower units of the Drauzug-Gurktal Nappe System juxtapose the structural highest units of the Ötztal-Bundschuh Nappe System. The structures observed show on the one hand an increasing mylonitisation of the rocks in structurally deeper levels (e.g., ultra-mylonitic dolomite marble of the Weißwände Lithodeme), and on the other hand decrease of deformation temperature that leads to the overprint of ductile mylonites by brittle-ductile structures (e.g., flanking structures). In hanging wall levels, the fault plane shows less evidence of cataclasis itself, which indicates that displacement along the detachment ceased at lower greenschist facies conditions. This fact also can be interpreted as ductile thinning in the first stages of exhumation.

This assumption is further supported by the occurrence of a 10-meter-thick quartzite mylonite directly above the detachment plane in hanging wall direction of the Spielriegel Complex. This gradient decreases continuously towards structural higher levels. A few shear sense indicators were found in the research area but in a large-scale normal fault setting much more indicators are expected. This fact is interpreted as strong coaxial (pure shear dominated) deformation and can be linked to ductile thinning. Further evidence of ductile thinning is given in the rheologic behaviour, according to research from Sean & Matthew, (2020). Their study showed that weaker rocks do not have the ability to transmit shear traction, this results in a pure shear dominated, thrust-normal thinning and transport-parallel stretching (e.g., Means, 1989; Camilleri, 1998; Yonkee, 2005; Law et al., 2013). In quartz rich lithologies, ductile thinning is at deformation temperatures of 300°C possible (e.g., Stipp et al., 2002; Yonkee, 2005; Long et al., 2011), with strain magnitude expected to increase with increasing deformation temperature (e.g., Ring and Kassem, 2007). Therefore, it can be shown that lithologies from the footwall show predominantly more rhombic clast geometries than lithologies from the hanging-wall. Possibly both exhumation models can be observed at the shear zone of Mount Kuster.

5.3 Estimation of the distance of displacement

As Stowasser (1956) reported the Stangalm Mesozoic cropping out at Mount Kuster show a thickness of 300-400 meters. The most western parts around Innerkrems are measured from maps from the Geological Survey of Austria show a thickness of 1600 meters. This nearly horizontal layered package thins from W to E out by a factor of 4 in the 25 kilometres in between. Due to these observations and with a few assumptions, it is possible to find a minimum distance of displacement the lithologies of the Stangalm Mesozoic s.l. have experienced. To get an idea of the magnitude of displacement during exhumation, a simplified trigonometric solution is presented.

For the calculation the angle of the Detachment is interpreted as the dip of the mylonitic foliation and for further calculation an angle of 10°, 15° and 20° is used. The hypotenuse in this case is interpreted as rough estimation of the distance of displacement (Fig. 32 B). It is also assumed that the angle of this detachment hasn't changed while exhumation.

The attempt is to use measured Raman temperatures and correlate them in terms of subduction depth and vertical uplift. An average geothermal gradient for upper crustal levels of 30°C/km for the upper 10 kilometres of the nappe stack is assumed.

In deeper horizons a geothermal gradient of 15°C/km is used. Therefore, an exhumation from 500°C peak temperature to 200°C shows a vertical exhumation (h) of approximately 16.6 kilometres.

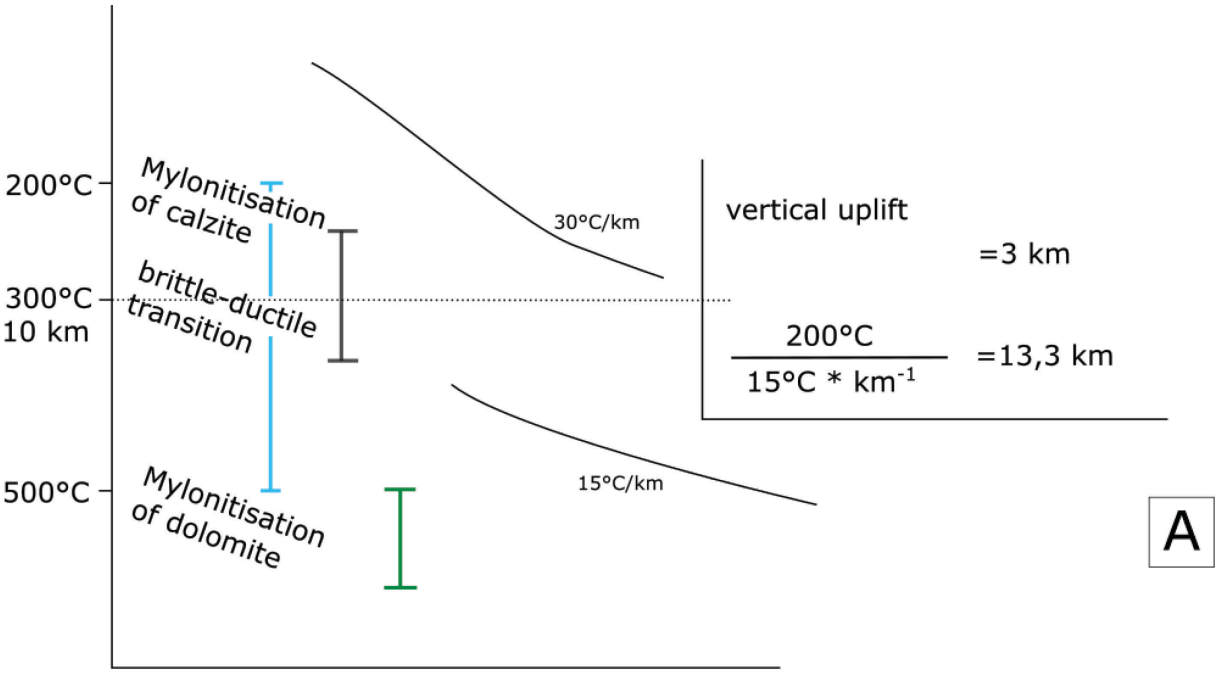

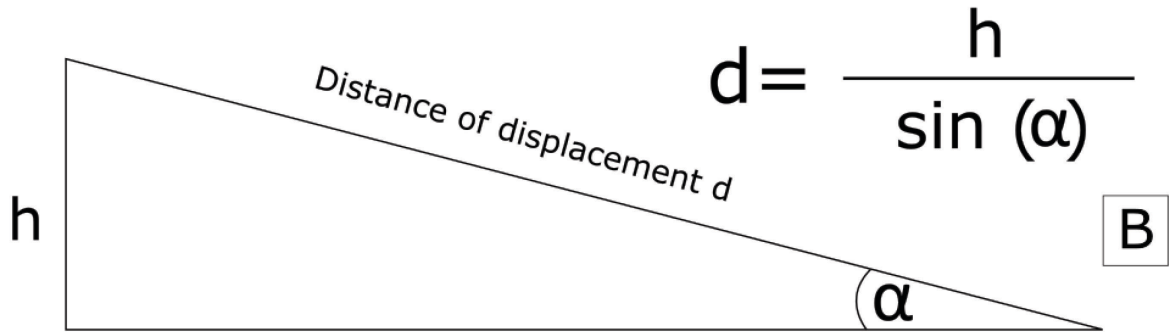

	Stangalm Mesozoic s.l.	Stangnock Fm.	Oberhof Lithodeme
angle α	h = 16.6 km	h = 4 km	h = 4.7 km
10°	95.96	23.03	27.07
15°	64.14	15.45	18.16
20°	48.54	11.69	13.74

C

Figure 32 A: schematic crustal profile and calculation of vertical exhumation; B: simplified trigonometrical illustration of the detachment & relation of the angle and the uplift distance. C: Calculation table with distances of displacement.

The same procedure can be done for lithologies of the Stangnock Formation. Which also show a thinning from W to E. In Western parts a thickness of 1000 m is reported (Iglseder et al., 2019) at the flank of mount Stangnock. The E most outcrops show a thickness of 250 meters measured from maps E of the Wintertalernock. Therefore, a thinning by the factor 4 is observed in 15 kilometres in between. Metamorphic peak temperatures range from 280-350°C (Rantitsch et al., 2020) from structural lower

to higher levels (ATA 2019, and references therein). The Thermal profile shows a vertical uplift of 4 kilometres and distances of displacement from 23.03 – 11.69 kilometres.

The Oberhof Lithodeme is cropping out in the Oberhof Window and show an apparent thickness of ~200 meters described by Hollinetz (2018). At Mount Kuster the apparent thickness is 50 meters described by Beck-Mannagetta (1959) and shown as a result of this study. Therefore, this lithodemic unit is thinning out in between five kilometres in W direction by a factor of 4. Modelled peak temperatures from Hollinetz (2018), indicates a metamorphic peak at 570°C in Oberhof. Raman temperatures from mount Kuster indicates a peak at 500°C. The resulting distance of displacement ranges from 13.7 – 27 kilometres.

In this highly simplified model, a thinning by the factor of four is shown for all affected units.

5.4 The Kuster Nappe

In the following point it will be discussed why it could be useful to introduce a new nappe named Kuster Nappe as the structural highest nappe of the Ötztal-Bundschuh Nappe System. The main reasons can be found in the (1) lithological composition, (2) the peak of metamorphism, as well as the apparent (3) deformation in this unit.

To clarify the lithological affiliation of the Oberhof Lithodeme and the Kuster Nappe the origin of these must be examined. The Oberhof Lithodeme was first described by Hollinetz (2018) as a higher metamorphic deformed equivalent of the Stangnock Formation.

The Stangnock Formation is an association of intercontinental sediments of the Upper Pennsylvanian (Iglseder, 2019 and references therein) which is the transgressively overlying cover of the Kaser Complex and the Spielriegel Complex. This cover was formed after the Variscan orogeny. Which means that the Stangnock Formation occurs due to Eo-Alpine thrust tectonics (D_{3a}) as “cover” formation in the (1) Königstuhl Nappe as well as the structurally uppermost formation in the (2) Stolzalpe Nappe. In the out of sequence thrusted Königstuhl Nappe this association shows a decreasing temperature gradient from E to W of 350°C in E parts and 260°C in W parts of the nappe (Rantitsch et al., 2020). (2) In the structurally uppermost Stolzalpe Nappe this cover experienced temperatures of 200-240°C (Rantitsch et al., 2020).

The Oberhof Lithodem therefore, is a relatively young term in the regional geology of the Upper Austroalpine unit. It is latterly described in the region of Oberhof by Hollinetz et al., (2018). The lithologies are distinguished as an association of graphite bearing metapelites and meta-psammites structurally above the Bundschuh-Orthogneis Lithodeme (Iglseder, 2019 & references therein). The main lithologies could be differentiated (1) garnet- and chloritoid-bearing graphite schist and (2) quartzitic mica schist and quartzite (Hollinetz et al., 2018). This earlier study suggests due to the similarities of the Permian graphite rich metasediments of the Stangnock Formation described in the Stolzalpe Nappe (Krainer, 1989) that the Oberhof Lithodem can be interpreted as a metamorphic equivalent of these. In the area around Flattnitz I interpret the occurring lithological association of graphite schists, meta-conglomerates, and mica schists intercalated into lithologies of the Stangalm Mesozoic s.l. as lithologies originating from the Stangnock Formation and due to the higher grade of metamorphose this lithological association corresponds to the Oberhof Lithodeme as described above. In comparison, the lithological units of the Stangalm Mesozoic s.l. consist mainly of carbonate-rich rocks, only the structural highest parts of the Stangalm Mesozoic shows lithological similarities. On closer examination, however, these have no genetic connection and can be clearly distinguished by the association of carbonate-rich lithologies with rare and low thickness intercalations of graphite schists and mica-rich horizons. No evidence for terrestrial deposition products is found in the units of the Stangalm Mesozoic. The exact lithological description is given in chapter 4.1. Besides of the lithological difference of the Stangalm Mesozoic s.l. and the Oberhof Lithodeme the age of the protolith should be considered. Therefore, as mentioned in Chapter 2.3 the deposition age of the Stangalm Mesozoic s.l. ranges from the uppermost Permian to the Jurassic, while the depositional age of the Stangnock Formation respective of the Oberhof Lithodeme was dated 310 – 305 Ma which corresponds to the lowermost Permian.

Another argument that should be considered is seen in (2) the peak of metamorphism, which affects both nappes (Kuster nappe & Stangalm Mesozoic s.l.) in the same way. Raman microspectroscopy data suggest for both units, maximum temperatures of metamorphism from 519±37°C to 435±39°C, as shown and discussed briefly in chapter 5.1. The Raman data from units of the DGNS in the research area show a lower temperature of metamorphism across the nappe system boundary of 380±70°C. Therefore, the Oberhof Lithodeme experienced much higher temperatures of metamorphism as the units of the DGNS have experienced, described in the literature. This indicates an earlier decoupling and deeper subduction of these parts of the former Stangnock Formation.

Like the metamorphic and thermal evolution of the units, the apparent deformation can be used as an argument to clarify the affiliation of the units. Therefore, both units show the same deformation caused by the same event.

Strong evidence for tectonic incorporation of the Oberhof Lithodeme while nappe stacking (D_{3a}) is obscured, although nearly all traces of thrusting are lost because of extensive D_{3b} shearing caused by the evolution of the shear zone. Arguments regarding to this can be found in the fact that the Oberhof Lithodeme at Mount Kuster is surrounded by Mesozoic units which can be shown by the inverse nappe stack found on the NE flank of Mount Kuster. This inverse nappe stack also can be found in lithologies of the Stangalm Mesozoic s.l. were the Weißwände Lithodeme is in hanging wall position of the Karnerboden Lithodeme (Fig. 16 A) and at the lake side where the Weißwände Lithodeme is on top of lithologies of the Murau Group (Fig. 16 B). This is good evidence for km scale (mountain ranged) isoclinal fold architecture as also described by Hollinetz (2018) in structural lower levels. The maximum temperatures of metamorphism which indicates the same peak temperature for both units indicate the same metamorphic peak and therefor the same depth of subduction during geodynamic evolution.

These facts lead to a possible model which focuses on the major ductile accretion structure bounden to D_{3a}, which got massively overprinted by the Top ESE Eo-Alpine Detachment structure related to the D_{3b} phase.

6 Conclusion

Lithological and structural geological mapping at mount Kuster and mount Hirnkopf is carried out, where a major Eo-Alpine Detachment is exposed. From structural investigations from outcrop to micro scale an interpreted evolution and deformation history of the lithologies in the research area is provided. The nappe system boundaries are classified and interpreted in terms of an Eo-Alpine Detachment where structurally lower units from the Drauzug-Gurktal Nappe System are juxtaposed against structurally higher units from the Ötztal-Bundschuh Nappe System.

The results of this study lead to following conclusions:

1) Several deformation phases from pre-Alpine (D_1 & D_2) to Eo-Alpine (D_3 & D_4) are preserved in different lithodemic units, whereby the D_{3b} phase is the dominant overprint in the research area and related to a major Top SE Detachment localised in the Stangalm Mesozoic s.l.
2) Paleopiezometry from nearly monomineralic units from the footwall and hanging wall of the Detachment is provided, which suggest the same differential stress for lithologies affected by the shear zone.
3) Raman Microspectroscopy data suggest a temperature peak of metamorphism of 519°C for units of the Oberhof Lithodeme. The Stangalm Mesozoic s.l. shows a peak at 485 °C, lower peak temperatures are determined across the nappe system boundary in hanging wall direction. Therefore, the Spielriegel Complex shows a maximum temperature of 388°C. These are the highest temperatures measured to date in the two last-mentioned units.
4) Lithologies originated from the Permian Stangnock Formation (Königstuhl Nappe) were systematically mapped and due to the grade of metamorphism assigned to the Oberhof Lithodeme, which is suggested to be a part of a new tectonic unit as structural highest unit of the Ötztal-Bundschuh Nappe system. The so called Kuster Nappe.
5) Due to the rheologic behaviour of quartz and carbonate rich lithologies in the footwall, the exhumation process is dominated by coaxial deformation driven by ductile thinning in the footwall and by non-coaxial deformation in the hanging wall, both of which are linked to a major low-angle detachment where units of the nappe stack got exhumed.
6) Comparison of the maximum thickness of outcropping units with their highly deformed equivalent lithologies show a thinning by the factor of 4 in the Stangalm Mesozoic s.l., in the Stangnock Formation, and in the Oberhof Lithodeme. Trigonometrical estimation of the distance of displacement indicates, depending on the assumed angle of the detachment an offset of approximately 60 kilometres for all three affected units.

7 References

Beck-Mannagetta, P. (1959). „Übersicht über die östlichen Gurktaler Alpen.“ – Jahrbuch der Geologischen Bundesanstalt, 102, 313–352.

Beyssac, O., B. Goffé, C. Chopin, J. N. Rouzaud (2002). “Raman spectra of carbonaceous material in metasediments: A new geothermometer.” – Journal of Metamorphic Geology, 20/9, 859–871. doi:10.1046/j.1525-1314.2002.00408.x.

Blenkinsop, T. G. (2000). „Deformation microstructures and mechanisms in minerals and rocks.” – Kluwer Academic Publishers, Dordrecht, p. 150.

Daniel, J. M., Jolivet, L., Goffe, B., Poinssot, C. (1996). “Crustal-scale strain partitioning: Foot wall deformation below the Alpine Oligo-Miocene detachment of Corsica.” – Journal of Structural Geology, 18/1, 41–59. doi: 10.1016/0191-8141(95)00075-O.

De Bresser, J. H. P, Ter Heege, J. H., Spiers C. J., (2001). “Grain size reduction by dynamic recrystallization: can it result in major rheological weakening?” – International Journal of Earth Sciences, 90, 28–45.

Decker, K. (1998). „Tektonik der spröden Kruste: Methoden der sprödtektonischen Strukturanalyse“ – Skriptum Universität Wien, 31-56.

Frimmel, H. (1987). “Strukturgeologische, geochemische und geochronologische Untersuchungen zur Entwicklungsgeschichte des NW-Randes der Gurktaler Decke (Oberostalpin).” – Dissertation. Universität Wien, p. 199.

Fritz, A. & Krainer, K. (2007). „Vegetationsgeschichtliche und florenstratigraphische Untersuchungen im Oberkarbon und Unterperm der Ost- und Südalpen (Teil 2).“ – Carinthia II, 197/117, 91–148.

Fritz, A., Boersma, M., Krainer, K. (1990). „Steinkohlenzeitliche Pflanzenfossilien aus Kärnten.“ – Sonderheft der Carinthia II, 49, p. 189.

Froitzheim, N., Plašienka, D., Schuster, R. (2008). “Alpine tectonics of the Alps and Western Carpathians.” - In: McCann, T. (Ed.): The geology of Central Europe. – Geological Society of London, 1141–1232.

Gautier, P., Brun, J., Jolivet, L. (1993). “Structure and kinematics of Upper Cenozoic extensional detachment on Naxos and Paros (Cyclades Islands, Greece).” – Tectonics, 12/5, 1180–1194. doi: 10.1029/93TC01131.

Grasemann, B., Wiesmayr, G., Draganits, E., Fusseis, F. (2004). “Classification of Refold Structures.” – The Journal of Geology, 112/1, 119–125.

Grasemann, B., Schneider, D. A., Stockli, D. F., Iglseder, C. (2012). “Miocene bivergent crustal extension in the Aegean: Evidence from the western Cyclades (Greece).” – Lithosphere, 4/1, 23–39. doi: 10.1130/L164.1.

Griesmeier, G.E.U. & Iglseder, C. (2019): „Arbeitstagung 2019 der Geologischen Bundesanstalt: Geologie des Kartenblattes GK25 Radenthein-Ost.“ – Geologischen Bundesanstalt, p. 285.

Haertel, M. & Herwegh, M. (2014). “Microfabric memory of vein quartz for strain localization in detachment faults: A case study on the Simplon fault zone.” – Journal of Structural Geology, 68/PA, 16–32. doi: 10.1016/j.jsg.2014.08.001.

Herwegh, M. & Jenni, A. (2001). “Granular flow in polymineralic rocks bearing sheet silicates: New evidence from natural examples.” – Tectonophysics, 332/3, 309–320. doi: 10.1016/S0040-1951(00)00288-2.

Hintersberger, E., Iglseder, C., Schuster, R., Huet, B. (2017). “The new database „Tectonic Boundaries” at the Geological Survey of Austria.” – Jahrbuch der Geologischen Bundesanstalt, 157, 195–207.

Hoinkes, G., Koller, F., Demény, A., Schuster, R., Miller, C., Thöni, M., Kurz, W., Krenn, K., Walter, F. (2010). „Metamorphism in the eastern Alps.” – Acta Mineralogica-Petrographica, Field Guide Series, 1, 1–47.

Hollinetz, M.S., Werdenich, M., Iglseder, C., Huet, B., Reiser, M., Schuster, R., Tropper, P., Rantitsch, G., Grasemann, B. (2019). „Bundschuh or not Bundschuh? Discussing criteria defining the Bundschuh Nappe in the light of new P-T-t data from two localities in the Gurktal Alps (Upper Austroalpine Unit, Eastern Alps).” – In: Griesmeier, G.E.U. & Iglseder, C. (Eds.): Arbeitstagung 2019 der Geologischen Bundesanstalt – Geologie des Kartenblattes GK25 Radenthein-Ost, 87– 95, Geologische Bundesanstalt, Wien.

Hollinetz, M.S. (2018). “Tectono-metamorphic evolution of the upper part of the Eo-Alpine extrusion wedge. A case study from the Oberhof window (Carinthia, Austria).” – Diplomarbeit, Universität Wien, p. 100.

Huet, B. (2015). “Strukurgeologie der Stolzalpe-Decke auf Blatt Radenthein-Ost (UTM 3106).” – Jahrbuch der Geologischen Bundesanstalt, 155, 121–145.

Iglseder, C. (2019). „Geologische und Tektonische Karte der Gurktaler Alpen 1:250.000.“ – In: Griesmeier, G.E.U. & Iglseder, C. (Eds.): Arbeitstagung 2019 der Geologischen Bundesanstalt – Geologie des Kartenblattes GK25 Radenthein-Ost, 48–54, Geologische Bundesanstalt, Wien.

Iglseder, C. & Huet, B. (2019). „Tektonische Einheiten auf GK25 Blatt Radenthein-Ost und angrenzenden Gebieten.“ – In: Griesmeier, G.E.U. & Iglseder, C. (Eds.): Arbeitstagung 2019 der Geologischen Bundesanstalt – Geologie des Kartenblattes GK25 Radenthein-Ost, 5–18, Geologische Bundesanstalt, Wien.

Iglseder, C. & Huet, B. (2015). “Evidence for Eoalpine top to the WNW thrusting and top to the ESE normal faulting in the Gurktal nappes (Drauzug-Gurktal nappe system, Upper Austro-Alpine, Austria).” – EGU series Emile Argand Conference – 12th Alpine Workshop, 13th – 19th September 2015, Montgenevre, Briancon, French Hautes-Alpes: Abstract Volume (2015), 22–23.

Iglseder, C. & Schuster, R. (2015). „Lithostratigraphy in low-grade metamorphic rocks – Examples from the Upper Austroalpine Stolzalpe Nappe and Bundschuh Nappe (Eastern Alps/Europe).“ – Berichte des Institutes für Erdwissenschaften Karl-Franzens-Universität Graz, 21, 173.

Iglseder, C., Huet, B., Rantitsch, G., Ratschbacher, L., Pfänder, J. (2016). „Age and structure of the Stolzalpe nappe – Evidence for Variscan metamorphism, Eoalpine top-to-the-WNW thrusting and top-to-the-ESE normal faulting (Gurktal Alps, Austria).” – In: Ortner, H. (Ed.): GeoTirol 2016: Annual Meeting DGGV: 25-28 September 2016, Innsbruck, Austria: Abstract Volume (2016), 137.

Iglseder, C., Huet, B., Schuster, R., Rantitsch, G., Dunkl, I., Ratschbacher, L. (2018). „A section through the uppermost Upper Austroalpine – Insights from the Gstoder, Bundschuh, Königstuhl and Stolzalpe Nappes (Gurktal Alps, Austria).“ – In: Koukal, V. & Wagreich, M. (Eds.): PANGEO AUSTRIA 2018 – Abstracts. – Berichte der Geologischen Bundesanstalt, 128, 66.

Iglseder, C., Van Husen, D., Huet, B., Knoll, T., Schönlaub, H.P. (2019). „Geologische Karte der Republik Österreich 1:25.000, Blatt Radenthein-Nordost.“ – Geologische Bundesanstalt, Wien.

Janák, M., Froitzheim, N., Lupták, B., Vrabec, M., Krogh Ravna, E.J. (2004). „First evidence for ultrahigh-pressure metamorphism in Pohorje, Slovenia: Tracing deep continental subduction in the Eastern Alps.” – Tectonics, 23, TC5014, Washington. doi: 10.1029/2004TC001641.

Jolivet, L., Daniel, J., Truffert, C., Goffé, B. (1994). “Exhumation of deep crustal metamorphic rocks and crustal extension in arc and back-arc regions.” Lithos, 33/1-3, 3–30. doi: 10.1016/0024-4937(94)90051-5.

Kabon, H. & Iglseder, C. (2019). „Fossile Floren der Stangnock-Formation in den Gurktaler Alpen (Turracher Höhe, Nesselbachgraben, Reißeck, Frauennock).“ – In: Griesmeier, G.E.U. & Iglseder, C. (Eds.): Arbeitstagung 2019 der Geologischen Bundesanstalt – Geologie des Kartenblattes GK25 Radenthein-Ost, 55–83, Geologische Bundesanstalt, Wien.

Kaindl, R. & Abart, R. (2002). “Reequilibration of fluid inclusions in garnet and kyanite from metapelites of the Radenthein Complex, Austroalpine Basement, Austria.” – Schweizerische Mineralogische und Petrographische Mitteilungen, 82, 467–486.

Koroknai, B., Neubauer, F., Genser, J., Topa, D. (1999). “Metamorphic and tectonic evolution of Austroalpine units at the western margin of the Gurktal nappe complex, Eastern Alps.” – Schweizerische mineralogische und petrographische Mitteilungen, 79, 277–295. doi: 10.5169/seals-60209.

Krainer, K. (1989). “Die fazielle Entwicklung der Oberkarbonsedimente (Stangnock-Formation) am NW-Rand der Gurktaler Decke.” – Carinthia II 179/99, 563–601.

Krenn, K., Kurz, W., Fritz, H., Hoinkes, G. (2011). “Eoalpine tectonics of the Eastern Alps: implications from the evolution of monometamorphic Austroalpine units (Schneeberg and Radenthein Complex).” – Swiss Journal of Geosciences, 104/3, 471–491, Basel.

Lopez-Sanchez, M. A. (2018). „GrainSizeTools: a Python script for grain size analysis and paleopiezometry based on grain size.” – Journal of Open Source Software, 3/30, 863, https://doi.org/10.21105/joss.00863.

Lünsdorf, N. K., Dunkl, I., Schmidt, B. C., Rantitsch, G., von Eynatten, H. (2017). “Towards a Higher Comparability of Geothermometric Data Obtained by Raman Spectroscopy of Carbonaceous Material. Part 2: A Revised Geothermometer.” – Geostandards and Geoanalytical Research, 41/4, 593–612. doi: 10.1111/ggr.12178.

Masuda T. & Fujimura A. (1981). „Microstructural development of finegrained quartz aggregates by syntectonic recrystallisation.” – Tectonophysics, 72, 105–128.

Neubauer, F.R., Koroknai, B., Genser, J., Handler, R., Topa, D. (1998). „Middle and Upper Austroalpine units of Gurktal Mountains/Nock region.” – Karpato-Balkanische Geologische Assoziation Kongress (KBGA), 16.F.1, 85–101, Salzburg.

Neubauer, F. & Pistotnik, J. (1984). “Das Altpaläozoikum und Unterkarbon des Gurktaler Deckensystems (Ostalpen) und ihre paläogeographischen Beziehungen.” – Geologische Rundschau, 73/1, 149–174. doi: 10.1007/BF01820365.

Neubauer, F. (1980). “Die Geologie des Murauer Raumes - Forschungsstand und Probleme.” – Mitteilungen Abteilung Geologisches Palaontologisches Bergbau Landesmuseum Joanneum, 41, 67–79.

Passchier, C. W. & Trouw, R. A. J. (2005). „Microtectonics 2nd ed.” – Springer Science & Business Media, p. 366. isbn: 9783540640035.

Pistotnik, J. (1973). “Zur Geologie des NW-Randes der Gurtaler Masse (Stangalm-Mesozoikum; Österreich).” Mitteilungen der geologischen Gesellschaft in Wien, 66-67, 127–141.

Rantitsch, G. & Russegger, B. (2000). „Thrust-related very low grade metamorphism within the Gurktal Nappe Complex (Eastern Alps). “ – Jahrbuch der Geologischen Bundesanstalt, 142/2, 219–225, Wien.

Rantitsch, G., Iglseder, C., Hollinetz, M.S., Huet, B., Schuster, R., Werdenich, M. (2020). „Organic metamorphism as a key for reconstructing pre-, syn- and post-orogenic processes: the Eoalpine upper plate (Eastern Alps) as a case study.” – International Journal of Earth Sciences, 109/2235-2253. doi:10.1007/s00531-020-01897-2.

Rantitsch G, Grogger W, Teichert Ch, Ebner F, Hofer C, Maurer E-M, Schaffer B, Toth M (2004). “Conversion of carbonaceous material to graphite within the Greywacke Zone of the Eastern Alps.” – International Journal of Earth Sciences, 93, 959–973. doi: 10.1007/s0053 1-004-0436-1.

Ree, J. H. (1994). “Grain boundary sliding and development of grain boundary openings in experimentally deformed octachloropropane.” – Journal of Structural Geology, 16/3, 403–418. doi: 10.1016 / 0191 - 8141(94)90044-2.

Schmid, S. M., Fügenschuh, B., Kissling, E., Schuster, R. (2004). “Tectonic map and overall architecture of the Alpine orogen.” – Swiss Journal of Geosciences, 97/1, 93–117. doi: 10.1007/s00015-004-1113-x.

Schmid, S. M., Panozzo, R., Bauer, S. (1987). “Simple shear experiments on calcite rocks: rheology and microfabric.” – Journal of Structural Geology, 9/5-6, 747–778. doi: 10.1016/0191-8141(87)90157-X.

Schönlaub, H.P. (2014a). “Stangnock-Formation.” – In: Piller, W.E. (Ed.): The lithostratigraphic units of the Austrian Stratigraphic Chart 2004 (sedimentary successions), Vol. I: The Paleozoic Era(them): 2nd Edition. – Abhandlungen der Geologischen Bundesanstalt, 66, 39–40, Wien.

Schuster, R. (1994). “Die Alpine Großüberschiebung an der Basis des Bundschuhkristallins.” Diplomarbeit. Universität Wien, 1–120. – (2015). “Zur Geologie der Ostalpen.” – Abhandlungen der Geologischen Bundesanstalt, 64, 143–165.

Schuster, R., & Frank, W. (1999). “Metamorphic evolution of the Austroalpine units east of the Tauern Window: Indications for Jurassic strike slip tectonics.” – Mitteilungen der Gesellschaft der Geologie-und Bergbaustudenten in Österreich, 42, 37–58.

Schuster, R., Kurz, W., Krenn, K., Fritz, H. (2010). “Introduction to the Geology of the Eastern Alps.” – Berichte der Geologischen Bundestanstalt, 99, 121–133.

Sean, P. L. & Matthew, J. K. (2020). “Distributed ductile thinning during thrust emplacement: A commonly overlooked exhumation mechanism.” – Geology, 48/4, 368–373. doi: 10.1130/G47022.1.

Stowasser, H. (1956). “Zur Schichtfolge, Verbreitung und Tektonik des Stangalm-Mesozoikums (Gurktaler Alpen).” – Jahrbuch der Geologischen Bundesanstalt, 99, 65–199.

Stüwe, K. & Schuster, R. (2010). “Initiation of subduction in the Alps: Continent or ocean?” Geology, 38/2, 175–178. doi: 10.1130/G30528.1.

Thöni, M. & Jagoutz, E. (1993). “Isotopic constraints for eo-Alpine high-P metamorphism in the Austroalpine nappes of the Eastern Alps: bearing on Alpine orogenesis.” Schweizerische Mineralogische und Petrographische Mitteilungen, 73/2, 177–189.

Tollmann, A. (1963). „Ostalpensynthese“. Vienna: Deuticke, p. 235. – (1977). „Die Geologie von Österreich“ - Band I: Die Zentralalpen. Vienna: Deuticke.

Tollmann, A. (1958). „Das Stangalm-Mesozoikum (Gurktaler Alpen).“ – Mitteilungen der Gesellschaft der Geologie- und Bergbaustudenten in Wien, 9, 57–74, Wien.

Twiss, R. J. (1977). „Theory and applicability of a recrystallized grain size paleopiezometer.“ – Pure and Applied Geophysics, 115, 227–244. doi: 10.1007/BF01637105.

Van Husen, D. (2019). „Eiszeitliche Entwicklung im Gebiet der Turrach zwischen dem Mur- und Draugletscher.“ – In: Griesmeier, G.E.U. & Iglseder, C. (Eds.): Arbeitstagung 2019 der Geologischen Bundesanstalt – Geologie des Kartenblattes GK25 Radenthein-Ost, 45–47.

Von Gosen, W., Haiges, K. H., Neubauer, F., Pistotnik, J., Thiedig, F. (1985). “Die tektonischen Baueinheiten am Nord- und Westrand der Gurktaler Decke (Österreich).” – Jahrbuch der Geologischen Bundesanstalt, 127, 693–699.

Walker, A. N., Rutter, E. H., Brodie, K. H. (1990). “Experimental study of grain-size sensitive flow of synthetic, hot-pressed calcite rocks.” – Geological Society, London, Special Publications 54/1, 259–284. doi: 10.1144/GSL.SP.1990.054.01.24.

Weissenbacher, M. (2015). „Strukturen der Bundschuh- und Murau Decke im Raum Flattnitz (Kärnten, Österreich).” – Masterarbeit, Universität Graz, p. 121., Graz.

8 List of Figures

9 List of Tables

10 Appendix

Point	001	001	002	003	004	004
Lithology	Qtz-Phyllit/ Quartzite	Qtz-Phyllit/ Quartzite	Dolomite	Dolomite	Calcitemarble myl	Calcitemarble myl
Comment	ca rich, refold structure		courser grained,	graphitic?, veins,	impure, Pyrit,	
Lithodemic unit	Murau	Murau	Weißwände	Weißwände	Leckenschober	Leckenschober
Nappe	Murau	Murau	Stangalm Mesozoic	Stangalm Mesozoic	Stangalm Mesozoic	Stangalm Mesozoi
Nappesystem	DG	DG	BS	BS	BS	BS
Plane (type)				S	S	S
Dip direction				069	080	066
Dip				12	27	25
Lineation (type)						Ls
Dip direction L						123
Dip L						20
Fold (type)	open	assym				
Generation	FA3	FA2				
FA dip direction	084	241				
FA dip	03	14				
AP dip direction	337	329				
AP dip	09	04				
UTM_N	5198134	5198134	5198625	5198577	5198578	5198578
UTM_E	427774	427774	427246	427222	427256	427256
Sample				MW1901	MW1902	

Point	004	004	004	004	005
Lithology	Calcitemarble myl	Calcitemarble myl	Calcitemarble myl	Calcitemarble myl	Dolomite myl
Comment					
Lithodemic unit	Leckenschober	Leckenschober	Leckenschober	Leckenschober	Leckenschober
Nappe	Stangalm Mesozoic	Stangalm Mesozoic	Stangalm Mesozoic	Stangalm Mesozoic	Stangalm Mesozoic
Nappesystem	BS	BS	BS	BS	BS
Plane (type)	S	S	S	S	S
Dip direction	125	105	052	068	234
Dip	25	01	28	10	32
Lineation (type)	Ls	Ls	Ls	Ls	
Dip direction L	104	108	122	108	
Dip L	01	04	09	10	
Fold (type)					
Generation					
FA dip direction					
FA dip					
AP dip direction					
AP dip					
UTM_N	5198578	5198578	5198578	5198578	5198625
UTM_E	427256	427256	427256	427256	427294
Sample					

Point	006	007	007	008
Lithology	Micaschist	Dolomite myl	Dolomite myl	Micaschist
Comment	contact Murau - Stangalm	shattered rock, fine joints, graphitic lense		phylonitic, course grained mica
Lithodemic unit	Murau	Weißwände	Weißwände	Murau
Nappe	Murau	Stangalm Mesozoic	Stangalm Mesozoic	Murau
Nappesystem	DG	BS	BS	DG
Plane (type)	S	S	S	S
Dip direction	168	262	268	202
Dip	33	20	44	07
Lineation (type)		Ls?		Ls
Dip direction L		337		286
Dip L		03		02
Fold (type)				iso
Generation				FA1
FA dip direction				133
FA dip				01
AP dip direction				200
AP dip				10
UTM_N	5198644	5198652	5198652	5198744
UTM_E	427326	427295	427295	426713
Sample	MW1903 (no)			

Point	008	008	008	008	008	008	008
Lithology	Micaschist	Micaschist	Micaschist	Micaschist	Micaschist	Micaschist	Micaschist
Comment							
Lithodemic unit	Murau	Murau	Murau	Murau	Murau	Murau	Murau
Nappe	Murau	Murau	Murau	Murau	Murau	Murau	Murau
Nappesystem	DG	DG	DG	DG	DG	DG	DG
Plane (type)	S	S	S	S	S	S	Sb
Dip direction	243	118	195	241	304	226	173
Dip	31	25	18	29	05	25	01
Lineation (type)	Ls	Ls	Ls	Ls	Ls	Ls	Lstr
Dip direction L	292	118	139	301	176	117	144
Dip L	11	15	09	12	01	02	02
Fold (type)	iso	iso	iso	iso	iso		
Generation	FA1	FA1	FA1	FA1	FA1		
FA dip direction	284	258	318	205	334		
FA dip	15	05	15	16	05		
AP dip direction	292	315	278	254			
AP dip	12	05	14	02			
UTM_N	5198744	5198744	5198744	5198744	5198744	5198744	5198744
UTM_E	426713	426713	426713	426713	426713	426713	426713
Sample							

Point	008	008	009	009	009	009
Lithology	Micaschist	Micaschist	Dolomite myl	Dolomite myl	Dolomite myl	Dolomite myl
Comment			flanking structure			
Lithodemic unit	Murau	Murau	Weißwände	Weißwände	Weißwände	Weißwände
Nappe	Murau	Murau	Stangalm Mesozoic	Stangalm Mesozoic	Stangalm Mesozoic	Stangalm Mesozoic
Nappesystem	DG	DG	BS	BS	BS	BS
Plane (type)	Sb	Sb	S	S	S	joint
Dip direction	118	126	238	258	247	134
Dip	35	31	12	09	12	85
Lineation (type)	Lstr	Lstr	Ls	Ls		
Dip direction L	133	130	294	297	298	
Dip L	26	32	09	06	07	
Fold (type)						
Generation						
UTM_N	5198744	5198744	5198730	5198730	5198730	5198730
UTM_E	426713	426713	426656	426656	426656	426656
Sample			Mw1911			

Point	009	009	009	009	009	009	009
Lithology	Dolomite myl	Dolomite myl	Micaschist	Micaschist	Micaschist	Micaschist	Micaschist
Comment			contact Stangalm - Murau				
Lithodemic unit	Weißwände	Weißwände	Murau	Murau	Murau	Murau	Murau
Nappe	Stangalm Mesozoic	Stangalm Mesozoic	Murau	Murau	Murau	Murau	Murau
Nappesystem	BS	BS	DG	DG	DG	DG	DG
Plane (type)	joint	contactplane S	S	S	S	S	S
Dip direction	130	354	294	334	311	286	272
Dip	87	04	03	10	12	17	18
Lineation (type)			Ls	Ls			
Dip direction L			217	231			
Dip L			04	05			
UTM_N	5198730	5198730	5198730	5198730	5198730	5198730	5198730
UTM_E	426656	426656	426656	426656	426656	426656	426656
Sample							

Point	009	009	009	009	009	010	010
Lithology	Micaschist	Micaschist	Micaschist	Micaschist	Micaschist	Dolomite myl	Dolomite myl
Comment							
Lithodemic unit	Murau	Murau	Murau	Murau	Murau	Weißwände	Weißwände
Nappe	Murau	Murau	Murau	Murau	Murau	Stangalm Mesozoic	Stangalm Mesozoi
Nappesystem	DG	DG	DG	DG	DG	BS	BS
Plane (type)	Sb	Sb	Sb	Sb	Sb	S	S
Dip direction	150	092	120	122	117	209	219
Dip	20	28	25	20	18	12	05
Lineation (type)	Lstr	Lstr	Lstr	Lstr	Lstr		Ls
Dip direction L	139	135	125	123	130		315
Dip L	19	20	30	19	18		01
Fold (type)							
Generation							
FA dip direction							
FA dip							
AP dip direction							
AP dip							
UTM_N	5198730	5198730	5198730	5198730	5198730	5198611	5198611
UTM_E	426656	426656	426656	426656	426656	426347	426347
Sample							

Point	010	010	010	010	010.1	010.2
Lithology	Dolomite myl	Dolomite myl	Dolomite myl	Dolomite myl	Dolomite myl	Dolomite myl
Comment						
Lithodemic unit	Weißwände	Weißwände	Weißwände	Weißwände	Weißwände	Weißwände
Nappe	Stangalm Mesozoic	Stangalm Mesozoic	Stangalm Mesozoic	Stangalm Mesozoic	Stangalm Mesozoic	Stangalm Mesozoi
Nappesystem	BS	BS	BS	BS	BS	BS
Plane (type)	S	joint	joint	joint	S	
Dip direction	222	125	123	124	272	
Dip	11	82	79	76	02	
Lineation (type)	Ls				Ls	
Dip direction L	304				314	
Dip L	01				01	
Fold (type)						
Generation						
FA dip direction						
FA dip						
AP dip direction						
AP dip						
UTM_N	5198611	5198611	5198611	5198611	5198611	5198611
UTM_E	426347	426347	426347	426347	426347	426347
Sample						

Point	011	011	011	011	011	011
Lithology	Dolomite myl	Dolomite myl	Dolomite myl	Dolomite myl	Dolomite myl	Dolomite myl
Comment						
Lithodemic unit	Weißwände	Weißwände	Weißwände	Weißwände	Weißwände	Weißwände
Nappe	Stangalm Mesozoic	Stangalm Mesozoic	Stangalm Mesozoic	Stangalm Mesozoic	Stangalm Mesozoic	Stangalm Mesozoi
Nappesystem	BS	BS	BS	BS	BS	BS
Plane (type)	S	S	S	S	S	S
Dip direction	249	232	204	221	216	221
Dip	37	15	15	30	29	40
Lineation (type)	Ls		Ls	Ls	Ls	Ls
Dip direction L	319		136	312	314	303
Dip L	15		08	01	01	01
Fold (type)						
Generation						
FA dip direction						
FA dip						
AP dip direction						
AP dip						
UTM_N	5198431	5198431	5198431	5198431	5198431	5198431
UTM_E	426787	426787	426787	426787	426787	426787
Sample	MW1904					

Point	011	011	011	011	011.1	011.2
Lithology	Dolomite myl	Dolomite myl	Dolomite myl	Dolomite myl	Dolomite myl	Dolomite myl
Comment						
Lithodemic unit	Weißwände	Weißwände	Weißwände	Weißwände	Weißwände	Weißwände
Nappe	Stangalm Mesozoic	Stangalm Mesozoic	Stangalm Mesozoic	Stangalm Mesozoic	Stangalm Mesozoic	Stangalm Mesozoi
Nappesystem	BS	BS	BS	BS	BS	BS
Plane (type)	joint	joint	joint	joint	S	joint
Dip direction	291	295	300	112	312	114
Dip	85	82	84	86	30	85
Lineation (type)						
Dip direction L					324	
Dip L					15	
Fold (type)						
Generation						
FA dip direction						
FA dip						
AP dip direction						
AP dip						
UTM_N	5198431	5198431	5198431	5198431	5198431	5198431
UTM_E	426787	426787	426787	426787	426787	426787
Sample						

Point	012	013	013
Lithology	Dolomite myl	Dolomite	Dolomite
Comment		h, s-parallel veins, mica on S-planes	
Lithodemic unit	Weißwände	Weißwände Karnerboden	Weißwände/Karnerboden
Nappe	Stangalm Mesozoic	Stangalm Mesozoic	Stangalm Mesozoic
Nappesystem	BS	BS	BS
Plane (type)	joint	joint	S
Dip direction	294	293	245
Dip	90	89	22
Lineation (type)			
Dip direction L			
Dip L			
UTM_N	5198431	5198332	5198332
UTM_E	426787	426970	426970
Sample		MW1905	

Point	013	013	013	013	014
Lithology	Dolomite	Dolomite	Dolomite	Dolomite	Dolomite
Comment					greyisch, Tremolit in joints
Lithodemic unit	Weißwände/Karnerboden	Weißwände/Karnerboden	Weißwände/Karnerboden	Weißwände/Karnerboden	Weißwände/Karnerboden
Nappe	Stangalm Mesozoic	Stangalm Mesozoic	Stangalm Mesozoic	Stangalm Mesozoic	Stangalm Mesozoic
Nappesystem	BS	BS	BS	BS	BS
Plane (type)	S	S	S	joint	S
Dip direction	293	280	324	288	355
Dip	17	20	23	90	20
Lineation (type)		Ls	Ls		Ls
Dip direction L		328	335		275
Dip L		15	20		03
Fold (type)					
Generation					
UTM_N	5198332	5198332	5198332	5198332	5198299
UTM_E	426970	426970	426970	426970	426991
Sample					MW1906

Point	014	015	015	015	015
Lithology	Dolomite	Calcitemarble myl	Calcitemarble myl	Calcitemarble myl	Calcitemarble myl
Comment		isoklinal folds, flanking structure			
Lithodemic unit	Weißwände/ Karnerboden	Leckenschober	Leckenschober	Leckenschober	Leckenschober
Nappe	Stangalm Mesozoic	Stangalm Mesozoic	Stangalm Mesozoic	Stangalm Mesozoic	Stangalm Mesozoic
Nappesystem	BS	BS	BS	BS	BS
Plane (type)	joint	S	S	S	S
Dip direction	115	130	122	186	112
Dip	88	41	45	40	42
Lineation (type)		Lcren2	Lcren2	Lcren2	Lcren2
Dip direction L		087	071	124	079
Dip L		37	30	25	35
Fold (type)		iso			iso
Generation		FA3			FA3
FA dip direction		099			072
FA dip		15			23
AP dip direction		334			110
AP dip		33			40
UTM_N	5198299	5197969	5197969	5197969	5197969
UTM_E	426991	427024	427024	427024	427024
Sample		MW1907			

Point	015	015	016	017	017	017
Lithology	Calcitemarble my	Calcitemarble	Qtz-Phyllit	Qtz-Phyllit	Qtz-Phyllit	Qtz-Phyllit
Comment			2 fold generations		FA1-FA2 / FA2-FA3 FIP	Foto SW
Lithodemic unit	Leckenschober	Leckenschober	Spielriegel	Spielriegel	Spielriegel	Spielriegel
Nappe	Stangalm Mesozc	Stangalm Mesozoic	Stolzalpe	Stolzalpe	Stolzalpe	Stolzalpe
Nappesystem	BS	BS	DG	DG	DG	DG
Plane (type)	S	S			S	
Dip direction	145	122			158	
Dip	40	30			09	
Lineation (type)	Lcren2	Lcren2			Lint	
Dip direction L	078	082			147	
Dip L	28	25			04	
Fold (type)	iso	iso	iso	assym	iso	assym
Generation	FA3	FA3	FA1	FA2	FA1	FA2
FA dip direction	076	061	119	228	234	187
FA dip	20	10	15	22	10	06
AP dip direction	140	120	148	251	222	226
AP dip	38	33	22	34	18	32
UTM_N	5197969	5197969	5197884	5197884	5197884	5197884
UTM_E	427024	427024	427008	427008	427008	427008
Sample						

Point	017	018	018	018	018	018
Lithology	Qtz-Phyllit	Qtz-Phyllit	Qtz-Phyllit	Qtz-Phyllit	Qtz-Phyllit	Qtz-Phyllit
Comment			nappe system boundary iso folded	FA2 - FA3 hook shaped FIP		
Lithodemic unit	Spielriegel	Spielriegel	Spielriegel - Leckenschober	Spielriegel	Spielriegel	Spielriegel
Nappe	Stolzalpe	Stolzalpe	Stolzalpe - Stangalm Mesozioc	Stolzalpe	Stolzalpe	Stolzalpe
Nappesystem	DG	DG	DG-BS	DG	DG	DG
Plane (type)		S	S	S		
Dip direction		111	088	208		
Dip		27	10	09		
Lineation (type)		Lcren2	Ls	Ls		
Dip direction L		059	138	129		
Dip L		10	09	04		
Fold (type)	open	open	open	open	iso	assym
Generation	FA3	FA3	FA4	FA3	FA1	FA2
FA dip direction	084	062	090	074	165	287
FA dip	01	13	08	08	18	17
AP dip direction	309	328	140	344	240	251
AP dip	21	13	10	37	44	21
UTM_N	5197884	5197866	5197866	5197866	5197866	5197866
UTM_E	427008	427115	427115	427115	427115	427115
Sample		MW1910				

Point	018	018	018	018	018	018
Lithology	Qtz-Phyllit	Calcitemarble myl	Calcitemarble myl	Calcitemarble myl	Calcitemarble myl	Calcitemarble myl
Comment					s-folds	z-folds
Lithodemic unit	Spielriegel	Leckenschober	Leckenschober	Leckenschober	Leckenschober	Leckenschober
Nappe	Stolzalpe	Stangalm Mesozoic	Stangalm Mesozoic	Stangalm Mesozoi	Stangalm Mesozoic	Stangalm Mesozoic
Nappesystem	DG	BS	BS	BS	BS	BS
Plane (type)		S		S	S	S
Dip direction		082		204	188	239
Dip		05		40	33	22
Lineation (type)		Lcren2	Ls		Ls	Ls
Dip direction L		064	124		104	294
Dip L		06	10		07	20
Fold (type)	open			iso		iso
Generation	FA3			FA3		FA4
FA dip direction	305			130		290
FA dip	24			08		20
AP dip direction	338			200		240
AP dip	28			30		20
UTM_N	5197866	5197866	5197866	5197866	5197866	5197866
UTM_E	427115	427115	427115	427115	427115	427115
Sample		MW1909				

Point	019	020	021	022	023	023
Lithology	Dolomite	Quartzite	Graphitschist	Micaschist/ Quartzit	Dolomite myl	Dolomite myl
Comment	greyisch	isoklinal folded	qtz rich, Boulders			
Lithodemic unit	Karnerboden	Oberhof	Oberhof	Murau	Weißwände	Weißwände
Nappe	tangalm Mesozo	Königsstuhl	Königsstuhl	Murau	Stangalm Mesozoic	Stangalm Mesozoic
Nappesystem	BS	DG	DG	DG	BS	BS
Plane (type)		S			S	joint
Dip direction		161			122	302
Dip		10			06	82
Lineation (type)		Ls			L	
Dip direction L		117			060	
Dip L		07			02	
Fold (type)						
Generation						
UTM_N	5198501	5198454	5198513	5197939	5198352	5198352
UTM_E	427232	427196	427088	427841	427464	427464
Sample			MW1912			

Point	023	023	024	024	024	024
Lithology	Dolomite myl	Dolomite myl	Calcitemarble myl	Calcitemarble myl	Calcitemarble myl	Calcitemarble myl
Comment			impure			
Lithodemic unit	Weißwände	Weißwände	Leckenschober	Leckenschober	Leckenschober	Leckenschober
Nappe	Stangalm Mesozoic	Stangalm Mesozoic	Stangalm Mesozoic	Stangalm Mesozoi	Stangalm Mesozoic	Stangalm Mesozoic
Nappesystem	BS	BS	BS	BS	BS	BS
Plane (type)	joint	joint	S	S?	S	
Dip direction	304	316	134	304	254	
Dip	85	80	01	12	04	
Lineation (type)			L		L	
Dip direction L			081		350	
Dip L			05		03	
Fold (type)					iso	iso
Generation					FA3	FA3
FA dip direction					250	248
FA dip					25	10
UTM_N	5198352	5198352	5198347	5198347	5198347	5198347
UTM_E	427464	427464	427461	427461	427461	427461
Sample						

Point	024	025	025	026
Lithology	Calcitemarble myl	Dolomite - Calcitmarble	Dolomite - Calcitmarble	Quartzite
Comment	Karnerboden-Leckenschober	Karnerboden-Leckenschober, Dolomitelense		Blockwerk
Lithodemic unit	Karnerboden - Leckenschober	Karnerboden - Leckenschober	Karnerboden - Leckenschober	Oberhof
Nappe	Stangalm Mesozoic	Stangalm Mesozoic	Stangalm Mesozoic	Königsstuhl
Nappesystem	BS	BS	BS	DG
Plane (type)	contactplane S	S?		
Dip direction	182	194	322	
Dip	06	17	26	
Lineation (type)		Ls		
Dip direction L		258		
Dip L		30		
Fold (type)	iso	iso		
Generation	FA3	FA3		
FA dip direction	220	260		
FA dip	06	30		
AP dip direction	152	264		
AP dip	10	42		
UTM_N	5198347	5198319	5198319	5198321
UTM_E	427461	427485	427485	427499
Sample				

Point	027	027	027	028	029
Lithology	Quartzite	Quartzite	Quartzite	Quartzite	Dolomite
Comment	meta conglomerate, folded, Qtz-clasts				greyisch veins
Lithodemic unit	Oberhof	Oberhof	Oberhof	Spielriegel	Weißwände
Nappe	Königsstuhl	Königsstuhl	Königsstuhl	Stolzalpe	Stangalm Mesozoic
Nappesystem	DG	DG	DG	DG	BS
Plane (type)	S	S	S	S	S
Dip direction	242	242	235	236	012
Dip	27	25	19	17	32
Lineation (type)	Ls	Ls	Ls		
Dip direction L	270	244	250		
Dip L	25	16	19		
Fold (type)	iso	iso			
Generation	FA3	FA3			
FA dip direction	243	256			
FA dip	05	05			
AP dip direction	240				
AP dip	30				
UTM_N	5197944	5197944	5197944	5197909	5198379
UTM_E	427692	427692	427692	427684	426686
Sample				MW1913	

Point	029	029	029	029	030
Lithology	Dolomite	Dolomite	Dolomite	Dolomite	Dolomite myl
Comment					
Lithodemic unit	Weißwände/ Karnerboden	Weißwände/ Karnerboden	Weißwände/ Karnerboden	Weißwände/ Karnerboden	Weißwände
Nappe	Stangalm Mesozoic	Stangalm Mesozoic	Stangalm Mesozoic	Stangalm Mesozoic	Stangalm Mesozoic
Nappesystem	BS	BS	BS	BS	BS
Plane (type)	S	S	joint	joint	S?
Dip direction	358	224	104	300	008
Dip	20	15	89	85	40
Lineation (type)	Ls	Ls			
Dip direction L	294	302			
Dip L	10	10			
Fold (type)					
Generation					
FA dip direction					
FA dip					
AP dip direction					
AP dip					
UTM_N	5198379	5198379	5198379	5198379	5198352
UTM_E	426686	426686	426686	426686	426519
Sample					

Point	030	030	031	032
Lithology	Dolomite myl	Dolomite myl	Dolomite	Dolomite
Comment			less deformed	
Lithodemic unit	Weißwände	Weißwände	Karnerboden	Karnerboden
Nappe	Stangalm Mesozoic	Stangalm Mesozoi	Stangalm Mesozoic	Stangalm Mesozoic
Nappesystem	BS	BS	BS	BS
Plane (type)	S	S		
Dip direction	224	270		
Dip	02	10		
Lineation (type)		Ls		
Dip direction L		270		
Dip L		08		
Fold (type)				
Generation				
FA dip direction				
FA dip				
UTM_N	5198352	5198352	5198250	5198177
UTM_E	426519	426519	427237	427261
Sample				

Point	033	033	034	034
Lithology	Dolomite/ Calcitmarble	Dolomite/ Calcitmarble	Qtz Phyllit/Micaschist	Qtz Phyllit/Micaschist
Comment	contact		corse grained mica	
Lithodemic unit	Karnerboden - Leckenschober	Karnerboden - Leckenschober	Murau?/ Bockbühel?	Murau?/ Bockbühel?
Nappe	Stangalm Mesozoic	Stangalm Mesozoic		
Nappesystem	BS	BS	DG/BS	DG/BS
Plane (type)	S	S	S	S
Dip direction	010	356	204	307
Dip	40	43	02	11
Lineation (type)	Ls	Ls	Ls	
Dip direction L	094	260	280	
Dip L	10	02	02	
Fold (type)				
Generation			FA3	FA3
FA dip direction			235	250
FA dip			05	01
AP dip direction			328	257
AP dip			08	10
UTM_N	5198149	5198149	5198605	5198605
UTM_E	427259	427259	426767	426767
Sample				

Point	034	034	034	034	035
Lithology	Qtz Phyllit	Qtz Phyllit/Micaschist	Qtz Phyllit/Micaschis	Micaschist	Dolomite/Dolomite dark
Comment					Weißwände-Karnerboden
Lithodemic unit	Murau?/ Bockbühel?	Murau?/ Bockbühel?	Murau?/ Bockbühel?	Murau?/ Bockbühel?	Weißwände - Karnerboden
Nappe					Stangalm Mesozoic
Nappesystem	DG/BS	DG/BS	DG/BS	DG/BS	BS
Plane (type)	S	S	S	Sb	S
Dip direction	277	148	289	320	191
Dip	22	20	30	01	17
Lineation (type)					Ls
Dip direction L					122
Dip L					07
FA dip direction	249				
FA dip	08				
AP dip direction	319				
AP dip	23				
UTM_N	5198605	5198605	5198605	5198605	5198525
UTM_E	426767	426767	426767	426767	426893
Sample					

Point	035	035	035	035
Lithology	Dolomite/Dolomite dark	Dolomite/Dolomite dark	Dolomite/Dolomite dark	Dolomite/Dolomit e dark
Comment	extension veins - Calcite			
Lithodemic unit	Weißwände - Karnerboden	Weißwände - Karnerboden	Weißwände - Karnerboden	Weißwände - Karnerboden
Nappe	Stangalm Mesozoic	Stangalm Mesozoic	Stangalm Mesozoic	Stangalm Mesozoic
Nappesystem	BS	BS	BS	BS
Plane (type)	S	S	joint	joint
Dip direction	193	202	315	272
Dip	07	16	89	70
Lineation (type)	Ls	Ls		
Dip direction L	119	120		
Dip L	01	04		
Fold (type)				
Generation				
FA dip direction				
AP dip				
UTM_N	5198525	5198525	5198525	5198525
UTM_E	426893	426893	426893	426893
Sample				

Point	035	035	035	036	037
Lithology	Dolomite/ Dolomite dark	Dolomite/ Dolomite dark	Dolomite/ Dolomite dark	Dolomite	Dolomite dark
Comment				greyisch	less deformed
Lithodemic unit	Weißwände - Karnerboden	Weißwände - Karnerboden	Weißwände - Karnerboden	Weißwände	Karnerboden
Nappe	Stangalm Mesozoic	Stangalm Mesozoic	Stangalm Mesozoic	Stangalm Mesozoic	Stangalm Mesozoic
Nappesystem	BS	BS	BS	BS	BS
Plane (type)	contactplane S	S	S	S	S
Dip direction	193	213	188	207	124
Dip	23	14	28	22	29
Lineation (type)		Ls	Ls		Ls
Dip direction L		139	121		130
Dip L		02	15		21
Fold (type)					
Generation					
UTM_N	5198525	5198525	5198525	5198359	5198073
UTM_E	426893	426893	426893	426990	427014
Sample					

Point	037.1	037.2	037.3	037.3	037.3
Lithology	Dolomite dark	Dolomite dark	Dolomite dark myl	Dolomite dark myl	Dolomite dark myl
Comment	increasing mylonitisation				
Lithodemic unit	Karnerboden	Karnerboden	Karnerboden	Karnerboden	Karnerboden
Nappe	Stangalm Mesozoic	Stangalm Mesozoic	Stangalm Mesozoic	Stangalm Mesozoic	Stangalm Mesozoic
Nappesystem	BS	BS	BS	BS	BS
Plane (type)	S		S	S	S
Dip direction	038		201	273	257
Dip	30		03	11	19
Lineation (type)			Ls		Ls
Dip direction L	100		084		284
Dip L	13		02		10
Fold (type)					
Generation					
FA dip direction					
FA dip					
AP dip direction					
AP dip					
UTM_N	5198128	5198128	5198104	5198104	5198104
UTM_E	426957	426861	426642	426642	426642
Sample					

Point	037.3	038	038	038.1	038.2	039
Lithology	Dolomite dark myl	Dolomite dark	Dolomite dark	Dolomite dark	Dolomite, Calcitemarble	Dolomite dark
Comment		courser grained			Leckenschober - Karnerboden	mylonitic
Lithodemic unit	Karnerboden	Karnerboden	Karnerboden	Karnerboden	Leckenschober - Karnerboden	Karnerboden
Nappe	Stangalm Mesozoic	Stangalm Mesozoi	Stangalm Mesozoic	Stangalm Mesozoic	Stangalm Mesozoic	Stangalm Mesozoic
Nappesystem	BS	BS	BS	BS	BS	BS
Plane (type)	joint	S	S	S		jointset1
Dip direction	286	277	292	276		106
Dip	87	20	28	28		84
Lineation (type)			Ls	Ls		
Dip direction L			296	312		
Dip L			25	01		
Fold (type)						
Generation						
UTM_N	5198104	5198051	5198051	5198051	5198051	5198171
UTM_E	426642	426567	426567	426567	426567	426542
Sample		MW1914				

Point	039	039	039	040	041	041
Lithology	Dolomite dark	Dolomite dark	Dolomite dark	Dolomite dark	Calcitmarble	Calcitmarble
Comment				course grained		
Lithodemic unit	Karnerboden	Karnerboden	Karnerboden	Karnerboden	Leckenschober	Leckenschober
Nappe	Stangalm Mesozoic	Stangalm Mesozoic	Stangalm Mesozoic	Stangalm Mesozoic	Stangalm Mesozoic	Stangalm Mesozoi
Nappesystsm	BS	BS	BS	BS	BS	BS
Plane (type)	jointset2	S	S		S fold limb	S fold limb
Dip direction	202	332	320		265	312
Dip	50	07	16		36	85
Lineation (type)		Ls	Ls		L	L
Dip direction L		270	292		246	226
Dip L		05	15		33	14
Fold (type)						
Generation						
FA dip direction						
FA dip						
AP dip direction						
AP dip						
UTM_N	5198171	5198171	5198171	5198228	5197980	5197980
UTM_E	426542	426542	426542	426663	426571	426571
Sample						

Point	041	041	041.1	042	042	042
Lithology	Calcitmarble	Calcitmarble	Calcitmarble	Calcitmarble	Calcitmarble	Calcitmarble
Comment				isoclinal folded		
Lithodemic unit	Leckenschober	Leckenschober	Leckenschober	Leckenschober	Leckenschober	Leckenschober
Nappe	Stangalm Mesozoic	Stangalm Mesozoic	Stangalm Mesozoic	Stangalm Mesozoic	Stangalm Mesozoic	Stangalm Mesozoi
Nappesystem	BS	BS	BS	BS	BS	BS
Plane (type)	S			S		
Dip direction	208			281		
Dip	45			23		
Lineation (type)	L			L		
Dip direction L	274			262		
Dip L	20			21		
Fold (type)	iso	iso		iso	iso	iso
Generation	FA3	FA3		FA3	FA3	FA3
FA dip direction	214	244		285	281	288
FA dip	39	14		05	04	10
AP dip direction	268			006	010	346
AP dip	65			83	86	89
UTM_N	5197980	5197980	5197980	5197906	5197906	5197906
UTM_E	426571	426571	426571	426574	426574	426574
Sample						

Point	042	042	043	044	044
Lithology	Calcitmarble	Calcitmarble	Calcitmarble	Qtz-Phyllit	Qtz-Phyllit
Comment			with Phyllitflachsen	Spielriegel	
Lithodemic unit	Leckenschober	Leckenschober	Leckenschober	Spielriegel - Leckenschober	Spielriegel - Leckenscher
Nappe	Stangalm Mesozoic	Stangalm Mesozoic	Stangalm Mesozoic	Stolzalpe - Stangalm Mesozioc	lpe - Stangalm Me
Nappesystem	BS	BS	BS	DG-BS	DG-BS
Plane (type)			S	S	
Dip direction			192	222	
Dip			80	35	
Lineation (type)			L	Ls	Lcren1
Dip direction L			274	105	284
Dip L			21	03	05
Fold (type)	iso	iso			
Generation	FA3	FA3			
FA dip direction	275	274			
FA dip	06	28			
AP dip direction		012			
AP dip		87			
UTM_N	5197906	5197906	5197851	5197847	5197847
UTM_E	426574	426574	426583	426579	426579
Sample			MW1915		

Point	045	046	046	047	047	047	048
Lithology	Qtz-Phyllit	Qtz-Phyllit	Qtz-Phyllit	Qtz-Phyllit	Qtz-Phyllit	Qtz-Phyllit	Qtz-Phyllit
Comment			2 foldings			Boulders	
Lithodemic unit	Spielriegel	Spielriegel	Spielriegel	Spielriegel	Spielriegel	Spielriegel	Spielriegel
Nappe	Stolzalpe	Stolzalpe	Stolzalpe	Stolzalpe	Stolzalpe	Stolzalpe	Stolzalpe
Nappesystem	DG	DG	DG	DG	DG	DG	DG
Plane (type)	S	S	S	S	S	Sb	
Dip direction	148	272	240	236	286	054	
Dip	25	17	22	25	32	06	
Lineation (type)	Lcren1	Lcren1	Ls				
Dip direction L	288	281	150				
Dip L	07	15	10				
Fold (type)		assym		assym			
Generation		FA2		FA2			
FA dip direction		249		240			
FA dip		15		22			
AP dip direction		245		275			
AP dip		25		32			
UTM_N	5197779	5197701	5197701	5197763	5197763	5197763	5197763
UTM_E	426612	426651	426651	426739	426739	426739	426739
Sample							

Point	049	049	050	051	052	053
Lithology	Qtz-Phyllit	Qtz-Phyllit	Qtz-Phyllit	Calcitmarble	Calcitmarble	Calcitmarble, Qtz-Phyllit
Comment				Phyllitflachsen	Phyllitflachsen	
Lithodemic unit	Spielriegel	Spielriegel	Spielriegel	Leckenschober	Leckenschober	enschober - Spielr
Nappe	Stolzalpe	Stolzalpe	Stolzalpe	Stangalm Mesozoic	Stangalm Mesozoic	alm Mesozoic-Stol
Nappesystem	DG	DG	DG	BS	BS	BS-DG
Plane (type)	S	S	S		S	nes with phyllitflac
Dip direction	224	195	110		178	
Dip	23	30	16		47	
Lineation (type)	Lcren1	Lcren1	Ls			
Dip direction L	292	272	120			
Dip L	10	01	15			
Fold (type)						
Generation						
UTM_N	5197909	5197909	5197911	5197973	5197952	5197955
UTM_E	426756	426756	426762	426757	426796	426821
Sample						MW1917 (no)

Point	054	055	056	056	056	057	057
Lithology	Qtz-Phyllit	Qtz-Phyllit	Qtz-Phyllit	Qtz-Phyllit	Qtz-Phyllit	Qtz-Phyllit	Dolomite myl
Comment	myl?						Mica on S-planes
Lithodemic unit	Spielriegel	Spielriegel	Spielriegel	Spielriegel	Spielriegel	Spielriegel	Weißwände
Nappe	Stolzalpe	Stolzalpe	Stolzalpe	Stolzalpe	Stolzalpe	Stolzalpe	Stangalm Mesozoi
Nappesystem	DG	DG	DG	DG	DG	DG	BS
Plane (type)	S		S	S	S	Sb	S
Dip direction	198		155	291	280	114	004
Dip	20		25	13	40	10	15
Lineation (type)	Ls		Ls	Lcren1		Lstr	Ls
Dip direction L	110		130	280		133	360
Dip L	03		21	10		12	03
Fold (type)			iso	open			
Generation			FA1	FA3			
FA dip direction			285	141			
FA dip			20	01			
AP dip direction			286	180			
AP dip			18	20			
UTM_N	5197930	5197953	5197880	5197880	5197880	5197880	5198902
UTM_E	426797	426834	426937	426937	426937	426937	426623
Sample							

Point	057	057	057	057	058	058
Lithology	Dolomite myl	Dolomite myl	Dolomite myl	Dolomite myl	Micaschist	Micaschist
Comment				course grained mica, S-C-Fabric		
Lithodemic unit	Weißwände	Weißwände	Weißwände	Weißwänd	Murau	Murau
Nappe	Stangalm Mesozoic	Stangalm Mesozoic	Stangalm Mesozoic	Stangalm Mesozoic	Murau	Murau
Nappesystem	BS	BS	BS	BS	DG	DG
Plane (type)	S	S	joint	S	S	S
Dip direction	017	041	129	290	221	249
Dip	15	20	87	15	14	04
Lineation (type)	Ls	L		Ls	Lcren	
Dip direction L	295	114		294	134	
Dip L	02	03		13	05	
Fold (type)					iso	iso
Generation					FA1	FA1
FA dip direction					306	298
FA dip					11	17
AP dip direction					248	
AP dip					10	
UTM_N	5198902	5198902	5198902	5198902	5198822	5198822
UTM_E	426623	426623	426623	426623	426665	426665
Sample						

Point	058	059	060	061	061	062
Lithology	Micaschist	Qtz-Phyllit	Phyllit	Qtz-chlorite-Phyllit	Qtz-chlorite-Phyllit	Qtz-chlorite-Phyllit
Comment	myl ,Bolders (		Excavation	Boulders		Fe-rich qtz veins
Lithodemic unit	Murau	Spielriegel	Spielriegel	Spielriegel	Spielriegel	Spielriegel
Nappe	Murau	Stolzalpe	Stolzalpe	Stolzalpe	Stolzalpe	Stolzalpe
Nappesystem	DG	DG	DG	DG	DG	DG
Plane (type)	Sb		S	S		S
Dip direction	254		203	180	160	255
Dip	30		80	56	50	30
Lineation (type)	Lstr			L	L	L
Dip direction L	143		240	134	190	265
Dip L	21		70	50	25	25
Fold (type)						
Generation						
FA dip direction						
FA dip						
AP dip direction						
AP dip						
UTM_N	5198822	5198052	5197373	5197191	5197191	5197144
UTM_E	426665	427688	427580	427515	427515	427487
Sample						

Point	062	063	064	065	066	067
Lithology	Qtz-chlorite-Phyllit	Qtz-chlorite-Phyllit	Qtz-chlorite-Phyllit	Qtz-chlorite-Phyllit	Phyllit Excavation	Qtz-chlorite-Phyllit
Comment			Qtz veins		folded Qtz veins	fabric, slope move
Lithodemic unit	Spielriegel	Spielriegel	Spielriegel	Spielriegel	Spielriegel	Spielriegel
Nappe	Stolzalpe	Stolzalpe	Stolzalpe	Stolzalpe	Stolzalpe	Stolzalpe
Nappesystem	DG	DG	DG	DG	DG	DG
Plane (type)	S	S				S
Dip direction	288	115				304
Dip	20	30				19
Lineation (type)	L	L				L
Dip direction L	308	135				269
Dip L	30	25				13
Fold (type)						
Generation						
FA dip direction						
FA dip						
AP dip direction						
AP dip						
UTM_N	5197144	5197072	5196904	5196991	5196990	5197043
UTM_E	427487	427397	427236	427171	427065	426805
Sample						

Point	067	067	067	068	069	069
Lithology	Qtz-chlorite-Phyllit	Qtz-chlorite-Phyllit	Qtz-chlorite-Phyllit	Qtz-chlorite-Phyllit	Qtz-chlorite-Phyllit	Qtz-chlorite-Phyllit
Comment						
Lithodemic unit	Spielriegel	Spielriegel	Spielriegel	Spielriegel	Spielriegel	Spielriegel
Nappe	Stolzalpe	Stolzalpe	Stolzalpe	Stolzalpe	Stolzalpe	Stolzalpe
Nappesystem	DG	DG	DG	DG	DG	DG
Plane (type)	S	S	S			
Dip direction	213	150	097			
Dip	21	30	26			
Lineation (type)			L			
Dip direction L			113			
Dip L			27			
Fold (type)					assym	iso
Generation					FA2	FA1
FA dip direction					294	187
FA dip					19	20
AP dip direction					019	278
AP dip					05	80
UTM_N	5197043	5197043	5197043	5196955	5197103	5197103
UTM_E	426805	426805	426805	426699	427362	427362
Sample						

Point	070	071	072	073	073
Lithology	Qtz-chlorite-Phyllit	Calcitemarble	Dolomite	Dolomite	Calcitmarble
Comment		with Phyllitflachsen, Boulders (m)	Breccia, Qtz veins,	folded	footwall
Lithodemic unit	Spielriegel	Leckenschober	Karnerboden	Karnerboden	Leckenschober
Nappe	Stolzalpe	Stangalm Mesozoic	Stangalm Mesozoic	Stangalm Mesozoic	Stangalm Mesozoi
Nappesystem	DG	BS	BS	BS	BS
Plane (type)	S				S
Dip direction	235				198
Dip	23				45
Lineation (type)	Lcren				L
Dip direction L	148				106
Dip L	12				10
Fold (type)	assym				iso
Generation	FA2				FA3
FA dip direction	329				104
FA dip	11				04
AP dip direction					228
AP dip					55
UTM_N	5197529	5197681	5197782	5197799	5197799
UTM_E	427474	427499	427541	427531	427531
Sample					

Point	073	073	073	073	073	073
Lithology	Calcitmarble	Calcitmarble	Calcitmarble	Calcitmarble	Calcitmarble	Calcitmarble with phyllitflachsen
Comment			hanging wall			
Lithodemic unit	Leckenschober	Leckenschober	Leckenschober	Leckenschober	Leckenschober	Leckenschober
Nappe	Stangalm Mesozoic	Stangalm Mesozoic	Stangalm Mesozoic	Stangalm Mesozoic	Stangalm Mesozoi	Stangalm Mesozoic
Nappesystem	BS	BS	BS	BS	BS	BS
Plane (type)	S	S	S	S	S	S
Dip direction	184	190	197	200	206	162
Dip	40	42	54	40	60	53
Lineation (type)	L	L	L	L	Ls	L
Dip direction L	112	088	111	106	287	108
Dip L	11	15	12	01	20	13
Fold (type)	iso	iso	open/assym	open/assym	open/assym	
Generation	FA3	FA3	FA4	FA4	FA4	
FA dip direction	109	116	272	246	260	
FA dip	05	06	20	05	06	
AP dip direction	201	272	183	204	178	
AP dip	47	22	43	04	15	
UTM_N	5197799	5197799	5197799	5197799	5197799	5197799
UTM_E	427531	427531	427531	427531	427531	427531
Sample						

Point	073	073	073	073	073	073
Lithology	Dolomite	Dolomite	Phyllit Quartzite	Phyllit Quartzite	Phyllit Quartzite	Phyllit Quartzit
Comment	lense		graphitic layer	Raman IGL 19/06		
Lithodemic unit	Leckenschober	Leckenschober	Leckenschober	Leckenschober	Leckenschober	Leckenschober
Nappe	Stangalm Mesozoic	Stangalm Mesozoic	Stangalm Mesozoic	Stangalm Mesozoic	Stangalm Mesozoic	Stangalm Mesozoic
Nappesystem	BS	BS	BS	BS	BS	BS
Plane (type)	S	joint	S	S	Sb	S
Dip direction	248	305	260	250	196	190
Dip	50	75	40	54	47	25
Lineation (type)	L		L		Lstr	
Dip direction L	276		265		137	
Dip L	50		25		27	
Fold (type)			open/assym		iso	
Generation			FA4		FA3	
FA dip direction			279		132	
FA dip			17		15	
AP dip direction			186		178	
AP dip			35		42	
UTM_N	5197799	5197799	5197799	5197799	5197799	5197799
UTM_E	427531	427531	427531	427531	427531	427531

Point	073	073	073	073	073
Lithology	Phyllit Quartzite	Phyllit Quartzite	Phyllit Quartzite	Phyllit Quartzite	Phyllit
Comment					Bockbühl?
Lithodemic unit	Leckenschober	Leckenschober	Leckenschober	Leckenschober	Leckenschober
Nappe	Stangalm Mesozoic	Stangalm Mesozoic	Stangalm Mesozoic	Stangalm Mesozoic	Stangalm Mesozoic
Nappesystem	BS	BS	BS	BS	BS
Plane (type)	Sb	Sb	S	Sb	S
Dip direction	187	178	210	170	120
Dip	60	30	30	52	30
Lineation (type)	Lstr	Lstr			Ls
Dip direction L	141	138			139
Dip L	50	25			32
Fold (type)					
Generation					
FA dip direction					
FA dip					
AP dip direction					
AP dip					
UTM_N	5197799	5197799	5197799	5197799	5197799
UTM_E	427531	427531	427531	427531	427531
Sample					

Point	073	073	073	073	073
Lithology	Phyllit	Phyllit	Phyllit	Phyllit	Phyllit
Comment	Bockbühl?				
Lithodemic unit	Leckenschober	Leckenschober	Leckenschober	Leckenschober	Leckenschober
Nappe	Stangalm Mesozoic	Stangalm Mesozoic	Stangalm Mesozoic	Stangalm Mesozoi	Stangalm Mesozoic
Nappesystem	BS	BS	BS	BS	BS
Plane (type)	S	S	S		Sb
Dip direction	155	223	245		178
Dip	30	43	50		47
Lineation (type)	Ls	L	L		
Dip direction L	134	285	320		
Dip L	26	10	25		
Fold (type)		open/assym	open/assym	open/assym	
Generation		FA4	FA4	FA4	
FA dip direction		295	274	314	
FA dip		15	34	15	
AP dip direction		200		180	
AP dip		45		40	
UTM_N	5197799	5197799	5197799	5197799	5197799
UTM_E	427531	427531	427531	427531	427531
Sample					

Point	074	074	074	074
Lithology	Calcitemarble, Dolomite	Calcitemarble, Dolomite	Calcitemarble, Dolomite	Calcitemarble, Dolomite
Comment	folded together, cal massiv, clastgeometries			
Lithodemic unit	Leckenschober	Leckenschober	Leckenschober	Spielriegel
Nappe	Stangalm Mesozoic	Stangalm Mesozoic	Stangalm Mesozoic	Stolzalpe
Nappesystem	BS	BS	BS	DG
Plane (type)	S	S	Sb	S
Dip direction	212	115	169	230
Dip	35	07	33	47
Lineation (type)	L	Ls	Lstr	L
Dip direction L	136	139	117	301
Dip L	03	07	27	15
Fold (type)		iso		
Generation		FA3		
FA dip direction		140		
FA dip		07		
AP dip direction		120		
AP dip		10		
UTM_N	5197819	5197819	5197819	5197819
UTM_E	427513	427513	427513	427513
Sample				

Point	074	075	075	075	077
Lithology	Calcitemarble, Dolomite	Quartzite	Quartzite	Quartzite	Qtz-chlorite-Phyllit
Comment		Metaconglomerate, detrital mica			chlorite + sericite
Lithodemic unit	Leckenschober	Oberhof	Oberhof	Oberhof	Spielriegel
Nappe	Stangalm Mesozoic	Königsstuhl	Königsstuhl	Königsstuhl	Stolzalpe
Nappesystem	BS	DG	DG	DG	DG
Plane (type)	S	S	S	S	S
Dip direction	169	226	142	225	188
Dip	33	17	35	20	82
Lineation (type)	Ls	Ls	Lcren	Ls	L
Dip direction L	117	139	214	260	100
Dip L	27	02	12	03	01
Fold (type)		open/assym		open/assym	
Generation		FA4		FA4	
FA dip direction		238		233	
FA dip		06		12	
AP dip direction		174		184	
AP dip		35		36	
UTM_N	5197819	5198194	5198194	5198194	5197979
UTM_E	427513	427453	427453	427453	427443
Sample		MW 1918			

Point	078	079	079	080	081
Lithology	Calcitemarble, Graphiteschist	Calcitemarble myl	Calcitemarble myl	Calcitemarble myl	Calcitmarble myl, Qtz-chlorite-Phyllit
Comment	fault	phyllit rich layers			Leckenschober - Spielriegel
Lithodemic unit	Leckensch ober	Leckenschober	Leckenschobe r	Leckenschober	Leckenschober
Nappe	Stangalm Mesozoic	Stangalm Mesozoic	Stangalm Mesozoic	Stangalm Mesozoic	Stangalm Mesozoic
Nappesystem	BS	BS	BS	BS	BS
Plane (type)	fault	S	S	S	S
Dip direction	200	146	148	202	209
Dip	70	20	23	32	17
Lineation (type)		L	Ls	L	L
Dip direction L		246	108	136	123
Dip L		15	19	25	06
Fold (type)			iso	iso	
Generation			FA3	FA3	
FA dip direction			105	095	
FA dip			18	30	
AP dip direction			150	200	
AP dip			22	30	
UTM_N	5197978	5197921	5197921	5197860	5197784
UTM_E	427392	427400	427400	427373	427283
Sample					

Point	081	081	081.1	081.1	081.1
Lithology	Calcitmarble, Qtz-chlorite-Phyllit	Calcitmarble, Qtz-chlorite-Phyllit	Qtz-chlorite-Phyllit	Qtz-chlorite-Phyllit	Qtz-chlorite-Phyllit
Comment			folds axis orthogonal		
Lithodemic unit	Leckenschober - Spielriegel	Leckenschober - Spielriegel	Spielriegel	Spielriegel	Spielriegel
Nappe	Stangalm Mesozoic - Stolzalpe	Stangalm Mesozoic - Stolzalpe	Stolzalpe	Stolzalpe	Stolzalpe
Nappesystem	BS-DG	BS-DG	DG	DG	DG
Plane (type)	S	S	S	S	
Dip direction	110	209	112	114	
Dip	34	17	36	20	
Lineation (type)	Lcren	Ls	Lcren	Lcren	
Dip direction L	144	123	174	127	
Dip L	40	06	26	12	
Fold (type)				assym	iso
Generation	FA1	FA2?		FA2	FA1
FA dip direction	130	050		125	269
FA dip	30	37		13	12
AP dip direction	110	054		246	106
AP dip	35	52		46	20
UTM_N	5197784	5197784	5197784	5197784	5197784
UTM_E	427283	427283	427283	427283	427283

Point	081.2	081.2	081.3	081.3	081.3	081.3
Lithology	Qtz-chlorite-Phyllit	Qtz-chlorite-Phyllit	Qtz-chlorite-Phyllit	Qtz-chlorite-Phyllit	Qtz-chlorite-Phyllit	Qtz-chlorite-Phyllit
Comment						
Lithodemic unit	Spielriegel	Spielriegel	Spielriegel	Spielriegel	Spielriegel	Spielriegel
Nappe	Stolzalpe	Stolzalpe	Stolzalpe	Stolzalpe	Stolzalpe	Stolzalpe
Nappesystem	DG	DG	DG	DG	DG	DG
Plane (type)		S	S		S	
Dip direction		117	125		137	
Dip		40	27		20	
Lineation (type)	Ls	L	Ls	Lcren	Lcren2	Lcren1
Dip direction L	102	135	130	163	076	128
Dip L	35	25	18	15	17	20
Fold (type)		open			open	
Generation		FA3			FA3	FA2
FA dip direction		092			075	130
FA dip		15			19	20
AP dip direction		352			140	232
AP dip		05			20	86
UTM_N	5197784	5197784	5197784	5197784	5197784	5197784
UTM_E	427283	427283	427283	427283	427283	427283
Sample						

Point	081.3	081.3	081.3	081.3	081.3	081.4
Lithology	Qtz-chlorite-Phyllit	Qtz-chlorite-Phyllit	Qtz-chlorite-Phyllit	Qtz-chlorite-Phyllit	Qtz-chlorite-Phyllit	Qtz-chlorite-Phyllit
Comment						
Lithodemic unit	Spielriegel	Spielriegel	Spielriegel	Spielriegel	Spielriegel	Spielriegel
Nappe	Stolzalpe	Stolzalpe	Stolzalpe	Stolzalpe	Stolzalpe	Stolzalpe
Nappesystem	DG	DG	DG	DG	DG	DG
Plane (type)	Sb	S				
Dip direction	121	125				
Dip	52	27				
Lineation (type)	Lstr	Ls	Lcren			
Dip direction L	142	130	163			
Dip L	47	18	15			
Fold (type)		iso	assym			
Generation		FA1	FA2	FA2	FA1	
FA dip direction		260	234	043	023	
FA dip		01	14	10	04	
AP dip direction		310	312	320	121	
AP dip		20	34	25	88	
UTM_N	5197784	5197784	5197784	5197784	5197784	5197784
UTM_E	427283	427283	427283	427283	427283	427283

Point	082	083	084	085	086
Lithology	Qtz-chlorite-Phyllit	Qtz Phyllit/ Quartzitee	Qtz-chlorite-Phyllit	Qtz-chlorite-Phyllit	Graphiteschist
Comment	deformed	course grained mica	metamorph than Murau		detrital mica, Raman IGL 1910
Lithodemic unit	Spielriegel	Murau	Spielriegel	Spielriegel	Oberhof
Nappe	Stolzalpe	Murau	Stolzalpe	Stolzalpe	Königsstuhl
Nappesystem	DG	DG	DG	DG	DG
Plane (type)				S	
Dip direction				188	
Dip				44	
Lineation (type)				Ls	
Dip direction L				190	
Dip L				37	
Fold (type)					
Generation					
FA dip direction					
FA dip					
AP dip direction					
AP dip					
UTM_N	5197458	5197651	5197765	5197708	5198190
UTM_E	428004	427912	427722	427657	427389
Sample					

Point	087	088	088	088
Lithology	Calcitmarble	Quartzite	Quartzite	Quartzite
Comment	graphitschist layer 0.5m	metaconglomerate inverse layering		
Lithodemic unit	Leckenschober	Oberhof	Oberhof	Oberhof
Nappe	Stangalm Mesozoic	Königsstuhl	Königsstuhl	Königsstuhl
Nappesystem	BS	DG	DG	DG
Plane (type)	S	S	S	S
Dip direction	230	216	214	260
Dip	50	34	33	10
Lineation (type)	Ls	Ls		
Dip direction L	298	298		
Dip L	28	07		
Fold (type)				
Generation				
FA dip direction				
FA dip				
AP dip direction				
AP dip				
UTM_N	5198320	5198370	5198370	5198370
UTM_E	427358	427303	427303	427303
Sample				MW 1919

Point	089	090	090	090
Lithology	Calcitmarble/ micaschist	Calcitemarble, Dolomite myl, Metakonglomerat	Calcitemarble, Metakonglomera	Dolomite myl, Metakonglo
Comment		contact Dol + Cal - Konglomerate		
Lithodemic unit	Murau	Leckenschober - Oberhof	Leckenschober - Oberhof	Leckenschober - Oberhof
Nappe	Murau	Stangalm Mesozoic - Königsstuhl	tangalm Mesozoic - Königsstu	Stangalm Mesozoic - Königsstuhl
Nappesystem	DG	BS-DG	BS-DG	BS-DG
Plane (type)		S	S	Smyl
Dip direction		187	226	238
Dip		25	34	30
Lineation (type)			Ls	Ls
Dip direction L			164	166
Dip L			12	06
Fold (type)				iso
Generation				FA3
FA dip direction				172
FA dip				07
AP dip direction				235
AP dip				30
UTM_N	5198678	5198477	5198477	5198477
UTM_E	427322	427308	427308	427308
Sample				

Point	091	092	093	093
Lithology	Calcitmarble myl	Calcitmarble, Dolomite	Dolomitemarble	Quartzite
Comment	graphitic, Raman IGL 1913	Dolomite Boudins, clast geometries Top E	graphitic, footwall carbonate	Metaconglomerate
Lithodemic unit	Leckenschober	Leckenschober	Weißwände	Oberhof
Nappe	Stangalm Mesozoic	Stangalm Mesozoic	Stangalm Mesozoic	Königsstuhl
Nappesystem	BS	BS	BS	DG
Plane (type)	Smyl			S
Dip direction	113			154
Dip	18			24
Lineation (type)	Ls			
Dip direction L	120			
Dip L	07			
Fold (type)				iso
Generation				FA3
FA dip direction				197
FA dip				20
AP dip direction				155
AP dip				25
UTM_N	5198468	5198444	5198423	5198423
UTM_E	427342	427357	427388	427388
Sample	MW 1920			

Point	094	095	096	097	097	098
Lithology	Mica schist	Mica schist	meta conglomerate	Quartzite	Quartzite	Dolomite greyisch
Comment	to S conglomerate more thick	no detrital mica	subanstehend			
Lithodemic unit	Oberhof	Bockbühel	Oberhof	Oberhof	Oberhof	Karnerboden
Nappe	Königsstuhl		Königsstuhl	Königsstuhl	Königsstuhl	Stangalm Mesozoic
Nappesystem	DG	BS	DG	DG	DG	BS
Plane (type)	S			S	joint	S
Dip direction	182			198	113	356
Dip	50			19	86	77
Lineation (type)	Ls			Ls		Ls
Dip direction L	277			108		085
Dip L	10			04		02
Fold (type)				iso		
Generation				FA3		
FA dip direction				203		
FA dip				23		
AP dip direction				180		
AP dip				20		
UTM_N	5198015	5198599	5198587	5198410	5198410	5198372
UTM_E	427659	426948	427008	427267	427267	427303
Sample	MW 1922					

Point	098	098	099	099	100
Lithology	Dolomite greyisch	Dolomite greyisch	Calcitmarble	Calcitmarble	Quartzite
Comment					metakonglomerate umyl, shearbands (Top E)
Lithodemic unit	Karnerboden	Karnerboden	Leckenschober	Leckenschober	Oberhof
Nappe	Stangalm Mesozoic	Stangalm Mesozoic	Stangalm Mesozoi	Stangalm Mesozoic	Königsstuhl
Nappesystem	BS	BS	BS	BS	DG
Plane (type)	S	joint	S	S	S
Dip direction	018	114	198	207	215
Dip	77	87	20	17	22
Lineation (type)	Ls		Ls	Ls	Ls
Dip direction L	112		103	290	135
Dip L	01		01	01	03
Fold (type)				iso	iso
Generation				FA3	FA3
FA dip direction				291	270
FA dip				02	19
AP dip direction				207	130
AP dip				17	05
UTM_N	5198372	5198372	5198367	5198367	5198343
UTM_E	427303	427303	427326	427326	427338

Point	101	101	101	101	101	102
Lithology	Qtz-chlorite-Phyllit	Qtz-chlorite-Phyllit	Qtz-chlorite-Phyllit	Qtz-chlorite-Phyllit	Qtz-chlorite-Phyllit	Qtz-chlorite-Phyllit
Comment						massive, Foto NW
Lithodemic unit	Spielriegel	Spielriegel	Spielriegel	Spielriegel	Spielriegel	Spielriegel
Nappe	Stolzalpe	Stolzalpe	Stolzalpe	Stolzalpe	Stolzalpe	Stolzalpe
Nappesystem	DG	DG	DG	DG	DG	DG
Plane (type)	S	Sb				
Dip direction	168	135				
Dip	13	45				
Lineation (type)		Lstr				
Dip direction L		114				
Dip L		45				
Fold (type)		iso	assym	assym	open	
Generation		FA1	FA2	FA2	FA3	
FA dip direction		092	200	022	054	
FA dip		10	03	04	12	
AP dip direction		335	333	300	126	
AP dip		28	55	58	50	
UTM_N	5197395	5197395	5197395	5197395	5197395	5197420
UTM_E	426764	426764	426764	426764	426764	426609
Sample						

Point	103	103	103	104	104
Lithology	Qtz-chlorite-Phyllit	Qtz-chlorite-Phyllit	Qtz-chlorite-Phyllit	Qtz-chlorite-Phyllit	Qtz-chlorite-Phyllit
Comment				SC-fabric Top ESE	
Lithodemic unit	Spielriegel	Spielriegel	Spielriegel	Spielriegel	Spielriegel
Nappe	Stolzalpe	Stolzalpe	Stolzalpe	Stolzalpe	Stolzalpe
Nappesystem	DG	DG	DG	DG	DG
Plane (type)	S	Sb	Sb	S	Sb (C') - FA3
Dip direction	209	177	208	168	120
Dip	14	28	27	24	44
Lineation (type)		Lstr		Lint	Lstr
Dip direction L		110		110	114
Dip L		12		10	44
Fold (type)	iso			open	
Generation	FA1			FA3	
FA dip direction	260			201	
FA dip	06			01	
AP dip direction	210			114	
AP dip	15			49	
UTM_N	5197375	5197375	5197375	5197567	5197567
UTM_E	426410	426410	426410	426384	426384
Sample					

Point	105	106	106	106	106	106
Lithology	Calcitmarble	Qtz-chlorite-Phyllit	Qtz-chlorite-Phyllit	Qtz-chlorite-Phyllit	Qtz-chlorite-Phyllit	Qtz-chlorite-Phyllit
Comment	Qtz mobilisate, Foto NE	nappe boundary iso folded	cal umyl	nappe boundary		
Lithodemic unit	Leckenschober	Spielriegel	Spielriegel	Spielriegel	Spielriegel	Spielriegel
Nappe	Stangalm Mesozoic	Stolzalpe	Stolzalpe	Stolzalpe	Stolzalpe	Stolzalpe
Nappesystem	BS	DG	DG	DG	DG	DG
Plane (type)	S	S	Sb	Sb	Sb	Sb
Dip direction	152	003	122	145	148	120
Dip	40	08	17	20	36	26
Lineation (type)	Ls	Lint	Lstr	Lstr	Lstr	Lstr
Dip direction L	102	287	146	140	129	133
Dip L	20	08	17	17	36	24
Fold (type)	iso	iso	assym			
Generation	FA3	FA1	FA2			
FA dip direction	150	280	200			
FA dip	40	01	07			
AP dip direction	100	022	289			
AP dip	20	13	35			
UTM_N	5197711	5197439	5197439	5197439	5197439	5197439
UTM_E	426279	426741	426741	426741	426741	426741
Sample						

Point	106	106	106	107	108	109
Lithology	Qtz-chlorite-Phyllit	Qtz-chlorite-Phyllit	tz-chlorite-Phyll	Chlorite-schist	Dolomite dark	Calcitmarble/Qtz-Phyllit
Comment					Fossil bearing (Diploporen?)	nappe system boundary
Lithodemic unit	Spielriegel	Spielriegel	Spielriegel	Spielriegel	Karnerboden	Leckenschober - Spielriegel
Nappe	Stolzalpe	Stolzalpe	Stolzalpe	Stolzalpe	Stangalm Mesozoic	Stangalm Mesozoic - Stolzalpe
Nappesystem	DG	DG	DG	DG	BS	BS-DG
Plane (type)	Sb	Sb	fault(gauche)	S		S
Dip direction	114	132	245	137		193
Dip	38	35	27	23		35
Lineation (type)	Lstr	Lstr				Ls
Dip direction L	130	122				109
Dip L	36	27				20
Fold (type)						
Generation						
UTM_N	5197439	5197439	5197439	5197721	5197828	5197799
UTM_E	426741	426741	426741	427035	426356	426467
Sample					FOS 1a/1b	

Point	110	110	111	111	112	113
Lithology	Dolomite dark	Dolomite dark	Dolomite dark	Dolomite dark	Calcitemarble	Calcitmarble/Qtz-Phyllit
Comment	Qtz layers iso folded		En-enchelion veins	folded in Leckenschober	Pyrit	nappe system boundary
Lithodemic unit	Karnerboden	Karnerboden	Karnerboden	Karnerboden	Leckenschober	Leckenschober - Spielriegel
Nappe	Stangalm Mesozoic	Stangalm Mesozoic	Stangalm Mesozoic	Stangalm Mesozoic	Stangalm Mesozoic	Stangalm Mesozoic - Stolzalpe
Nappesystem	BS	BS	BS	BS	BS	BS-DG
Plane (type)	S		S	vein	S	S
Dip direction	076		151	128	177	230
Dip	22		30	72	54	16
Lineation (type)	Ls		Ls		Ls	Lcren
Dip direction L	114		084		096	300
Dip L	16		15		13	11
Fold (type)	ios	assym/open			iso	open (SE-vergent)
Generation	FA3	FA4			FA3	FA4
FA dip direction	096	273			095	264
FA dip	10	08			15	01
AP dip direction	050	199			175	339
AP dip	22	32			55	32
UTM_N	5197747	5197747	5197682	5197682	5197596	5197547
UTM_E	426413	426413	426229	426229	426021	425887
Sample						

Point	ci14/247	ci14/248
Lithology	Calcitemarble	Greenschist
Comment		
Lithodemic unit	eckenschobe	Spielriegel
Nappe	ngalm Mesoz	Stolzalpe
Nappesystem	BS	DG
Plane (type)	S	S
Dip direction	140	219
Dip	20	15
Lineation (type)	Ls	Ls
Dip direction L	124	284
Dip L	20	5
Fold (type)		
Generation		
UTM_N	5198185	5198018
UTM_E	425043	424976
Sample		

Point	113	114	115	ci17/070	ci17/070
Lithology	Calcitmarble/Qtz-Phyllit	Calcitemarble	Dolomite	Micaschist	Micaschist
Comment	decoppeled qtz veins	next to nappe boundary	with veins - less deformed	carbonatic, graphitic	
Lithodemic unit	Leckenschober - Spielriegel	Leckenschober	Karnerboden	Murau	Murau
Nappe	Stangalm Mesozoic - Stolzalpe	Stangalm Mesozoic	Stangalm Mesozoic	Murau	Murau
Nappesystem	BS-DG	BS	BS	DG	DG
Plane (type)		S	S	S	Sb (C')
Dip direction		164	312	238	145
Dip		40	46	26	32
Lineation (type)		Ls		Ls	Lstr
Dip direction L		101		281	119
Dip L		23		20	27
Fold (type)				iso	down
Generation		FA3		FA1	
FA dip direction		100		282	
FA dip		20		19	
AP dip direction		160		250	
AP dip		40		28	
UTM_N	5197547	5197557	5198208	5198786	5198786
UTM_E	425887	425908	425113	426721	426721
Sample					

Point	ci17/071	ci17/071	ci17/026	ci17/026	ci18/006	ci18/006
Lithology	Dolomit myl	Dolomit myl	Cal-Micaschist	Cal-Micaschist	Micaschist/ Greenschist	Micaschist/ Greenschist
Comment	invers folded				carbonatic	
Lithodemic unit	Weißwände	Weißwände	Murau	Murau	Murau	Murau
Nappe	Stangalm Mesozoic	angalm Mesozo	Murau	Murau	Murau	Murau
Nappesystem	BS	BS	DG	DG	DG	DG
Plane (type)	S	joint	S	Sb (C')	S	S
Dip direction	293	128	206	109	289	2
Dip	7	86	27	6	20	38
Lineation (type)	Ls		Lcren-int	Lstr	Lmin	Lcren
Dip direction L	286		118	116	289	286
Dip L	9		1	5	20	8
Fold (type)					iso	
Generation					FA1	
FA dip direction					285	
FA dip					20	
AP dip direction					285	
AP dip					020	
UTM_N	5198726	5198726	5198622	5198622	5198694	5198694
UTM_E	426631	426631	427589	427589	427834	427834